DESIGN OF A VEHICLE BASED INTERVENTION SYSTEM TO PREVENT OZONE LOSS

The 1994/95 NASA/USRA Advanced Design Project Team
Presents:

The Aeolus

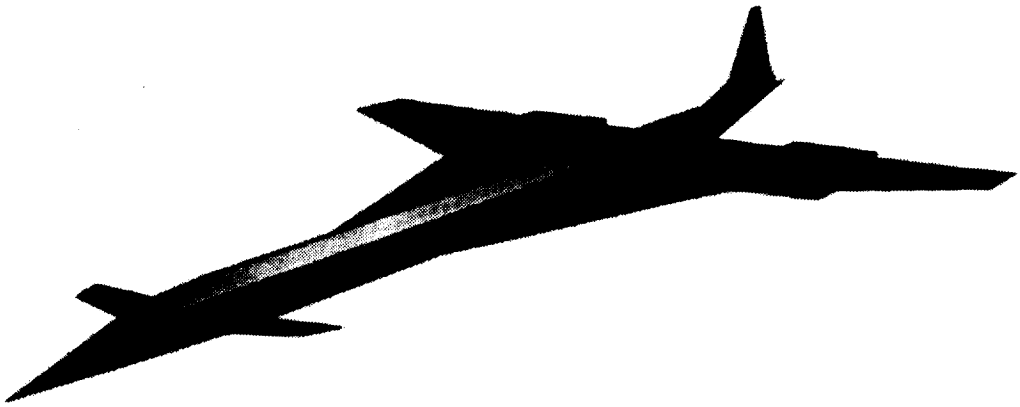

Department of Aerospace and Ocean Engineering
Virginia Polytechnic Institute and State University
May 3, 1995

Team Members:

Robin Cole
Matt Meade
Kristin Olson
Anne Valdivia
Daniel Fisher
James Neel
Andrew Pittman
Aria Wibisono

Consulting Professors:
Dr. William H. Mason
Professor Nathan Kirschbaum

ACKNOWLEDGMENT

The 1994/95 NASA/USRA ADP group would like to thank NASA/USRA for sponsoring this project. Furthermore, we would like to thank Dr. William H. Mason and Professor Nathan Kirschbaum for their assistance and guidance. Finally, we would like to thank the graduate students who also provided much assistance: Paul Crisafulli, Valery Razgonyaev, and Pete McMillan.

Abstract

Purpose

This project was designed to be completed over a period of three years. Overall project goals were:

- To understand the processes that contribute to stratospheric ozone loss
- To determine the best prevention scheme for loss
- To design a delivery vehicle to accomplish the prevention scheme

The 1994-1995 design objectives included:

- To review the results of the 1993-1994 design team, including a reevaluation of the major assumptions and criteria selected to choose a vehicle
- To evaluate preliminary vehicle concepts and perform quantitative trade studies to select the optimal vehicle concept

Ozone Hole

Chlorine from chlorofluorocarbons (CFCs) and natural sources initiates the destruction of stratoshperic ozone through a free radical chain reaction. Reduced quantities of ozone in the stratosphere allows greater levels of ultraviolet (UV) radiation to reach the earth's surface. High levels of UV radiation are known to cause cancer and other medical problems in humans.

Prevention Schemes

A plan proposed by R.J. Cicerone, Scott Elliot, and R.P. Turco in late 1991 was used for the prevention scheme because of its research support and economic feasibility. This scheme uses hydrocarbon (propane) injections into the Antarctic ozone hole to form stable compounds with the destructive atomic chlorine, thereby reducing the chemical reactions causing ozone depletion. Most ozone destruction takes place during a 3-4 week period each year. For this reason, the hydrocarbons must be injected during this time interval.

Propane Delivery and Storage

Propane delivery and mixing techniques were investigated by the 1993/1994 design team to determine the best mixing technique available. Classical diffusion theory was used by the 1993/1994 design team to determine the mixing requirements. A multi-tank propane storage system was designed, and vehicle loading techniques were examined.

Selection Criteria

A set of baseline vehicle requirements and a baseline mission profile were generated using parameters developed from the 1993-1994 design report and current supersonic transport research. A selection criteria was generated based on an assessment of applicable existing and proposed designs in conjuction with the developed baselines.

Aircraft Configuration Studies

Selected concepts were assessed and modeled using analytical methods. The primary analysis tool used in defining the original concepts was an aircraft synthesis code, ACSYNT. Additional analysis was conducted using FORTRAN programs to study the aerodynamic, stability and control, and structural considerations of the concepts.

Final Concept

The final concept, called the Aeolus, was chosen to be the canard version of the High Speed Civil Transport. The aircraft is unique in its ability to load the payload through its swinging tailcone.

Table of Contents

List of Figures

List of Tables

Variable and Acronym Definitions

ACSYNT	AirCraft SYNthesis
APAS	Aerodynamic Preliminary Analysis System
APU	Auxilary Power Unit
C_D	Drag Coefficient
C_{D0}	Drag Coefficent at Zero Lift
C_L	Lift Coefficient
C_{La}	Lift Curve Slope with respect to Angle of Attack
C_{La}	Lift Curve Slope with respect to Angle of Attack
$C_{L;p}$	Lift Curve Slope with respect to Roll Rate
C_{Lq}	Lift Curve Slope with respect to Pitching Rate
C_{Lr}	Lift Curve Slope with respect to Yaw Rate
$C_{Ld\ canard}$	Lift Curve Slope with respect to Canard Deflection
C_{ma}	Pitch Moment Slope with respect to Angle of Attack
C_{mq}	Pitch Moment Slope with respect to Pitching Rate
$C_{md\ canard}$	Pitch Moment Slope with respect to Canard Deflection
C_{yb}	Side Slip Coefficent with respect to Side Slip Angle
C_{yp}	Side Slip Coefficient with respect to Roll Rate
C_{yr}	Side Slip Coefficent with respect to Yaw Rate
$C_{yd\ aileron}$	Side Slip Coefficient with respect to Aileron Deflection
$C_{yd\ rudder}$	Side Slip Coefficient with respect to Rudder Deflection
C_{lb}	Rolling Moment Coefficent with respect to Side Slip Angle
C_{lp}	Rolling Moment Coefficent with respect to Roll Rate
C_{lr}	Rolling Moment Coefficent with respect to Yaw Rate
$C_{ld\ aileron}$	Rolling Moment Coefficent with respect to Aileron Deflection
$C_{ld\ rudder}$	Rolling Moment Coefficent with respect to Rudder Deflection
C_{mp}	Pitching Moment Coefficent with respect to Roll Rate
C_{mr}	Pitching Moment Coefficent with respect to Yaw Rate
C_{nb}	Yawing Moment Coefficent with respect to Side Slip Angle
C_{np}	Yawing Moment Coefficent with respect to Roll Rate
C_{nr}	Yawing Moment Coefficent with respect to YawRate
$C_{nd\ aileron}$	YawingMoment Coefficent with respect to Aileron Deflection
$C_{nd\ rudder}$	Yawing Moment Coefficent with respect to Rudder Deflection
CFC	Chloroflourocarbons
cg	Center of Gravity
CMC	Ceramic Matrix Composites
EPM	Enabling Propulsion Materials
FAA	Federal Aviation Association
FADEG	Fully Automated Digital Engine Control
FAR	Federal Aviation Regulation
FBL	Fly-By-Light
FCC	Flight Control Computer
FPR	Fan Pressure Ratio
g	Gravity
GE	General Electric
GPS	Global Positioning System
HSCT	High Speed Civil Transport
IMC	Intermetallic Matrix Composites
INS	Inertial Navigational System
L/D	Lift to Drag Ratio
LPP	Lean-Premixed-Prevaporized
LTA	Lighter Than Air
M	Mach Number
M_{avail}	Mach Available

M_{req}	Mach Required
MFD	Multi-Function Display
MIL-STD	Military Standard
MTF	Mid-Tandem Fan
NASA	National Association of Space and Aeronautics
NO_X	Nitrous Oxide Emissions
OAS	Optical Amplifier System
OPR	Overall Pressure Ratio
PSC	Polar Stratospheric Clouds
PFCC	Primary Flight Control Computer
P&W	Pratt & Whitney
RAT	Ram Air Turbine
RFP	Request for Proposals
RQL	Rich-Burn, Quick-Quench, Lean-Burn
SFC	Specific Fuel Consumption
SAS	Stability Augmentation System
SST	Supersonic Transport
TBE	Turbine-Bypass Turbojet
TOGW	TakeOff Gross Weight
tr	Time Constant of Roll Mode
T2	Time to Double Amplitude of Spiral Mode
UV	Ultraviolet
wd	Natural Frequency of Dutch Roll
zd	Damping Ratio of Dutch Roll
zp	Damping Ratio of Phugoid Mode
zsp	Damping Ratio of Short Period Mode

1.0 INTRODUCTION

The depletion of ozone over Antarctica was first discovered in the early 1970's. The discovery of this hole has a direct bearing on supersonic transport (SST) research because many scientists believe the NO_x emissions from the jet engines cause the depletion (Dornheim, 1994). Scientists and environmentalists have since been working to determine the cause and global effects of this hole. Their research has identified two of the main sources of the problem to be chloroflourocarbons and NO_x. Ground based ozone depletion intervention schemes are being implemented by the government and industries to slow and eventually eliminate further depletion. However, surface level changes will take decades to have an effect at the stratospheric altitudes containing the ozone layer. Along with intervention comes the possibility of fixing the existing hole. Solutions to this problem are currently being studied.

Scientists have proven that decreases in the ozone level can lead to a significant increase of skin cancer and cataracts. The presence of the ozone level shields the Earth surface from harmful ultraviolet (UV) radiation which can contribute to these diseases. The thinning ozone layer may also lead to major changes in the ecosystem such as the photosynthesis of phytoplankton. These problems have led to the proposal of direct vehicle-based intervention schemes (Kay, 1992).

This is the third and final year of the Virginia Tech NASA/USRA Advanced Design Program to design a vehicle-based intervention system to prevent ozone loss. The goals of the three year project is to 1) study the causes which contribute to the depletion of the ozone layer, 2) examine and propose different intervention schemes and choose the most effective, and 3) design a man made, environmentally sound system to carry out the chosen scheme. This is the primary goal of the current team. The goal of the 1994/1995 team also includes reviewing and reevaluating the decisions of the previous two years.

A good understanding of the ozone depletion mechanisms and chemistry is essential to determine an effective intervention scheme. Chapter 2 explains the ozone cycle including the production and destruction specifically over Antarctica. It also discusses future predictions if the problem is not corrected and the ozone layer continues to deteriorate.

2.0 OZONE

Ozone (O_3) is a natural atmospheric gas, 90 percent of which is found in the stratosphere at an altitude between 49,000-98,000ft (Hamill, 1991). The ozone layer is responsible for blocking the Sun's harmful ultraviolet (UV) radiation. This layer of ozone is essential to maintaining life on Earth as we know it to exist.

2.1 Ozone Equilibrium

Ozone molecules in the stratosphere are constantly formed and destroyed as they intercept the sun's harmful UV radiation of wavelengths (λ) ranging from 240-320nm. As UV rays less 240nm interact with molecular oxygen found in the outer layer of the stratosphere, a reaction occurs which produces atomic oxygen as shown in reaction (1). This atomic oxygen then seeks out other molecular oxygen and the two join to produce an ozone molecule as in reaction (2). The ozone is then destroyed as it absorbs the UV rays between the wavelengths 240-320nm before they reach the earth. Again, atomic oxygen is produced as shown in (3) which combines with an oxygen molecule and the process repeat (NASA/USRA, 1994). As shown in equation (1) and (3), "h" represents Planck's Constant and "v" is the radiation frequency corresponding to the radiation wavelength (Kay, 1992).

$$O_2 + hV \rightarrow O + O \qquad (\lambda < 240nm) \qquad (1)$$

$$O + O_2 \rightarrow O_3 \qquad (2)$$

$$O_3 + hV \rightarrow O_2 + O \qquad (240nm < \lambda < 340nm) \qquad (3)$$

Other reactions, as shown below in (4) and (5), also occur throughout the stratosphere but they are less frequent.

$$O + O_3 \rightarrow O_2 + O_2 \qquad (4)$$

$$O + O \rightarrow O_2 \qquad (5)$$

These reactions are less common because oxygen molecules are much more abundant than either atomic oxygen or ozone molecules. Therefore, the formation of ozone, reaction (2), is most common (NASA/USRA, 1994).

About thirty years ago, scientists predicted the amount of ozone which should be present using the above equations. When measured, the amount of actual ozone present was found to be much less. This indicated that other ozone reducing reactions must also naturally exist. The reactions were found to be as shown in (6) and (7) (NASA/USRA, 1994).

$$X + O_3 \rightarrow XO + O_2 \quad (6)$$
$$XO + O \rightarrow X + O_2 \quad (7)$$
$$\text{NET}\quad O + O_3 \rightarrow 2O_2$$

The X term represents either ClO, NO, OH or BrO in the above reactions (Zurer, 1993). The catalytic reaction between these naturally present elements and the ozone layer could potentially result in the destruction of many ozone molecules. This, fortunately, does not occur because these elements only exist in trace amounts in the atmosphere (NASA/USRA, 1994).

The combination of the above seven reactions describes the natural cycle and balance of ozone in the atmosphere.

2.2 Cloroflourocarbons

Scientists have discovered that the main reason for the current ozone depletion is due to the increased levels of chlorine radicals in the atmosphere. Man-made cloroflourocarbons (CFC's) are the source of over 80 percent of the chlorine now present in the atmosphere (Chipperfield, 1993). CFC's are normally, as developed, stable and inert until they are subjected to intense UV rays which are present in the stratosphere. At this point they breakdown, such that a chlorine atom is released (Zurer, 1993). The reactions for the two most common CFC's on the market, which account for approximately 47 percent of the destructive chlorine, are shown in (8) and (9) (Prather, 1990). These newly formed chlorine atoms (Cl) are capable of destroying ozone molecules as in reactions (6) and (7) (NASA/USRA, 1994).

CFC-11 $CF_2Cl_2 + hV \rightarrow CF_2Cl + Cl$ (8)

CFC-12 $CFCl_3 + hV \rightarrow CFCl_2 + Cl$ (9)

The atomic chlorine atoms formed do not continuously destroy ozone molecules. Because chlorine has a high reactivity, it can react with many other trace elements in the atmosphere, thus temporarily retaining it from the ozone destroying cycle (Kay, 1992). These chlorine atoms are deemed to be in

reservoirs. Reservoirs are stable compounds which tie-up the ozone depleting species (*Stratospheric Ozone*, 1987). Over 90 percent of ozone depleting chlorine atoms in the high-latitude stratosphere are in the form of hydrochloric acid (HCl) or chlorine nitrate ($ClONO_2$) (Kawa, 1992).

A direct result of the increased chlorine in the atmosphere, is an increase in the destruction of ozone as shown in reactions (6) and (7) (NASA/USRA, 1994). Although this process helps to explain the reduced amounts of ozone detected in the atmosphere as a whole, the question of the obvious hole and excessive depletion over Antarctica still has not been answered.

2.3 The Ozone Hole and the Polar Winter

The cause for the significant decrease in atmospheric ozone over Antarctica has been researched since the discovery of the hole in the early 1970's. During the Southern Hemisphere's spring, research has shown almost all of the ozone at certain altitudes is destroyed as the sun rises. The size of the ozone hole was measured to cover an area of 9 million square miles including the tip of South America (Svitil, 1993). The unique atmospheric conditions specific to Antarctica during the winter causes the extreme ozone depletion compared to the milder depletion elsewhere.

As the Southern hemisphere's winter begins, the air over the pole is essentially isolated from the rest of the atmosphere due to the strong westerlies which encircle the polar region. "As the air cools, contracts, and descends, a cyclonic system termed the polar vortex is formed" (NASA/USRA, 1994). Figure 2.1 shows the structure of the polar vortex. During the polar winter, the region is covered in darkness and no solar energy is present to heat the air inside the polar vortex. This results in an extreme temperature drop to as low as 193K. At this point, type I polar stratospheric clouds (PSC's) consisting of condensed particles of nitric acid and water particles form. When temperatures drop as low as 187K, type II PSC's of ice particles form (Hamill, 1991).

Polar stratospheric clouds alone are not responsible for the massive ozone depletion. PSC's provide the surface for chemical reactions which change the stable chlorine reservoirs of hydrogen chloride (HCl) and chlorine nitrate ($ClONO_2$) into photolytically reactive molecular chlorine (Cl_2) and hypochlorous acid (HOCl) as shown in reactions (10) and (11) (Hamill, 1991).

$$HCl + ClONO_2 \rightarrow Cl_2 + HNO_3 \quad (10)$$

$$H_2O + ClONO_2 \rightarrow HOCl + HNO_3 \quad (11)$$

The sun finally rises nearing the end of the polar winter. The incoming solar energy releases chlorine atoms from the molecular chlorine and hypochlorous acid as shown in (12) and (13). The product of these reactions are then free to catalytically react with the ozone as in the ozone reducing reactions shown in (6) and (7), and therefore resulting in increased ozone depletion.

$$Cl_2 + hV \rightarrow 2Cl \quad (12)$$

$$HOCl + hV \rightarrow OH + Cl \quad (13)$$

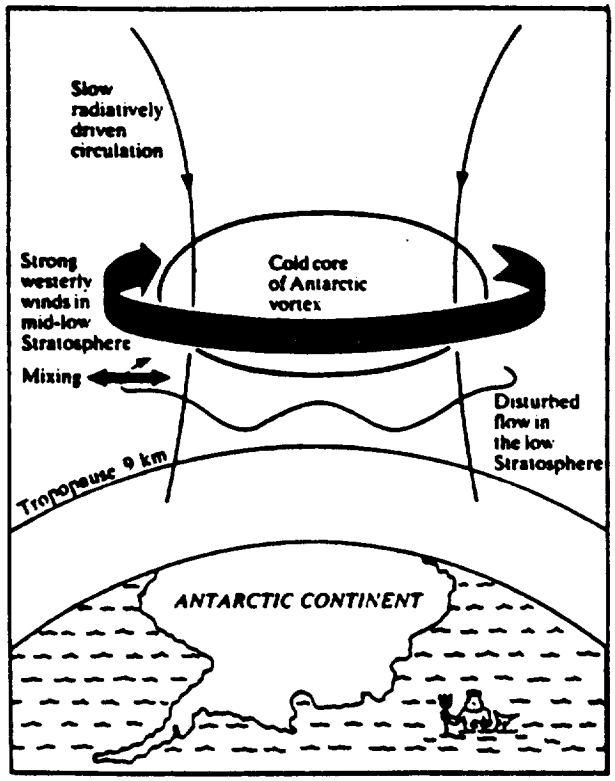

Figure 2.1
Structure of Antarctic Polar Vortex
From: Wayne, 1991

This cycle evolves over a three week period causing the destruction of most of the ozone present over the polar vortex. This destroyed ozone accounts for approximately 3 percent of the total global

stratospheric ozone (Hamill, 1991). At the end of the three week period, the necessary extreme winter conditions no longer exist and the depleting of ozone essentially ceases until the following polar winter.

2.4 Conclusions

Since the detection of the ozone hole, the levels of chlorine in the atmosphere have continued to rise. Figure 2.2 shows the increase in chlorine levels over the past 30 years as well as the predicted levels under the restrictions of the Montreal protocol, and its recent revisions, which calls for the complete phase out of CFC's by 1996.

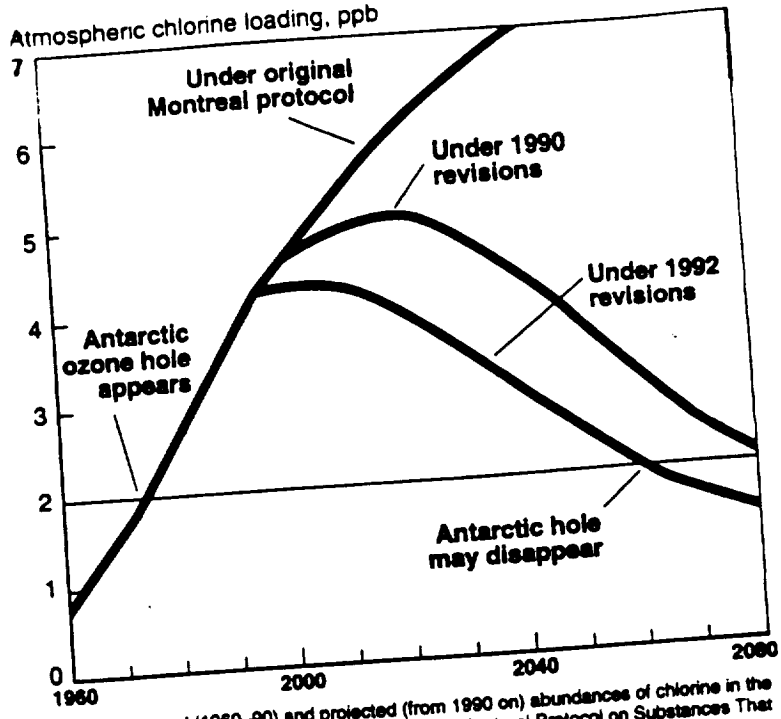

Figure 2.2
Prediction of Future Atmospheric Chlorine Concentrations
From: Prather, 1990

Studies show that for every one percent decrease in ozone, there is a two percent increase in the UV dose proven to cause skin cancer (Kay, 1992). The definite effects of increased UV radiation exposure are uncertain, only estimates have been made. If the depleting ozone problem is not soon cured, it has been predicted that a 10 percent loss of ozone would result in 1.75 million more cases of cataracts a year as well as 26 percent increase in skin cancer (Lipske, 1992). In addition to being harmful to humans, the depleting ozone could have negative effects on the agricultural and plant world as well as the marine food chain (NASA/USRA, 1994). In order to ensure the continued balance of our sensitive ecosystem, an environmentally sound ozone depletion intervention scheme must be developed.

3.0 INTERVENTION SCHEMES

Scientists have proposed several intervention schemes in response to the increasing concern for the depleting ozone layer. Proposed schemes included the deflection of UV radiation by mechanical means, the possible production and distribution of man-made ozone or the complete clean-up of CFC's by chemical means. The problem with any intervention scheme is the inherent risks involved. These risks include possible wrong assumptions or unpredicted side effects as well as the wasted time and resources (NASA/USRA, 1994).

3.1 Hydrocarbon Injections

The first year of this study was devoted to the task of researching the possibilities and choosing the most effective intervention scheme. The 1992/1993 Virginia Tech NASA/USRA team decided the injection of hydrocarbons into the ozone layer during the period of catalytic ozone destruction by atomic chlorine could help control the depleting ozone layer. The active chlorine is predicted to rapidly react with the hydrocarbon, minimizing the amount of ozone destroyed. If the hydrocarbon is injected during the polar winter, the chlorine atoms will be diverted until the conditions for the release of atomic chlorine atoms passes. At this time, the injections will no longer be necessary until the following polar winter (Cicerone, 1991).

This scheme was proposed and researched by R.J. Cicerone, Scott Elliott, and R.P. Turco in a paper titled "Reduced Antarctic Ozone Depletion in a Model with Hydrocarbon Injections" (Cicerone, 1991). The general reaction of a hydrocarbon with atomic chlorine is shown in equation (14).

$$Cl + C_xH_y \rightarrow HCl + C_xH_y \qquad (14)$$

Propane is the hydrocarbon of choice since it reacts at a 1:1 ratio with the active chlorine. Therefore, the amount of active chlorine present in the stratosphere dictates the necessary amount of propane which must be injected into the atmosphere (Cicerone, 1991). The amount of active chlorine present in the stratosphere will need to be determined just before the time the propane is scheduled to be released.

4.0 DELIVERY SYSTEM

Once the intervention scheme was chosen, a delivery system to release the propane into the stratosphere was developed. The main design requirements are that the propane must be delivered within a three week period, and the delivery system must be able to withstand the harsh winds and weather conditions present over Antarctica at an altitude of 66,000ft.

Several vehicles were investigated to implement the Cicerone method. Lighter-then-air (LTA) vehicles were eliminated because of their low speed and altitude restrictions as well as their susceptibility to damage from the high winds present at the high altitudes. Missiles were ruled out due to their low payload to gross weight ratio and debris problems. Subsonic aircraft were also investigated but eliminated due to their inability to fly at the altitudes and payloads needed as well as the harsh gusts over Antarctica. The first year NASA/USRA team chose a fleet of supersonic aircraft as the most effective delivery system. The second year, 1993/1994 team, reviewed the previous year's analysis and updated their delivery scheme. They performed an operational analysis and trade studies to more clearly understand the hydrocarbon insertion initially proposed and to understand its capabilities. The 1993/1994 team chose the preliminary size of the supersonic delivery aircraft as well as alternate uses of this vehicle.

4.1 The Supersonic Delivery System

The supersonic aircraft was considered the viable vehicle with which to implement the propane delivery system. The aircraft needed to be capable of carrying the necessary payload, approximately 62,620lbs, and fly at the high altitudes required for this mission. At supersonic speeds, the aircraft would be able to withstand the harsh weather conditions present during the polar winter including the gusts up to 195 knots. A fleet of planes traveling supersonically will be able to deliver the propane over the entire 9 million square miles within the three week time frame. The remainder of this paper concentrates on the design of a cost effective, supersonic aircraft as well as the mission it must accomplish to complete the necessary deliveries.

5.0 Mission Definitions

The NASA/USRA Request for Proposals (RFP) requirements generated primary mission parameters for use in this study. These requirements were then used to define an initial mission, which has been refined and optimized throughout the study. A secondary mission is also currently being studied and designed to generate revenues for the vehicle concept as a commercial transport when not employed in propane delivery.

5.1 Mission and Aircraft Requirements

The Request for Proposals (RFP) for the NASA Advanced Design Project (ADP) generated various baseline parameters and selection criteria which were used in this study. The primary mission must be accomplished in a three week time window. Vehicle technology used for this study must be available in the next twelve years. The chosen concept should be able to accomplish an economically efficient, alternate purpose. The vehicle must be able to reach its base from the center of the polar vortex without tanker support (3,700 nmi). NO_x emissions released by the vehicle into the atmosphere should be kept to a minimum. Noise standards must be met and the vehicle must be able to be serviced and loaded with the propane payload in less than four hours. Table 5.1 shows the baseline aircraft and mission parameters.

Aircraft Parameters	
Cruise Mach	2.4
Cruise SFC	<=1.3
Cruise L/D	<=11
Payload	78000 lbs
Mission Parameters	
Range	6500 nmi
Curise Altitude	66000 ft
Refuelings	1
Cround Time	4hrs
Propane Payload	62620 lbs
Plume Radius	3228 ft
Aircraft Fleet Size	83

Table 5.1 Baseline Parameters
From: 1993/1994 NASA/USRA Design Report

5.2 Primary Mission

The primary mission for the vehicle concept, the delivery of propane into the polar vortex environment, is shown graphically in Figure 5.1. This mission is composed of two subsonic and two supersonic phases. The aircraft will takeoff from its base at an airport in South America and climb to Mach 0.9 and an altitude of 36,000 ft. The plane cruises for 900 nmi. at this flight condition. The plane then performs a rendezvous with a tanker and refuels; this refueling adds approximately 1,500 nmi. to the range of the aircraft. After refueling, the plane accelerates and climbs to M=2.4 at approximately 66,000 ft. The aircraft cruises at this speed back and forth through the polar vortex releasing propane continuously, and performs a 1.6g turn at each end of the vortex (see insert in Figure 5.1). The aircraft then returns to its base, cruising first at supersonic speeds, then cruising subsonically and finally decelerating and descending for landing. The longest distance through the vortex is approximately 2725 nmi. Only one pass through and back will be made at this section. As the aircraft fly further away from the center, more passes during a single operation may be made until the entire payload is released.

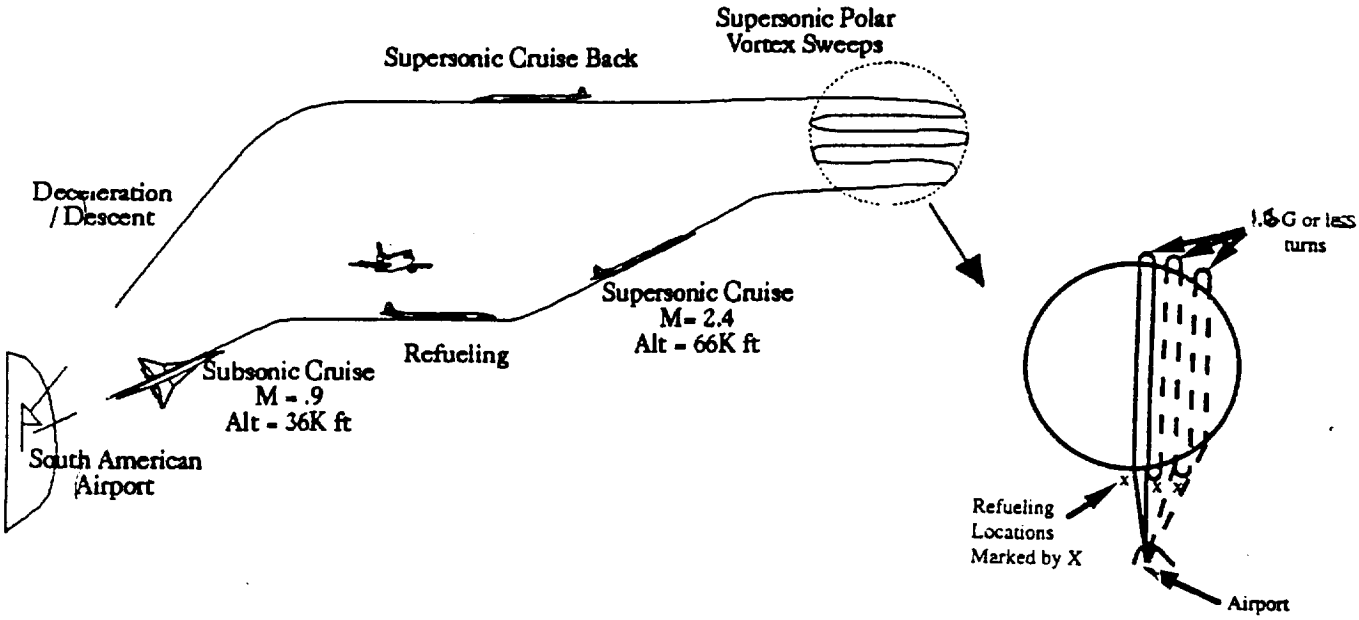

Figure 5.1
Polar Mission

5.3 Commercial Mission

The secondary, or commercial mission, is crucial to the feasibility of this design concept. The primary polar mission only spans three weeks of the year, leaving 49 weeks for the aircraft to earn revenue by fulfilling the commercial mission. The aircraft will carry approximately the equivalent weight of passenger/luggage load as the polar mission payload (propane and tankage), 76,162 lbs. This figure is equivalent to about 237 passengers and their baggage. This is the reason larger aircraft concepts were considered. The primary mission could be completed by a smaller supersonic plane, built specifically for the mission, but such an aircraft would have very limited alternative uses. A larger vehicle, however, can adequately fulfill a profitable commercial mission. The commercial mission itself is very similar to the primary mission, excluding the refueling leg, and substituting straight supersonic cruise for the polar vortex sweep phase. The vehicle concept unrefueled range is designed to be 5,500 nmi. in order to complete trans-pacific crossings.

5.4 ACSYNT Mission

ACSYNT is a multi-disciplinary design and analysis program developed by NASA that uses fundamental sizing and analysis methods along with a non-linear optimization method to perform multidisciplinary optimization (Myklebust, 27). Initially, the geometry of the vehicle concepts and an equivalent mission statement was input into ACSYNT. This mission statement differed slightly from the RFP required mission in that the refueling leg could not be modeled. The initial climb segments were modeled as four discontinuous climb phases up to 36000 ft. The aircraft flew in subsonic cruise, M = .9 and then accelerated and climbed to M = 2.4 at 66000ft. The turns at the ends of the polar vortex were modeled in ACSYNT as combat phases, in which the G loads are specified. The aircraft then returned to base in two legs, the first while continuing to fly at M=2.4, then decelerating and descending to cruise at M=.9 and about 30000 ft before final descent and landing. The commercial mission was modeled in ACSYNT in the same way, neglecting the "combat phase". These missions were connected to the various geometries and analyzed. The output from these runs was used to compare the vehicle concepts. Once the final concept had been chosen, the ACSYNT mission was further modified to more accurately model the propulsion system.

Two ACSYNT files had to be used to model the chosen variable bypass ratio propulsion system because, as yet, ACSYNT does not model such an engine; the first file optimized the engine for the turn in the polar vortex using a low bypass ratio engine and the second file sized the engine at takeoff using higher bypass ratio engines. The file that sized the engine at takeoff was used to determine the weights and performance criteria for the concept, excluding the weight of the fuel used in the 1.6g turn, which was calculated separately. This file was used because, excluding the turn segment, this file more accurately modeled the aircraft at takeoff and cruise. ACSYNT was also further utilized to optimize and refine the final concept and mission altitudes and speeds.

6. Concept Selection

6.1 Technologies

Three major areas were studied where emerging technologies could make the Aeolus High Speed Civil Transport concept both more economically feasible and safe. These areas, which will be further discussed in later chapters, were :

- Materials
- Propulsion
- Aircraft Systems

Technological improvements in these areas are occurring rapidly thus these new technologies are expected to be commonly used in future high performance aircraft designs. For this reason, the added cost of research, development, and incorporation of these emerging technologies into the Aeolus concept is expected to be minimal.

Materials

Newly developed composites and advanced metals were incorporated into a large percent of the Aeolus concept to reduce the weight of the aircraft while maintaining high structural strength. These materials include: titanium for the leading edges of the wings, fuselage, and tail; graphite for the longerons, frames, spars, ribs, and midchord surfaces of the fuselage and wing; and kevlar for the trailing edges and inner decks. The bulkheads were chosen to be made of a honeycomb composite with metal inserts where concentrated loads enter the bulkheads. Without these metals inserts, the honeycomb structure could deform or tear. According to analysis using ACSYNT, the use of composites in a large percentage of the aircraft components reduced the weight of the aircraft by almost 25%.

Propulsion

The primary mission of the Aeolus concept centered on the reduction of the ozone hole; therefore the propulsion system used by the Aeolus needed to environmentally safe with low NOx emissions. For

this reason and for its supersonic and subsonic capabilities, a new Rolls-Royce mid-tandem turbofan concept was chosen for its lower emissions and high levels of technological advancement.

Aircraft Systems

A fly-by-light system was chosen as the flight control package for the Aeolus concept. Although this technology is currently being perfected and is more expensive, it is expected to be fully developed, employed in other vehicles, and less costly by the onset of production of the Aeolus. A multi-purpose viewing screen will be employed to convey trajectory and flight control information to the crew. This screen will also act as a virtual reality viewing screen that displays computer generated images of crucial areas outside the aircraft. The virtual reality view screen eliminates the need for a droop nose at landing and takeoff.

6.2 Supersonic Transports: Current Capabilities

A comparator aircraft study was conducted to determine the current capabilities of the world's supersonic aircraft fleet. Comparator aircraft were selected according to their speed, payload capacity, and range. Table 6.1 shows a cross section of the capabilities of the comparator aircraft studied.

	Concorde	[illegible]	[illegible]	Boeing 2707 SST (unbuilt)
Cruise Mach	2.04	1.9	2.0	2.7
Range (nmi)	3,360	3,500	6,475	4,000
Payload (lbs)	28,000	33,000	64,000	72,400

Table 6.1
Comparator Aircraft
From: 1993/1994 NASA / USRA Design Report

These aircraft were used as comparisons throughout the study, but none were chosen to be modified for this mission for various reasons. None of the above aircraft met all of the requirements (required payload capacity, range, and speed) necessary to accomplish the mission in the polar vortex gust

environment and neither did they contain any of the technologies that have emerged since their production that had the potential to cut both the weight and operating costs.

6.3 Initial Concept Exploration

In September 1994, each team member set out to modify or create an aircraft that could fulfill the mission set out in the NASA RFP. These individual efforts produced seven preliminary designs that were examined for their potential to solve the problem. These seven designs were narrowed to four initial concepts based upon their potential speed and payload capacity using research on current High Speed Civil Transport (HSCT) vehicles. Of these four initial concepts, shown in Figure 5.1, two are currently being researched in the HSCT community. These were (a) canard concept, which is currently being studied by the European HSCT community (Poisson-Quinton, pg. 38) and (b) a horizontal tail concept, currently being studied by NASA. The third initial concept chosen was (c) a delta wing planform and the fourth concept was the (d) 1993/1994 Va Tech / USRA tailless, straked delta HSCT concept. Each concept was then evaluated on the basis of takeoff gross weight (TOGW), performance, economic feasibility, and ability to meet the mission requirements.

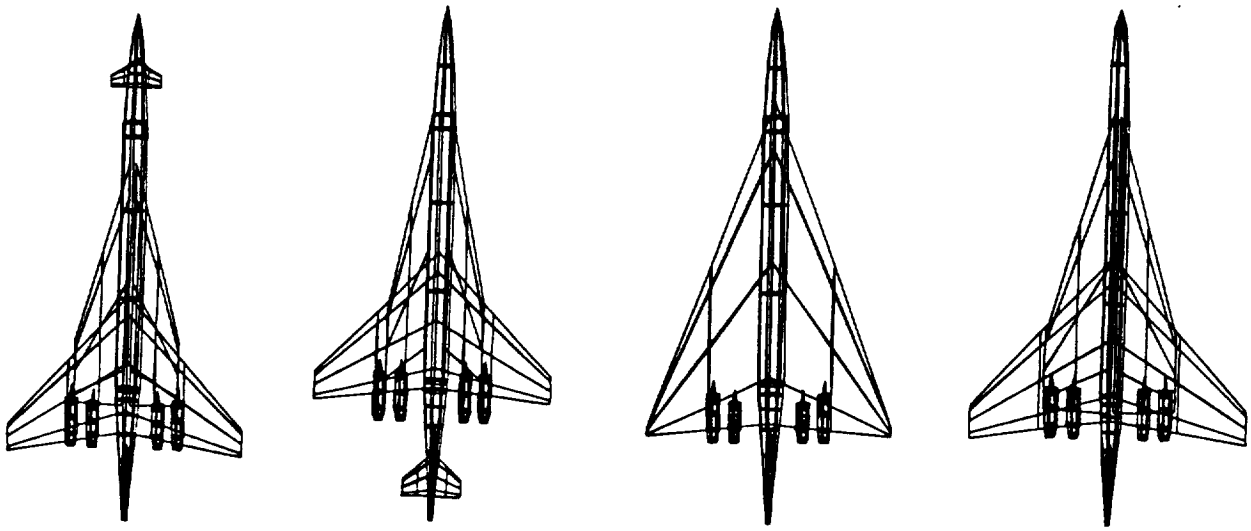

(a) (b) (c) (d)

Figure 6.1
Four Initial Concepts

6.4 Concept Evaluation

Initial Analysis Methods

The four concepts were investigated using ACSYNT and various FORTRAN sizing codes to see if they were feasible designs. The concepts were modeled in ACSYNT using 3-D geometric methods. The aircraft components for each concept were chosen and sized by the designer using interactive graphics. The results from the 1993/1994 design concept optimization were compared to preliminary ACSYNT results of the three other concepts, which were updated and optimized in ACSYNT throughout the initial design process.

Initial Aircraft Sizing

The initial size of the concepts was determined not by the primary mission of propane delivery to the polar vortex, but instead by the secondary commercial mission. A smaller plane with an adequate payload capacity such as the Dedicated Aircraft studied in the 1993/1994 USRA ADP Design Report (see Figure 6.2) would have been able to accomplish the propane mission, however it would not be able to carry enough passengers to be economically feasible as a transport. The initial size of the Aeolus (length = 300 ft.) was therefore determined by passenger load capabilities.

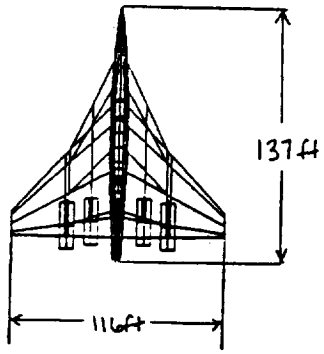

Dedicated
Aircraft

Figure 6.2
1993/1994 NASA USRA Dedicated Aircraft

Comparator aircraft studies and ACSYNT analysis were used to locate the center of gravity (cg) on the vehicle concepts. It was estimated to be approximately 61% of the fuselage length for the 1993/1994 version, slightly forward for the canard version and further back for the horizontal tail version due to the weight of the added surfaces. Preliminary landing gear placements were located with respect to the estimated CG to allow rotation on takeoff. Retracted stowage areas were then estimated to determine if each concept could retract and stow its landing gear. Once it was determined that each concept was viable, further analysis with respect to aerodynamic, structural, and stability and control was conducted in ACSYNT and numerical routines to differentiate the concepts.

Concept Performance

ACSYNT was utilized to assess the basic performance capabilities of the initial four concepts. The ACSYNT data, presented in Table 6.2, along with comparative aircraft studies and numerical analysis a sizing code and ACSYNT, was used to differentiate the initial concepts. Due to its excessive TOGW and the unrealistic ACSYNT results, the delta concept analysis was disregarded.

	Canard	Horizontal Tail	1993 USCT (Data from 1993/1994 NASA ADP Report)	Delta
Maximum TOGW, lbs.	604711	700060	709910	989714
Wing Loading, lbs/ft	95.3	110.3	86	37.6
Thrust to Weight T/W	.53	.31	.35	.30
Takeoff Field Length, ft	5558.1	8765	6217	5323.5
Supersonic Cruise L/D	9.1	8.8	11.13	10.02
Fuel Used, lbs.	385687	378821	374743	273137

Table 6.2
ACSYNT Concept Performance Comparison
(Commercial 5500 nmi Mission)

Canard Concept

The canard version was based on the HSCT concept currently being studied by the European HSCT community. (Poisson-Quinton, pg. 40) It had a wing span of 138 ft, wing area of 9950 sq. ft (including the highly swept strakes), a fuselage length of 300 ft, and a maximum fuselage diameter of 12 ft. The wing sweep for this concept was 47 degrees and the strakes were swept 79 degrees. The concept had an aspect ratio of 3. The canard has a planform area of 477.5 ft, approximately 5% of the total wing area, as optimized by ACSYNT. As shown in the above table, the T/W ratio is quite high. This excess thrust is necessary at takeoff so the Aeolus has adequate thrust at altitude to execute the 1.6g turn. The canard concept also fulfilled the required aircraft parameter of L/D <= 11, having a supersonic cruise L/D of 9.1.

Horizontal Tail Concept

The horizontal tail concept used the same fuselage and basic wing planform as the canard concept, except the strake and wing were located further forward along the fuselage. The horizontal tail had a plan area of almost 600 sq. ft. As shown in the table above, the wing loading for this concept was higher than that of the canard concept. The TOGW was approximately 100,000 lbs heavier and the T/W ratio was significantly lower than the canard concept. This concept was eliminated because of the added weight of the horizontal tail and its possible interference with other components of the plane as the tailcone was swung 90^{o} to allow for the loading of the propane tankage assembly into the fuselage.

Delta Wing Concept

The last new preliminary concept utilized a delta wing planform. This highly swept delta wing had a very large wing area, twice that of the other concepts, and, as shown in Table 6.2, a high TOGW. This resulted in reduced thrust to weight ratios and excessive drag. Even while operating with the largest achievable thrust at altitude, the increase in weight of this aircraft concept reduced its ability to execute the 1.6g turn at the edge of the polar vortex . These reasons caused this design to be eliminated as a feasible concept.

1993 HSCT Concept

The 1993 HSCT concept was the aircraft chosen by the 1993/1994 Va.Tech NASA/USRA design team to perform the mission required in the RFP. This aircraft concept was a straked delta with a wing span of 150 ft, a wing area of 8250 sq. ft. and a fuselage length of 284 ft. It used no horizontal surfaces such as a canard or horizontal tail for longitudinal control. Although the 1993 NASA ADP HSCT was a competitive concept capable of accomplishing the required mission, Table 6.2 shows that it had a larger TOGW, higher supersonic L/D ratio and significantly lower T/W ratio than the canard concept. For these reasons, this concept was eliminated.

6.5 Internal Configuration

Commercial Mission Version

In order to be economically feasible, the Aeolus concept had to have a passenger capacity greater than 220 people. This passenger capacity corresponds to the weight of the propane payload required in the primary mission. The passenger layout was divided into first and economy class sections. The first class cabin, shown in Figure 6.3a, consisted of eight rows of four seats each, two seats either side of a central aisle. A galley and restroom were placed at the front of this section. This forward placement was necessary so the restroom and galley could remain in place for use by the propane discharge crews during the primary mission, when the passenger seats and mid and aft located restrooms and galleys must be removed. The larger economy cabin, shown in Figure 6.3b, consisted of 41 rows of five seats each, two seats on one side of the aisle, three seats on the other side.

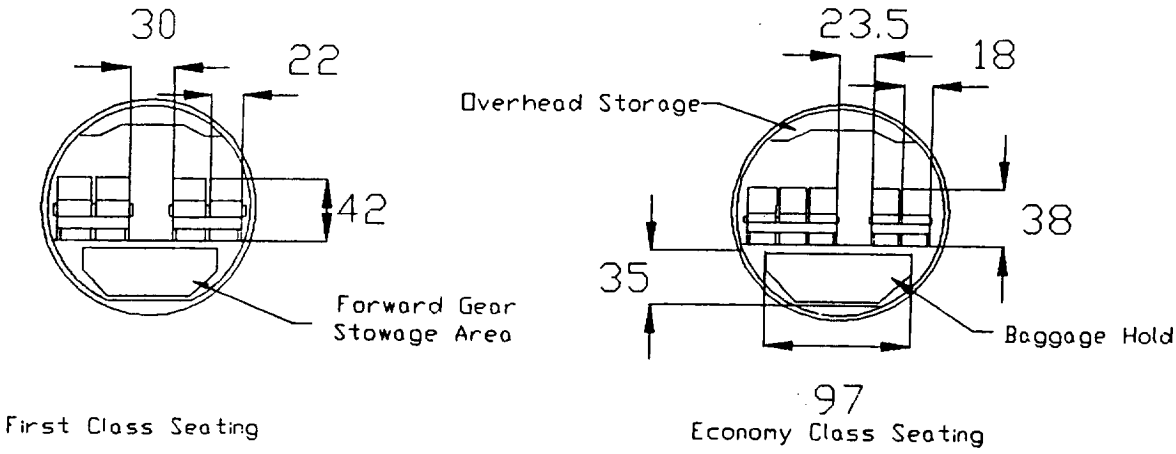

Figure 6.3a and 6.3b
First Class and Economy Class Seating

Two galleys were located in the economy section, one at the rear of the first group of seats, and one at the rear of the aircraft. Four restrooms were also placed in the economy section, one across from the forward galley, and three at the rear. The seat sizes, spacing and arrangements proposed for each section were standard for transport aircraft. (Torenbeek, pg. 75) Overhead storage compartments and cargo holds were also included in the design of the fuselage sections. The complete top view of the passenger version of the Aeolus showing its mixed class seating is shown in Figure 6.4.

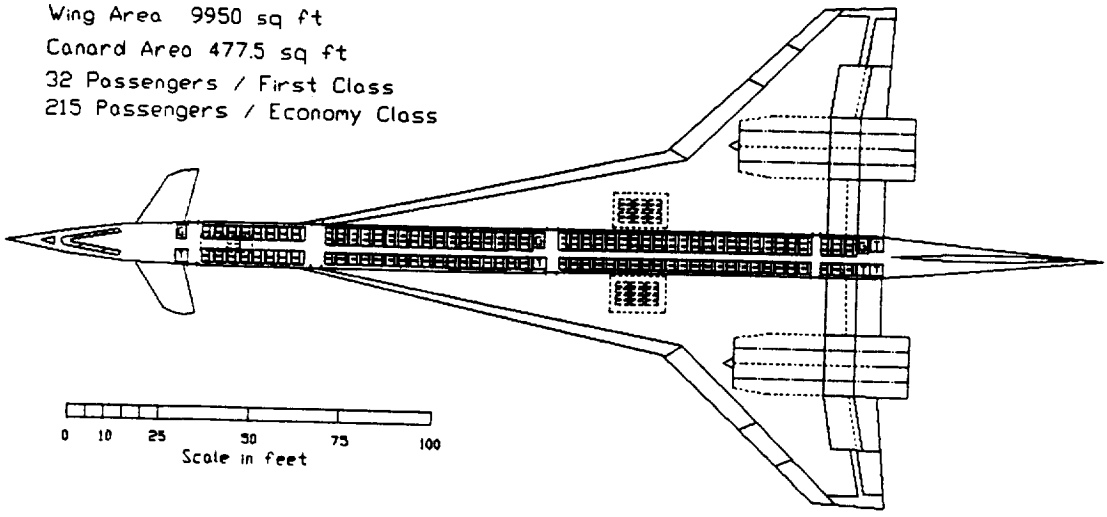

Figure 6.4
Overhead View of the Passenger Version of the Aeolus Concept

Propane Mission Version

The Aeolus' primary mission is to distribute propane into the polar vortex environment to reduce the destruction of ozone in the ozone layer. All passenger amenities except the forward restroom and galley are removed for this mission to reduce the aircraft weight and allow room for the insertion of the propane tank packs. The propane is stored in nine tanks each with a radius of 1.64 ft. The tanks are grouped in pyramids of three tanks that are loaded as an integrated pack through the rear of the aircraft via the swinging tailcone of the aircraft. The cg of the propane tankage system is located at the aircraft's center of gravity. A cross-sectional view of the propane storage system is shown in Figure 6.5 and a top view of the propane version of the aircraft can be seen in Figure 6.6.

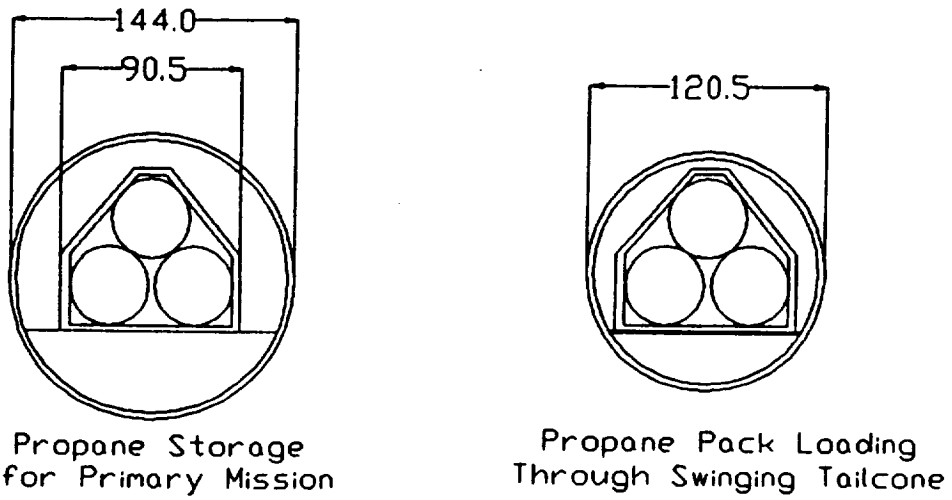

Figure 6.5
Propane Delivery System

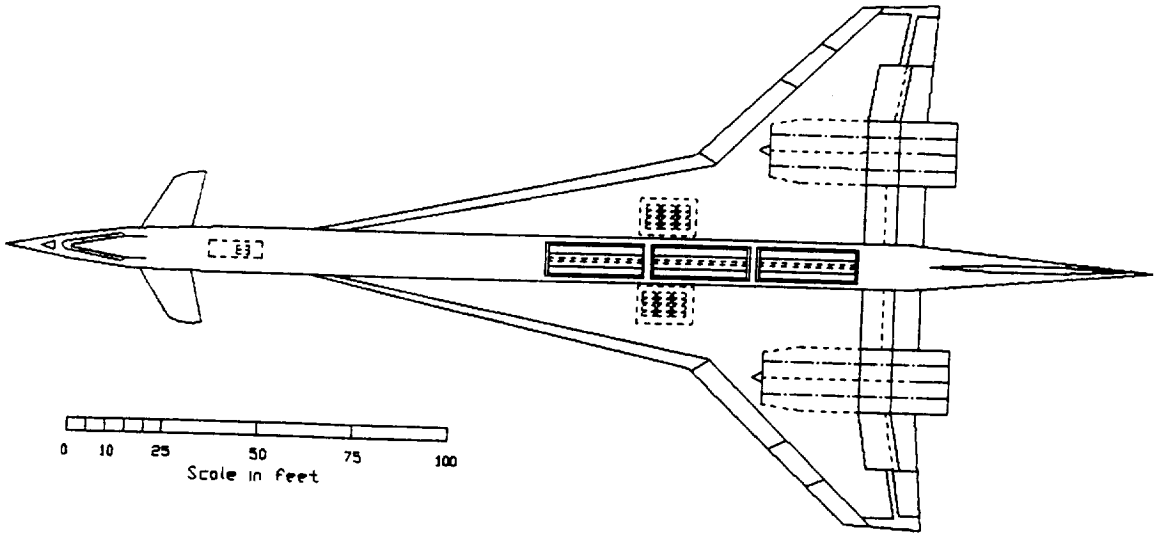

Figure 6.6
Overhead View of the Propane Version of the Aeolus Concept

7.0 AERODYNAMICS

In consideration of the aerodynamics of Aeolus, the cruise conditions of supersonic as well as subsonic speeds are the most important. The cruise mach numbers of interest are Mach 2.4 and Mach 0.9, which are the cruise mach numbers for the propane delivery mission. The aerodynamics involved in these two cruise conditions are widely different and must be examined separately. While the subsonic 0.9 Mach number is normally considered in the transonic range, the highly swept and extremely thin wing of Aeolus delays the response of the drag rise due to compressibility. Therefore, the Aeolus exhibits little transonic effects. The supersonic cruise conditions are a more complex problem and require the aid and insight of complex aerodynamic codes. This chapter will describe : supersonic wing design, supersonic lift due to drag, cruise drag, friction and wave drag, subsonic aerodynamic concerns, and takeoff and landing aerodynamic performance for the Aeolus.

7.1 Supersonic Wing Design

The design of a supersonic wing is an entirely different process than designing a conventional subsonic wing. The goal is to distribute the load over the wing chordwise as well as the span, so supersonic wings are highly swept. The straked foremost section of the wing, is the higher swept portion. This accomplishes the load distribution as mentioned above, and also serves to generate leading edge vortices, which provide a large percentage of lift at takeoff and landing.

The design goals for the Aeolus were primarily for a wing which exhibits the lowest possible supersonic drag, as well as minimum trim drag. With an aircraft which cruises the majority of its flight supersonically, the supersonic aerodynamic demands outweigh the subsonic aspects. The planform area was initially sized with a cruise lift coefficient estimate of 0.1. This analysis coupled with thrust to weight considerations at takeoff and cruise set constraints on the wing loading. A chart illustrating these constraints can be seen in later in Figure 8.5. A lift coefficient of 0.10 was also used in the design of the wing. Advanced supersonic wings have subsonic inboard leading edges. A subsonic leading edge dictates

that the leading edge of the wing sees a Mach number normal to the surface that is less than one. This allows for leading edge design to obtain a high leading edge suction.

The suction on the leading edge of the wing is an important design factor as well. Leading edge suction is due to the acceleration of the flow around the leading edge of the wing, which produces a force called leading edge thrust which acts in the opposing direction of drag. (Figure 7.1)

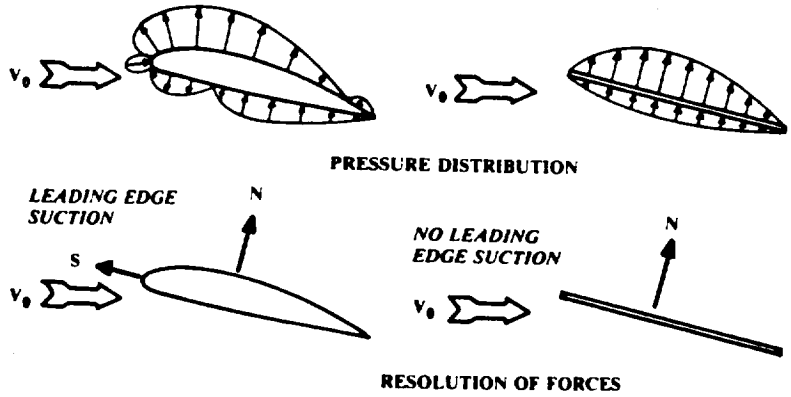

Figure 7.1
Leading edge suction definition
(taken from Raymer, *Aircraft Design: A Conceptual Apporach*, pg.298)

If this leading edge force is utilized, the supersonic drag due to lift can be reduced, and at supersonic speeds every drag count saved is a great deal of fuel, and consequently money saved. At supersonic cruise each drag count translates to 455 pounds of thrust and an increment of 0.165 pounds per second of fuel usage. If the entire flight is considered, the TOGW of the aircraft increases dramatically with each additional drag count. This increased drag idea is shown for various planforms in Figure 7.2. The planforms are plotted versus the drag for both no leading edge suction and full leading edge suction values. Corresponding planforms on both charts show an overall decrease in drag. A computer panel code called WingDes was utilized to design the wing for optimum leading edge thrust. The code takes a basic input of the planfrom geometry and design force coefficients, and iteratives to produce an optimized leading edge as well as wing

camber. The program outputs leading edge suction coefficients for varied angle of attacks. The suction coefficient for the design lift coefficient of 0.1 was obtained this way.

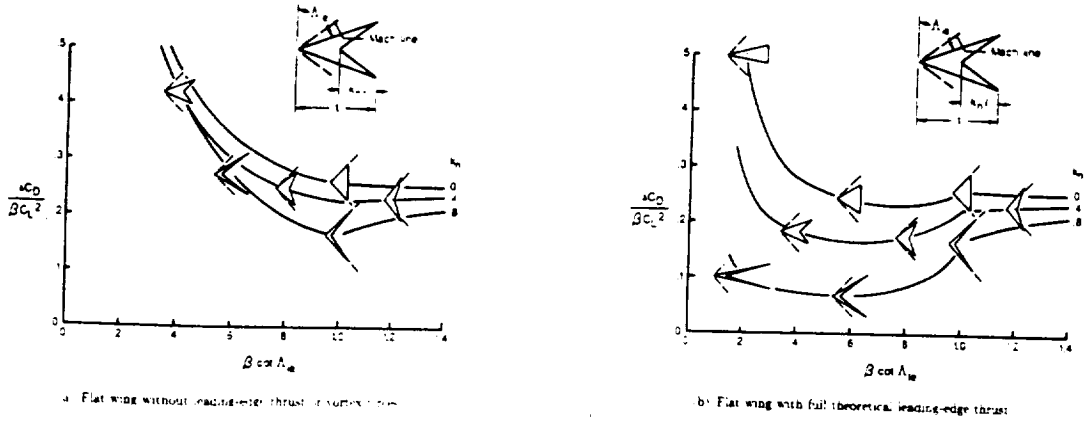

Figure 7.2
Effect of leading edge suction on Drag
(taken from Carlson, Mann pg.65)

The drag coefficients out of WingDes are computed with respect to an input of the center of gravity location. This allows for the design of trim drag with respect to the static margin. Figure 7.3 shows the supersonic drag due to lift as a function of static margin(supersonic). The minimum drag appears when the static margin is about 0.03 - 0.02. As the graph shows, this is for a supersonic nuetral point of 192 feet back from the nose tip. This demonstrates Aeolus is obtaining close to maximum trim drag efficiency from its wing at cruise conditions. In actual cruise conditions the C.G. location as well as the stability of the aircraft are augmented through in flight control systems.

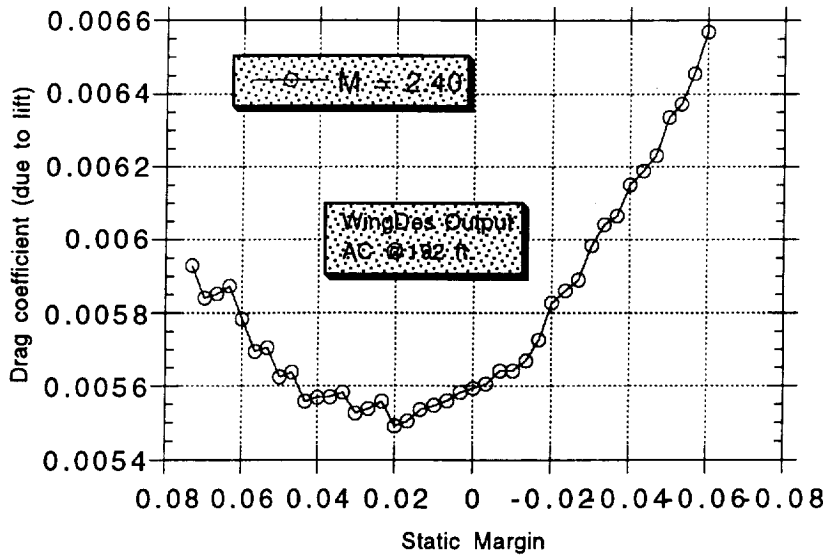

Figure 7.3
Static Margin vs. Drag due to lift

7.2 Friction and Wave Drag

Low friction and wave drag are essential to a successful design. These components make up 49% of total drag at supersonic cruise conditions. Subsonically, they comprise 52% of the total drag. Friction drag can be reduced through maintaining a very smooth skin on the surface of the aircraft and also by laminar flow technologies. It is anticipated that the Aeolus would require the use of these technologies if it were to go into production. This is based on the assumption that high Reynolds number flows could be economically controlled by laminar flow technology. As it stands presently, the technology would place too high a burden on this already expensive project. By the year of actual production, the tecnologies would hopefully be more feasible due to economic factors and growing technology in the area. If the technology would successfully reduce turbulence as much as 25%, Aeolus would see a great weight savings in fuel due to the lower skin friction drag. For the Aeolus concept, program FRICTION was utilized to calculate the

friction and form drag for the subsonic and supersonic cruise conditions. The flow was assumed to be fully turbulent. Friction and form drag components are shown in Table 7.1.

	Geometry		Subsonic cruise (M = 0.90)				Supersonic cruise (M = 2.40)			
Component	Swet (sq ft)	Length (ft)	Re x10^9	C_{fric}	$C_{D}S_w$	C_{Dfm}	Re (sq ft)	C_{fric}	$C_{D}S_w$	C_{Dfm}
Fuselage	8132	300	.852 E+09	.00146	11.903	-	0.398 E+09	.00121	9.842	-
Wing	6120	50	0.392 E+09	.00162	11.350	-	0.183 E+09	.00135	15.054	-
Nacelle	11152	138	0.142 E+09	.00185	18.032	-	0.663 E+08	.00157	9.608	-
Vertical Tail	569	36	0.102 E+08	.00206	1.105	-	0.318 E+08	.00176	0.955	-
Canard	513	24	0.681 E+09	.00194	1.057	-	0.477 E+08	.00165	0.991	-
Total	26488			.00893	43.45	.00014		.00754	36.35	.00012

- form drag values not specified for individual components

Sub: $C_{Dfriction}$ = 0.00437; C_{Dform} = 0.00014 Sup: $C_{Dfriction}$ = 0.00365; C_{Dform} = 0.00012

Table 7.1

For supersonic flight conditions it is necessary to keep wave drag to a minimum. Wave drag is pressure drag due to shocks, and is a direct result of the way in which the aircraft's volume is distributed. (Raymer 228) To keep this component of drag to a minimum, the wing and fuselage must be kept very thin. The wing's maximum thickness to chord ratio is 2.5 %, while the fuselage is 4% thick. The ideal volume distribution for minimum wave drag is that of a Sears-Haack body which is shown in Figure 7.4. The next step in wave drag reduction would be to area rule the fuselage so that the cross sectional area plot for Aeolus resembles the smooth curve of the Sears-Haack body cross sectional area distribution. Aeolus' wave drag was estimated using APAS. This program was also used in determination of the supersonic stability derivatives, and will be described in more detail later. The results show that at Mach 2.40 cruise,

the wave drag coefficient is 0.002042. While Aeolus has the thrust required to overcome this value of wave drag, the production of Aeolus would require an area ruling to further reduce this value.

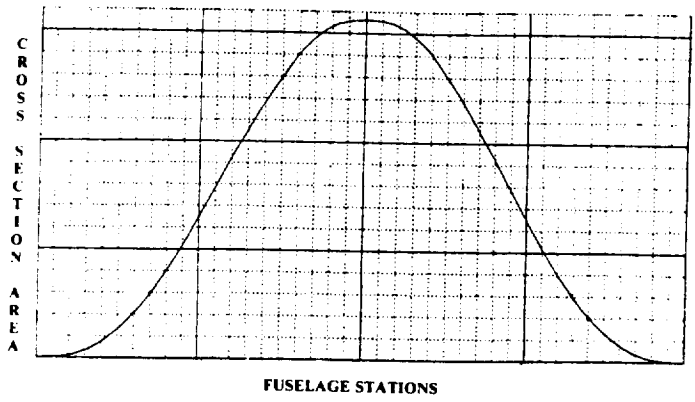

Figure 7.4
Sears-Haack Volume Distribution
(taken from Raymer pg. 157)

7.3 Supersonic and Subsonic Cruise

The Aeolus is to be extensively used as a transport when not dispersing propane to the polar region. In either case, cruise is the primary flight condition. With the exception of a 1.6 - g turn high angle of attack, and strong G maneuvers will not need further aerodynamic consideration. In cruise it is desired to determine the amount of drag encountered to figure out how much thrust is needed. All components of the drag at mach 2.4, and mach 0.9 cruise have been determined, friction & form, wave, and drag due to lift. To determine the drag encountered for the cruise lift coefficient, the drag polar must be constructed. The drag polar takes the form:

$$C_D = C_{D0} + KC_L^2$$

The "K" factor differs between the supersonic case and the subsonic case. For the subsonic case, "K" is the inverse of the aspect ratio multiplied by pi assuming 100% leading edge suction. For Aeolus, WingDes would not output any subsonic data, so a leading edge suction of 100% was assumed. Since the thrust required at subsonic cruise is significantly lower than the allowable thrust, this assumption does not effect the actual design at all. It may, however, cause the drag estimates at subsonic cruise to be overly

optimistic, resulting in more fuel burned in subsonic flight. Since Aeolus has a surplus of fuel storage volume, this assumption is not considered dangerous to the design. For the supersonic case, the K factor is more dependent on the leading edge suction percentage. Figure 7.5 shows this relation. Figure 7.6 shows the drag polars for different values of leading edge suction to show its influence on overall drag. The leading edge suction coefficient was an output of the WingDes code. It was found to be 12%, the corresponding value for a lift coefficient of 0.1. The K factor for 12% leading edge suction is 0.353 which was used in constructing the supersonic drag polar.

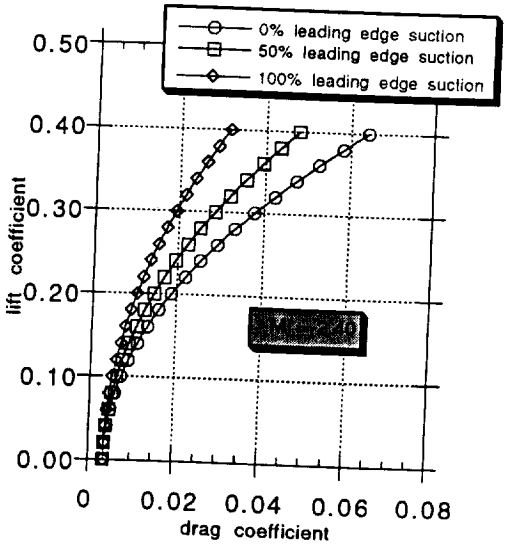

Figure 7.5
Drag polar comparison of
varying leading edge suction values

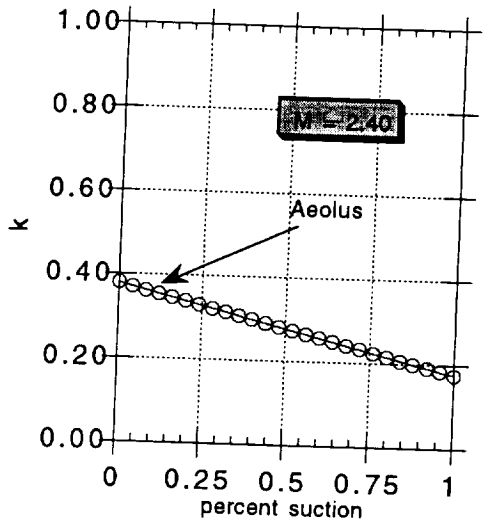

Figure 7.6
K vs. leading edge suction %

Now, the drag polar can be constructed. They were constructed so that the subsonic and supersonic cruise conditions were demonstrated. They appear on the same plot in Figure 7.7 below.

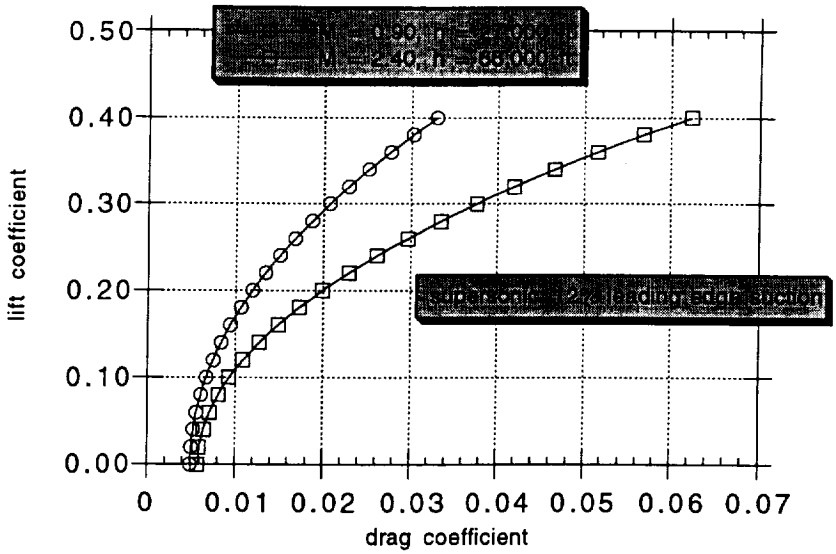

Figure 7.7
Drag polars for Aeolus

Utilizing these drag polars, the thrust required at both cruise conditions can be found. For the supersonic case, the drag coefficient corresponding to the actual lift coefficient(not the design lift coefficient) of 0.13 is 117.8 counts. This translates to a thrust required of 54,000 pounds with a L/D of 9.17. For the subsonic case, the drag coefficient is 94.2 counts with thrust required of 35,800 pounds and a L/D of 16.9. These drag polars were further used in the performance analysis of Aeolus, especially in the 1.6 - g turn.

7.4 Takeoff and Landing

Achieving the necessary lift at takeoff for a supersonic transport is very different aerodynamically from a conventional subsonic aircraft. The potential component of lift is not as great, due to the low $C_{L\alpha}$ of the thin, highly swept wing. At Aeolus' takeoff angle of attack of 10 degrees this component of lift is only approximately half the required lift needed for takeoff. High lift devices, such as flaps give an increment of lift coefficient of about 0.2 - 0.3.(N. Kirschbaum) In this case Aeolus expects to get about 0.2 lift increment out of trailing edge flaps. Since the lift coefficient needed by Aeolus to takeoff at a velocity of 145 knots is about 0.85, the difference will be made up through vortex lift and ground effect.

From wind tunnel testing, it has been determined that the Concorde gets about 30% of its lift at takeoff from vortex lift.(ONERA) Vortices are generated by the highly swept strakes and produce a low pressure region above the wing. At increasing angles of attack, these vortices get stronger, and the pressure in the regions above the wings decrease accordingly. These low pressure regions create the extra "vortex" lift. Without it, the Aeolus would not leave the ground. This increment in lift is shown in Figure 7.8.

Figure 7.8 shows only the vortex and flap increments of lift. These are for the takeoff configuration, but can be scaled down to create the same percentage of contribution at landing since Aeolus will require a smaller lift coefficient. Figure 7.8 also neglects the contribution of ground effect as it has been shown not to vary significantly with angle of attack.

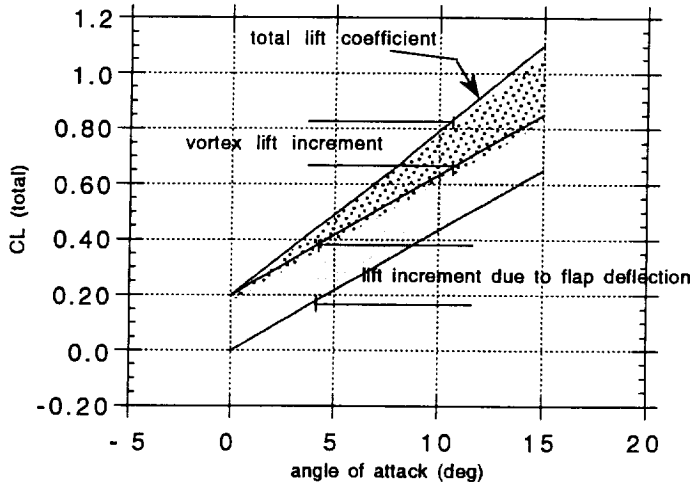

Figure 7.8
Takeoff lift w/flaps and vortex contributions

Ground effect has been shown to be quite favorable for thin wings, however, no methods can accurately predict the ground effect on highly swept wings. Therefore, the ground effect for the Aeolus was calculated using an interpolation curve which utilizes Gersten's theory and Kirkpatrik's theory. (Kuchemann) Figure 7.9 shows the components of lift at takeoff for a constant angle of attack of 10 degrees.

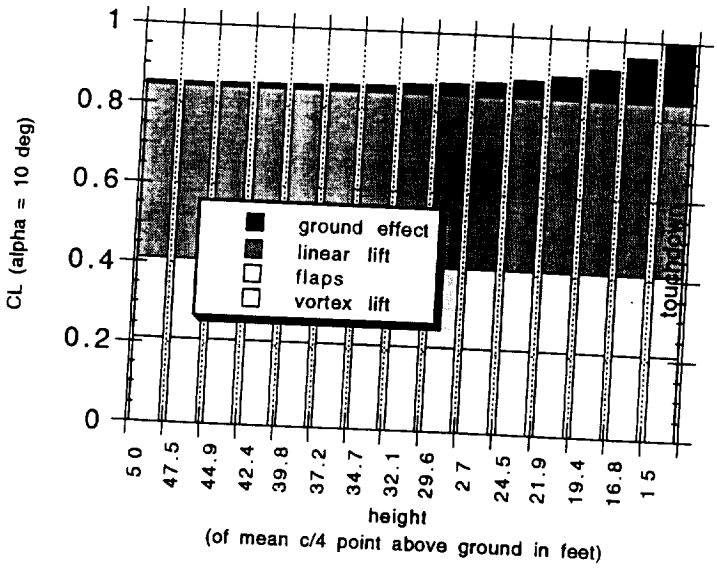

Figure 7.9
Lift coefficient generated vs. height above ground

As shown by the plot in Figure 7.9, the increment in lift due to ground effect is very favorable. At the point where Aeolus touches down, it is receiving approximately 15% of its lift from ground effect. In tests done on the Concorde, this effect has also shown to increase damping on roll and pitch during landing. This creates less dependance on active controls to land the aircraft. (Sforza, *Space/Aeronautics,*)

8.0 PERFORMANCE

Many of the performance requirements of the Aeolus were discussed in previous chapters. These requirements demonstrated the need for an aircraft capable of excellent supersonic as well as subsonic performance characteristics. The Aeolus is required to have a range of 5500 nmi, cruise at Mach 2.4, and fly at an altitude around 66,000 feet. To disburse the propane correctly, Aeolus must fly at an altitude as low as 50,000 feet in order to disburse the propane at the lower levels of the vortex. These are the baseline parameters. To illustrate Aeolus' capability to fulfill the RFP requirements the following parameters will be examined: subsonic cruise conditions and range, supersonic range, turning performance, takeoff and landing capabilities, and wing loading vs. thrust to weight constraints. Specifically, the turning capability is examined in response to the requirement for Aeolus to execute a "2-G" turn or less, so as to fly back through the polar region before returning to base. This chapter will detail this turn, and how Aeolus will execute it.

8.1 Supersonic Cruise

The largest factor in the design of the Aeolus was its requirement to cruise at Mach 2.4. As described in the mission outline in chapter 5, the aircraft is required to deliver 62,620 lbs of propane per mission to achieve the required concentration of propane in the polar atmosphere. This can only be accomplished in a feasible manner by using a large fleet of supersonic aircraft. A high speed of Mach 2.4 reduces the mission time significantly, enabling fewer planes to deliver the necessary amount of propane. The high velocity also allows the aircraft to resist large wind gusts produced by the volatile polar vortex environment.

The cruise requirments of Aeolus are a Mach number of 2.4 and an altitude of 66,000 feet. This is a restraint placed on the design which is specific to the mission. It has been determined through analysis of the molecular distribution in the polar atmosphere that the altitudes needed to release the propane at 50,000 feet at the lowest and 66,000 feet at the highest. These altitudes take into account the changing plume radii of the propane. In this chapter, the reference cruise condition will be Mach 2.4 at 66,000 feet. The range at

these conditions must be sufficient to complete the release of propane and guarantee a safe return back to the nearest airport form any point in the mission.

The required lift coefficient for the propane delivery mission is 0.133 assuming TOGW. This lift coefficient accounts for the refueling of the aircraft before its supersonic leg of the mission. It represents the maximum lift coefficient which will be required for Mach 2.4 cruise. Therefore, the average needed cruise C_L will be lower, about 0.1. Correspondingly, the lift to drag ratio for the supersonic leg is 9.17. The total thrust required is 54,000 lbs. From this thrust required, and an assumed constant SFC of 1.3, the fuel needed to make one pass through the vortex is 130,500 lbs. This figure is based on a flying distance of 1,360 nautical miles. The Aeolus is capable of carrying 425,000 lbs of fuel, which is more than sufficient for this mission. In addition, the mission where the aircraft is required to fly 2720 nautical miles (through and back) represents the maximum flying distance required for propane distribution, as this is a flight through the widest part of the vortex. A table summarizing the supersonic performance characteristics is shown below.

Supersonic Performance for Aeolus				
C_L	L/D	thrust req. (lbs)	fuel req. (lbs) (for 1360 nmi flt.)	sp. range (nmi/lbf)
0.133	9.17	54,000	130,500	0.01042

Table 8.1
Supersonic performance parameters

8.2 Subsonic Cruise

There were not as many requirements restricting the subsonic cruise case. The need to cruise subsonically lies in the requirement to refuel for the polar vortex mission. The refueling is to take place at an altitude of 38,000 feet at a mach number of 0.8, due to KC-10 requirements. After refueling the climb to 66,000 feet and mach 2.4 is made. The range over which the Aeolus will be cruising subsonically is the

distance from the airport to the refueling rendezvous point with the tanker. This distance is approximately 900 nautical miles. Due to this relatively small distance, the altitude for best specific range will be the desired cruise altitude. Since the subsonic cruise leg of the mission with the exception of transporting the propane to the area of interest, is useless, it is of course desirable to cruise for the best fuel usage.

To determine the best specific range, the optimum cruise altitude (C_L) also have to be considered. The best C_L for cruise will occur at approximately the value of maximum lift to drag ratio. A plot showing this relation for the Aeolus at a mach number of 0.9 is shown in Figure 8. 1. This plot is for an altitude of 27,000 feet, which as Figure 8.2 shows is the altitude at best specific range. The graph shows that the cruise C_L desired for cruise is about 0.16 , corresponding to a L/D of 16.9.

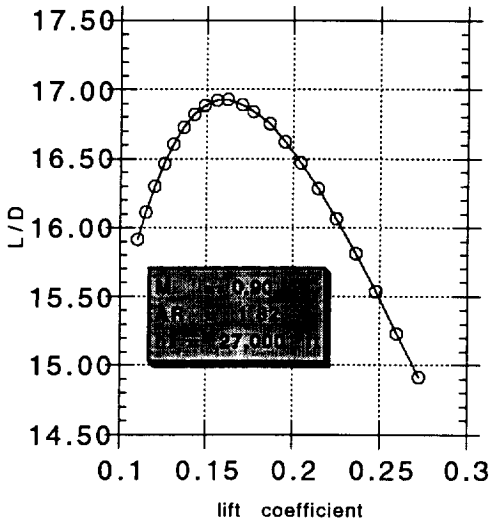

Figure 8.1
Cruise C_L vs. L/D

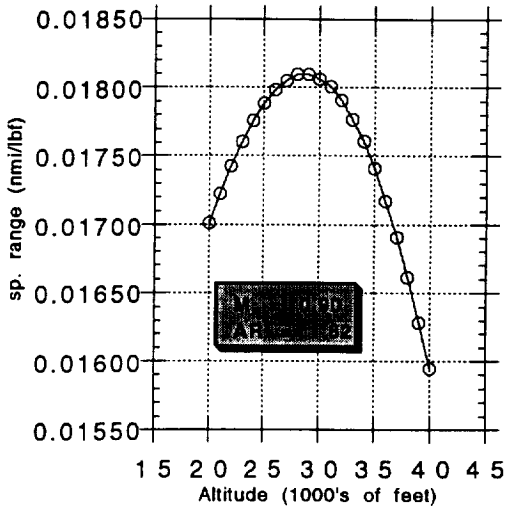

Figure 8.2
Specific range vs. Altitude

As stated above, the best cruise altitude with respect to specific range is about 27,000 feet as shown in Figure 8.2 above. The specific range at this altitude gives the fuel used for a 900 nautical mile flight of about 50,000 pounds. This amount does not include fuel consumed during takeoff and climb to altitude, just the Mach 0.9 cruise at 27,000 feet. At the end of this subsonic leg, the Aeolus would then climb to 38,000 feet and Mach 0.8 to refuel, and then climb to supersonic cruise and altitude.

8.3 Supersonic Turning Capabilities

The mission of disbursing the propane requires the aircraft to make a 180 degree turn after flying through the polar region to fly back through distributing the remaining propane. The turn was originally assumed to be a 2-g turn, however, this required too much thrust. Therefore the selection of a turn which can be executed by Aeolus must be examined from the aerodynamic, propulsive, and performance point of view. Another criteria for selecting the turn is that it is desired to have the minimum radius possible in order to maintain an even distribution of propane without any gaps in concentration. To keep the choreography of the required mission as simple as possible, this turn would enable the aircraft to sweep back through the vortex covering the area with propane evenly; starting where the previous pass left off, such as the sweeping action of mowing the lawn. So, the turn is to have the smallest radius possible, but yet lie within the limits of the thrust available at 66,000 feet. These are the criteria with which the turn was analyzed.

The turn as stated above is to be of as high a load as possible. The limiting factor is the engine weight. As the propulsion chapter will discuss later for each pound of engine weight added, the TOGW increases dramatically. Therefore, the constraint of available thrust became the turning constraint as well. In the preliminary analysis of this turn, a 2-g load factor was examined. The thrust required for this maneuver is way over the available thrust of 100,000 pounds at around 140,000 pounds. A 1.5 - g turn was also examined and produced a thrust required of about 90,000 pounds. To determine the actual value of the load of the turn the fuel used in turn was plotted against the load factor. The thrust required was also plotted against the load factor. The turn desired was specified to have the lowest amount of fuel burnt in the turn while still below the available thrust constraint. The plots showing this analysis can be found below in Figures 8.3 and 8.4. The optimum turn was found to be at 1.7 - g's. The thrust required is about 99,000 pounds for this turn, and only 6400 pounds of fuel are burned. The load of the turn chosen however was 1.6 - g's. This value was chosen because the thrust required is 99,000 pounds, 9,000 pounds less than the 1.7 - g turn, with a fuel penalty of less than 50 pounds per turn. The thrust required lies right under the constraint due to engine size. In addition to this, the fuel burned for this turn is very close to the minimum, with a fuel weight penalty of only about 50 pounds.

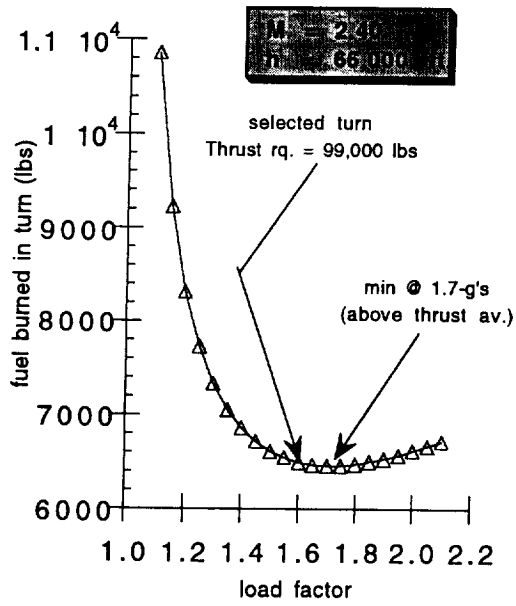

Figure 8.3
Fuel burned vs. load factor

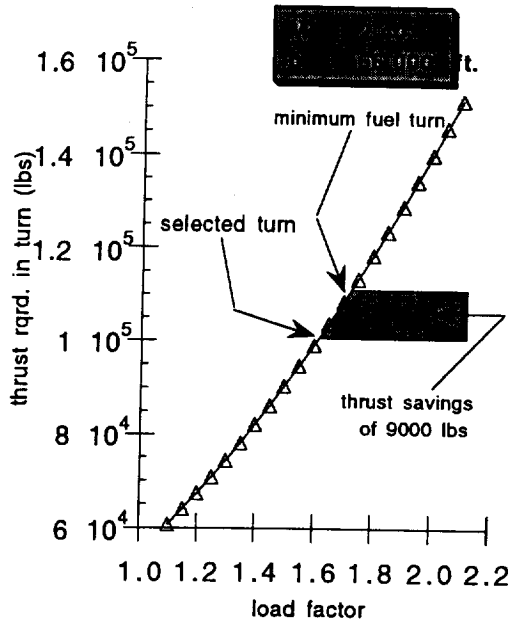

Figure 8.4
Thrust rqrd. vs. load factor

8.4 Takeoff and Landing Performance

The Aeolus, since it will serve as both the propane delivery system and as a commercial transport, will need to be able to takeoff and land from a conventional airfield. The takeoff and landing field length are therefore limited. The takeoff field length which is used in ACSYNT is the field length analyzed for the Aeolus. The length is 6000 feet, which places a constraint in the wing loading - thrust to weight analysis in the next section. Aeolus can takeoff in much less than 6000 feet, but this was chosen to put a realistic length on the constraint chart. Analysis done with a takeoff field length of 6000 feet will also coincide with ACSYNT analysis. The landing field length requirement set by the 1993/94 NASA/USRA ADP group is 12,000 feet. This places another restraint in the wing loading-thrust to weight analysis. The $C_{L\alpha}$

for takeoff and landing which ACSYNT produced is 2.483. The angle of attack is 10 degrees with a maximum angle of rotation of 11 degrees. Chapter 7.0 on the aerodynamics contains a detailed description of the components of lift at takeoff and landing.

8.5 Wing loading vs. Thrust to Weight Analysis

In the design of an aircraft, two major design factors are the size of the wing as well as the size of the engines used. These factors are used to get a preliminary size of the aircraft, and used to design for certain mission requirements, such as a 1.6 - g turn. If not designed with these factors in mind, an aircraft will not be able to perform in the required manner, and in an extreme circumstances, may not be able to takeoff. Figure 8.5 shows the W/S vs. T/W plot for the Aeolus. Each line on the plot represents the constraint placed on wing loading and thrust to weight ratio due to a certain flight condition.

Figure 8.5 accounts for all constraints which effect the design of the aircraft for the propane mission, as well as cruise without refueling for the commercial transport mission. The thrust to weight ratios on the plot as well as the wing loadings are all takeoff equivalent values at sea level static conditions. These were obtained by converting all the specific parameters back to takeoff conditions. This was done so that all the design constraints could be viewed and compared on the same plot.

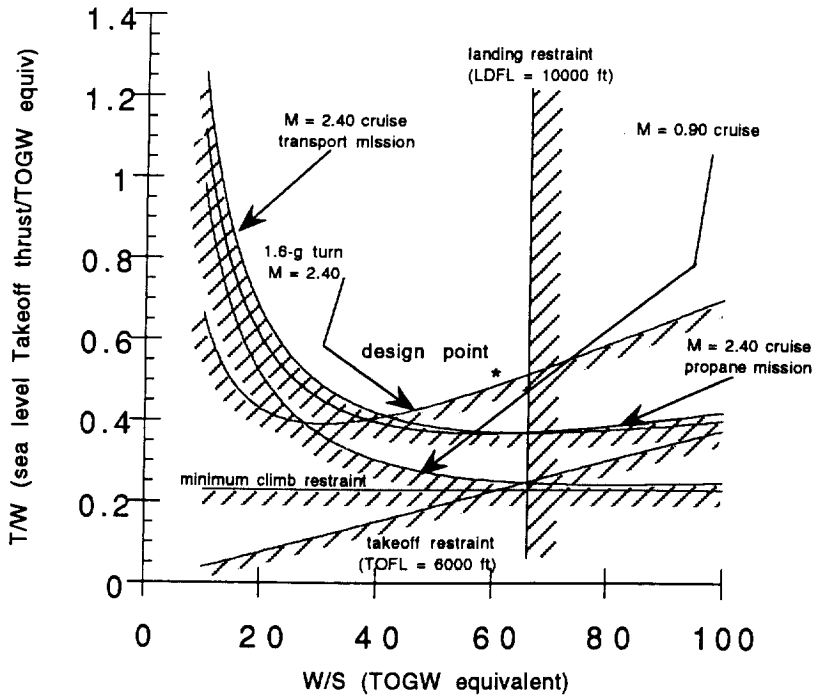

Figure 8.5
W/S vs. T/W sizing/constraint chart

Note that the constraint line for the 1.6 - g turn lies directly beneath the design point which is the takeoff configuration for Aeolus. This means that Aeolus has just the right amount of thrust at altitude to execute the turn. Any decrease in the thrust to weight ratio at altitude would prohibit Aeolus from performing the turn, and would have to execute a lighter "g" maneuver. The current design for Aeolus lies within the "flyable" range on the plot meaning that the wing size and the engine size are consistent with the performance requirements.

9.0 PROPULSION

Components of the engine and its installation must meet aircraft requirements. In this study, primary emphasis is placed on the inlet geometry, combustor and nozzle. Other features researched included aerodynamics, engine sizing and the materials of the various components. It will be important to optimize all of the components involved in the design of the powerplant to keep the TOGW of the Aeolus low and reduce the specific fuel consumption (SFC).

Powerplants for new HSCT concepts are currently being researched by several different companies. Pratt & Whitney (P&W) and General Electric (GE) are researching propulsion designs for the American HSCT program while Rolls Royce, Snecma, Fiat Avio and Motoren-und Turbinen-Union have been working for the European propulsion team (Kandebo, 1994). This study only includes engines designed to travel at Mach 2.4 at an altitude of 66,000 ft, the operating requirements for the Aeolus. The engine analysis code ONX/OFFX (Mattingly, ONX and OFFX User Guide) was used to estimate and compare the uninstalled thrust, SFC, and air mass flow of various engines at both on and off design Mach numbers and altitudes. This extended data was used to evaluate the Aeolus throughout its flight regime and mission.

9.1 Initial Engine Selection

The baseline engine design chosen was the Rolls-Royce Mid-Tandem Fan (MTF). The Mid-Tandem Fan, shown in Figure 9.1, is a non-afterburning, variable-bypass engine predicted to produce between 60,000-80,000 lb of thrust at takeoff. It measures 260-350 in. in length and has a diameter of 80-100 in. This baseline engine is utilized on the European HSCT project study. Although the MTF is still in its preliminary stages, it was chosen because it is predicted to produce a higher amount of thrust than most other designs with quieter operation. Another favorable feature is the MTF's auxiliary fan is partially hidden behind the low-pressure compressor reducing the frontal area (Kandebo, 1993, p. 22). The fact that the MTF is a variable-bypass engine will allow the engine to produce more thrust at takeoff at reduced noise levels and, with a reduced bypass and its convergent-divergent nozzle, increased thrust at supersonic speeds.

Since the MTF is only a baseline engine and has not been developed, thrust and specific fuel consumption at supersonic cruise have not yet been disclosed. The components such as the combustor and

the nozzle have not been finalized. These engine components are designed and chosen to meet the specific mission requirements and are described in the following sections.

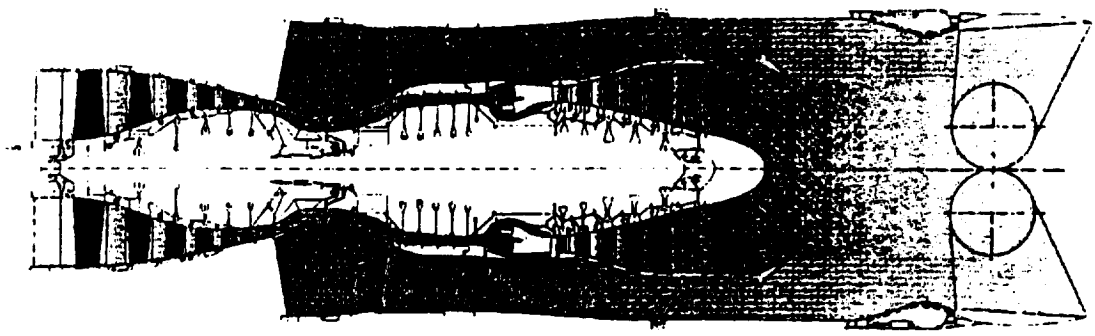

Figure 9.1
The Selected Base Engine: The Mid-Tandem Fan
From: *The Concorde Story*, p. 121

9.2 Engine Sizing

Factors considered in sizing the engine for segments of the Aeolus mission were takeoff, climb to subsonic and supersonic cruise, subsonic cruise, supersonic cruise and the supersonic turn at the end of each pass through the polar vortex. Using comparative engine decks which had similar mission requirements to those of the Aeolus mission, the list was narrowed down to the two most important factors: takeoff and the supersonic turn. The other conditions were checked to ensure they could be met.

The supersonic turn was the first situation analyzed. Trade-off studies were done between the fuel used during the turn and the required weight of the engine versus the number of g's pulled. The weight of the fuel consumed and the weight of the engines needed to be minimized. Figure 9.2 shows a graph of the two variables versus the g's pulled. The calculations which produced this graph are shown in Appendix A. The reference engine weight was assumed to be 15,500 lb (including the inlet and the nozzle) with a reference installed thrust at Mach 2.4 and 66,000 ft of 25,000 lb. It was also initially assumed four engines,

two on each wing, would be used. Since the MTF did not have a published specific fuel consumption, a specific fuel consumption (SFC) of 1.3, as chosen by the 1993/1994 USRA team, was used for the calculations.

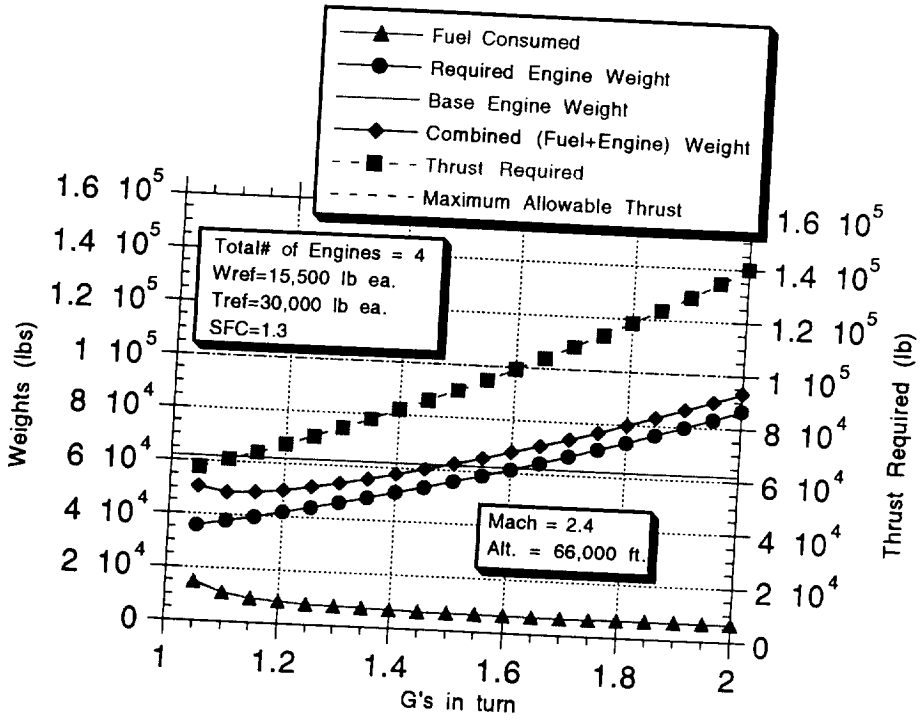

Figure 9.2
Graph of the Required Engine Weight and the Fuel Consumed versus the Number of G's Pulled

The least amount of fuel was consumed at the 1.7g turn. The solid horizontal line on the graph shows the limit where the engine weight would not have to be increased to meet the turn requirement. The intersection of the horizontal line and the required engine weight line occurred at approximately a 1.6g turn. The time and fuel calculations show that a 1.6g turn would consume only approximately 50 lb more fuel than a 1.7g turn which is compensated for in the engine weight savings, therefore a 1.6g turn was chosen. The engine weight required for this turn was approximately 62,000 lb for all four engines. This number includes the use of light weight composite materials so the weight of each engine will be at the most 15,500 lb per engine.

The preliminary calculations (shown in Appendix A) predicted the required total thrust for a 1.6g to be approximately 99,030 lb. The dashed horizontal line shows the maximum allowable thrust using four engines producing 25,000 lb of thrust each (100,000 lb of total thrust). The thrust required line for each turn, also included in Figure 9.2, shows that the 1.6g turn falls below this maximum. Therefore, the required thrust per engine was less than 25,000 lb, so the size of the engine is adequate.

In order to achieve 25,000 lb of thrust at Mach 2.4 and 66,000 ft, the static takeoff thrust must be large enough to allow for the loss of thrust at the higher altitudes which always occurs in aircraft powerplants. Therefore, the largest scale of the MTF engine was chosen resulting in a static takeoff thrust of 80,000 lb with an engine length of 350 in. (not including the inlet) and an engine diameter of 100 in. The necessary takeoff thrust was optimized using ACSYNT. ACSYNT results showed a non-afterburning engine producing 80,000 lb of thrust was adequate for the Aeolus to takeoff.

9.3 Engine Inlet

For a supersonic aircraft, the inlet must allow for variable air intake area and oblique shock shaping at supersonic conditions to decelerate the airstream from supersonic to subsonic speeds at the engine face. At takeoff, the intake of air must be large to produce the necessary thrust. To provide the necessary amount of air at takeoff the intake area must be 80 percent of the engine diameter. The necessary thrust is lower for supersonic cruise, therefore, the needed air intake is then smaller and the inlet must reduce in area in order to be most efficient. At the same time, oblique shocks and a normal shock must be formed to slow the air to the necessary subsonic speeds without producing large total pressure losses (Talbot, 1962).

NASA-Lewis and McDonnell Douglas are focusing their studies on an axisymmetric, variable-diameter, centerbody inlet. (Kandebo, 1993. p. 47) This configuration resembles two umbrellas with their handles connected together. As more air is needed, the canopy portion of the umbrella is collapsed. The canopy is expanded when the air flow must be restricted. In testing, this inlet has met and surpassed its anticipated performance.

Two different modifications of this inlet concept were initially studied. The first design considered was an independent nacelle which held only one engine. The second design considered was a dual nacelle which held two engines. After comparative studies the two engine nacelle design was chosen. This design provided more efficient trailing edge control surfaces and reduced the wetted area of the nacelles by almost one third which was one of the driving design considerations. The dual engine nacelle was designed with a common vertical wedge system to avoid an engine unstart propagating into the adjoining inlet.

A detailed drawing of the inlet design is shown in Figure 9.3. This design is a two-dimensional, variable-diameter inlet similar to the three dimensional, variable diameter inlet being researched by NASA-Lewis and McDonnell Douglas. The inlet ramp retracts at takeoff so the required larger air flow will reach the engine. At supersonic cruise conditions, the ramp angles increase allowing less air into the engine. Also shown on the drawing are auxiliary doors on the sides of the nacelle and the variable angle lip at the intake which open at takeoff to increase the amount of air reaching the engine. The increasing cross-sectional areas (A-A, B-B and C-C) of the inlet duct show that as the air enters the inlet and approaches the engine face, the intake area increases ensuring that the air velocity will slow to low subsonic Mach numbers after the normal shock at the inlet choke, before entering the engine. The inlet ramp is shaded to show that the surface is perforated. This perforation causes the air to be drawn to the ramp creating an ideal boundary layer along the ramp. The nacelle is equipped with an aft facing, auxiliary exhaust ramp on the bottom to provide the suction on the perforated ramp faces and to allow the boundary layer air to be dumped out the bottom of the nacelle.

9.4 Engine Nozzle

Noise reduction is a main design restriction for the HSCT powerplant. The Concorde often produces jet noise greater than 120 decibels at takeoff (NASA, No Noisy Neighbor). The goal for future HSCT concepts is to meet current FAA Stage 3 noise requirements or future standards (possibly Stage 4 noise requirements) for community noise levels near airports (Phillips, 1991).

The non-afterburning, MTF engine, by design, uses a two-bucket nozzle similar to the one used on the Concorde's engine. This nozzle has good noise characteristics which, along with the high bypass/lower

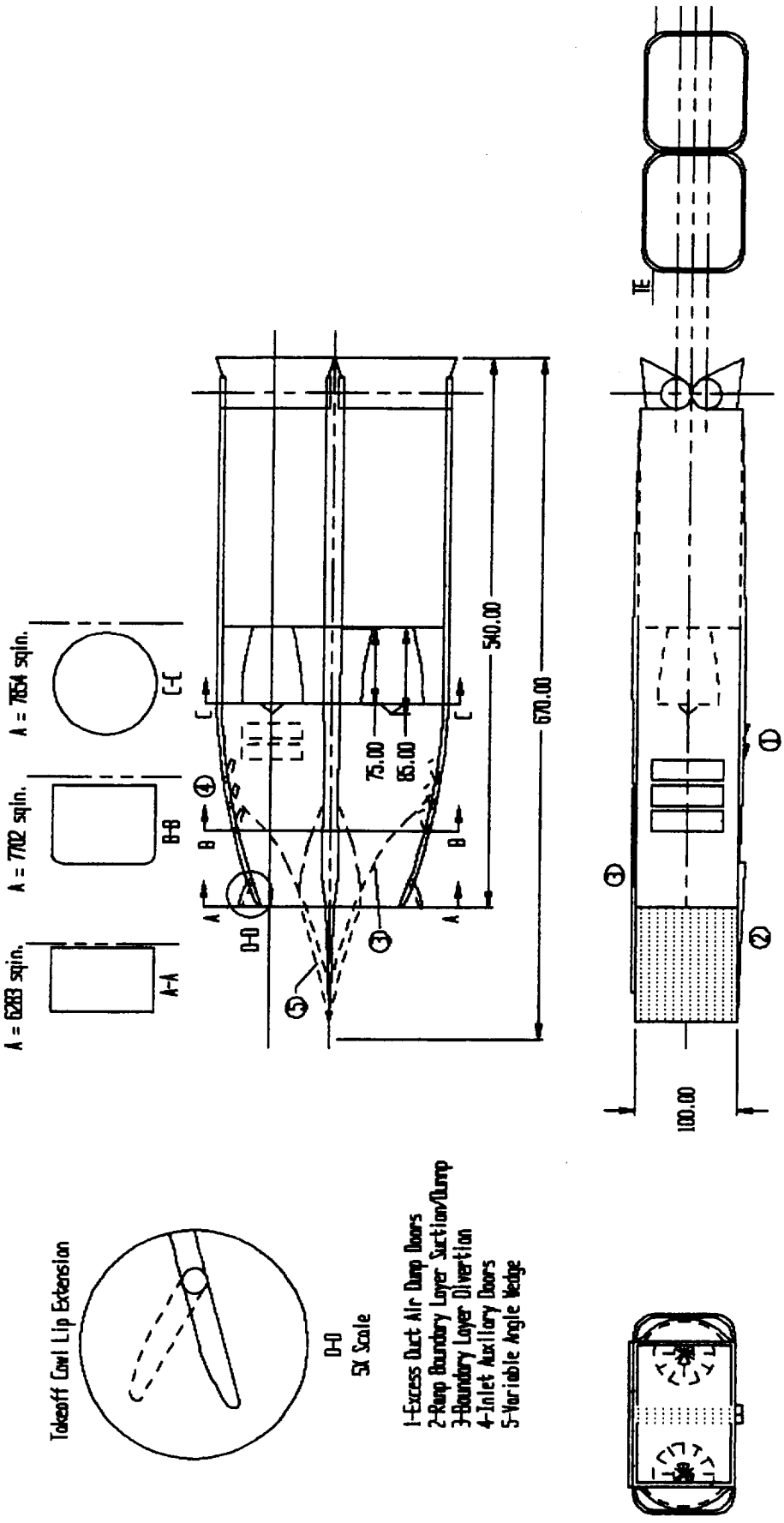

Figure 9.3 Nacelle Design: Two Engines in One Pod

exhaust velocity, should meet the necessary noise requirements. Also, the two-bucket design is simple with few moving parts (Kandebo, 1993, p. 22). The two-bucket nozzle is included in Figure 9.3.

9.5 Combustors

The primary concern of a combustor is that its gases and NO_x byproducts do not, within limits, effect the ozone layer. The purpose of this project is to design an aircraft that will not exacerbate the ozone. Therefore, it will be important for the powerplant of the aircraft not to have the damaging NO_x emissions of current supersonic cruise aircraft powerplants.

NASA's combustor program goal was to reduce NO_x emissions by approximately 90 percent. The two main combustor designs being studied to date are the Lean-Premixed-Prevaporized (LPP) combustor and the Rich-Burn, Quick-Quench, Lean-Burn (RQL) combustor, shown in Figure 9.4. The LPP combustor mixes fuel and air upstream of the burning zone. Ideally, the fuel is completely vaporized and perfectly blended with the air before the mixture enters the combustion system. The burning takes place where the velocities are lower downstream of the flame stabilizer (NASA, Ultra-Low NO_x Emissions).

The LPP process, on which GE is focusing their efforts (Kandebo, 1994), is fairly simple but it still has some potential problems. When a combustible mixture exists upstream of the combustion system, there is always a possibility that flame could flash back and damage the engine. Researchers are now trying to eliminate this hazard. Also, the LPP combustor will need to be operated in a parallel staged configuration with another burner (NASA, Ultra-Low NO_x Emissions), making the combustor system more complicated.

The RQL combustor, on which P&W is concentrating (Kandebo, 1994), is more complicated than the LPP combustor. The RQL combustor has two burning zones. In the first burning zone, excess fuel is injected into a small amount of air making a rich burn zone. The chemical reactions which occur in this fuel rich environment causes the chemistry to take certain paths which reduces NO_x production. Air must then be added quickly and uniformly downstream to complete the reactions in order to minimize additional NO_x production. A final burnout stage is also necessary. This process has been hard to optimize in experiments and the RQL research has not progressed as far as the LPP approach (NASA, Ultra-Low NO_x Emissions).

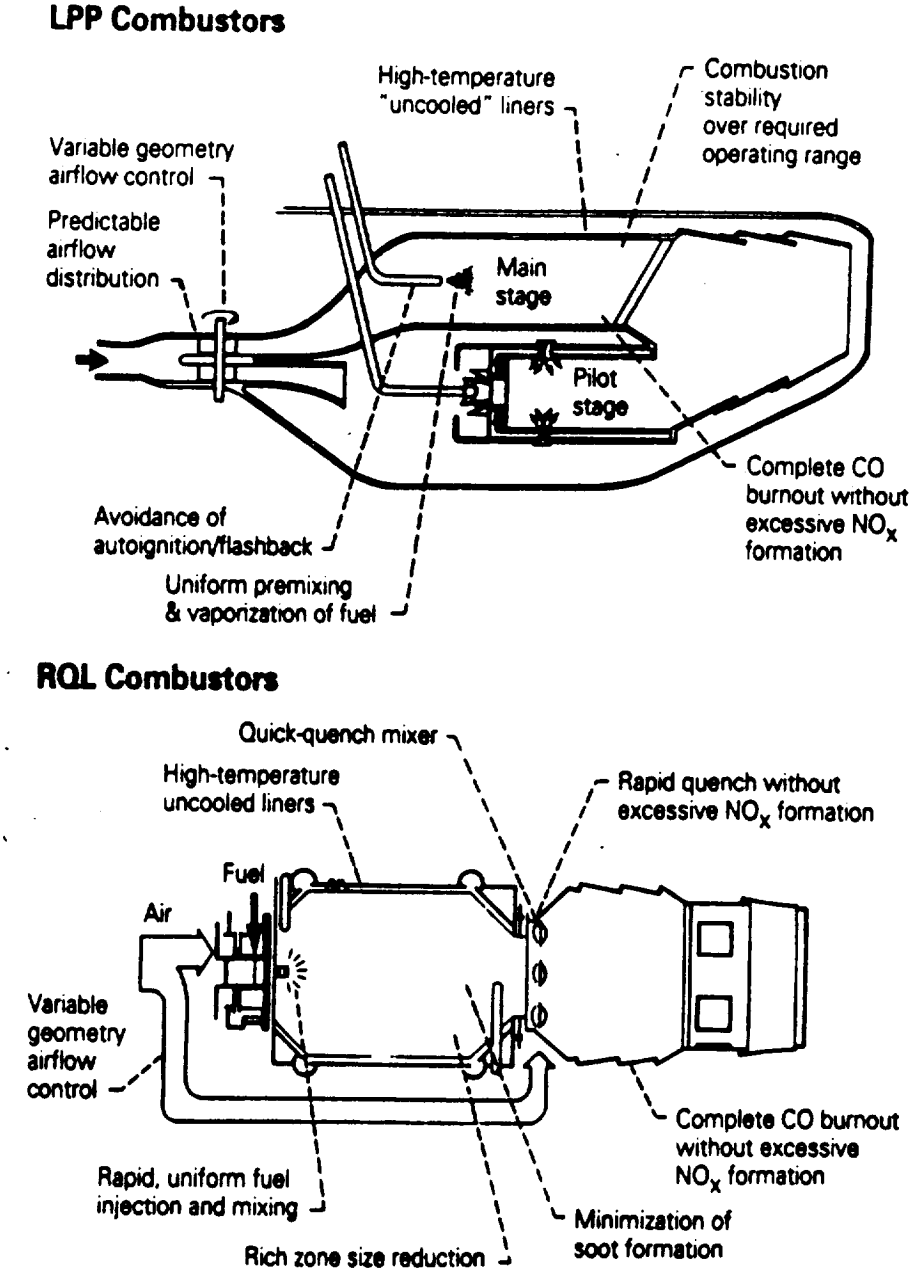

Figure 9.4
LPP and RQL Combustors
(From: NASA Headquarters Office of Aeronautics and Space Technology)

Both the LPP and RQL experiments show the NO_x emissions meet the clean air requirements, the LPP combustor producing less NO_x than the RQL combustor. Soot emission from both combustors are also much lower than current combustors. This helps eliminate some of the pollution associated with

aircraft powerplants and avoid environmental problems in the stratosphere. Again, the LPP soot emissions were much lower than the RQL soot emissions (NASA, Ultra-Low NO_X Emissions).

The materials which will be necessary for the production of these two combustors is still in the research stage. Both of NASA's low emissions combustors lack the internal cooling present in combustors of today's aircraft (NASA, Ultra-Low NO_X Emissions). The combustors will have to operate over a wide range of conditions. At taxi/idle and at altitude relight the combustor will have to withstand low temperatures and pressures. At takeoff and supersonic cruise, the combustor must withstand very high temperatures and pressures (NASA, Ultra-Low NO_X Emissions).

The LPP combustor was chosen to be used in the modified MTF. As noted, the LPP combustor produced lower NO_X and soot emissions in the tests conducted to date. The LPP combustor, as previously mentioned, is also easier to optimize than the RQL combustor (NASA, Ultra-Low NO_X Emissions).

9.6 ONX/OFFX

The engine analysis program ONX/OFFX (Mattingly, ONX and OFFX User Guide), was used to compare different engine types and cycles. The P&W turbine-bypass turbojet (TBE) and an afterburning turbojet were analyzed using this code. Both engines were analyzed with an overall pressure ratio (OPR) of 15.5 and a fan pressure ratio (FPR) of 3.5 (NASA, Report 4233, 1994). The design point for both engines was Mach 2.4, altitude of 66,000 ft, temperature leaving the combustor 3200 R and a design thrust of 12,000 lbf.

ONX/OFFX calculates parameters such as uninstalled thrust, air mass flow and SFC at various altitudes and Mach numbers. The most important of these parameters is SFC. If the SFC consumption is improved by one percent, the TOGW will be reduced by more than 8,000 lb (NASA, Report 4233, 1989). Figure 9.5 shows a comparison of the SFC of the two P&W engines at the various altitudes and off-design Mach numbers. The afterburning turbojet was eliminated due to its high SFC. ONX/OFFX is not capable of modeling variable-bypass engines. However, the program helped eliminate the idea of afterburning for the MTF engine, since it is not necessary for takeoff or for climb to cruise conditions. ONX/OFFX also helped show a SFC of 1.3 was feasible.

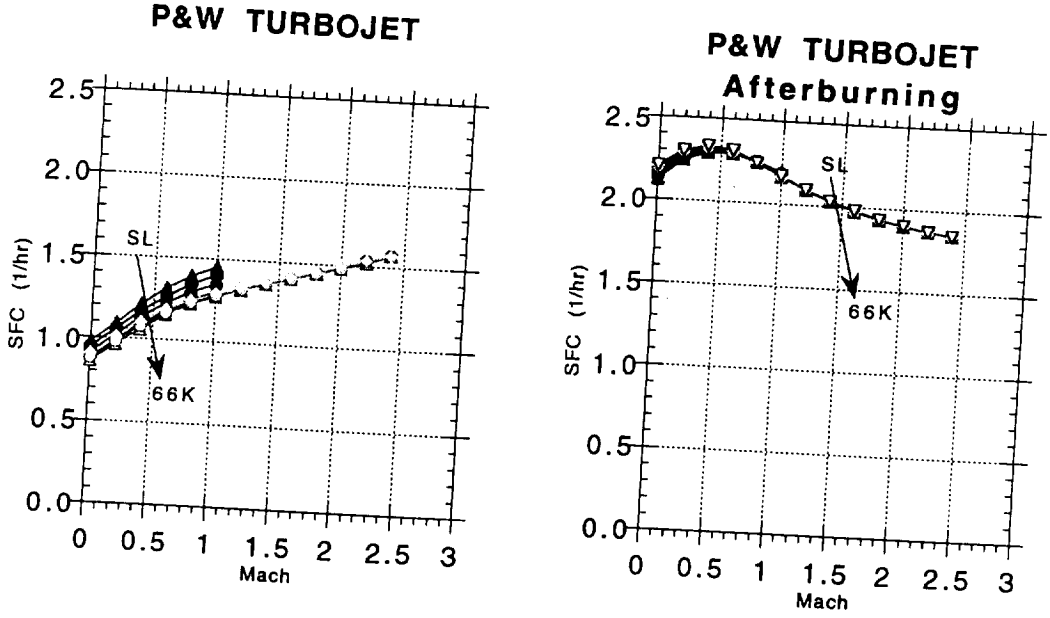

Figure 9.5
ONX/OFFX SFC Comparison

9.7 Engine Materials

HSCT engine materials are, like the engines themselves, still in the development stages. Overall weight of the engine is of great importance. Studies have shown that 1,000 lb pounds of engine weight becomes 24,000 lb of TOGW (NASA, Report 4233, 1989). European manufacturers are developing polymeric matrix composites specifically designed for engine intakes as well other titanium matrix composites (Proctor, 1994) which may also be used for the nacelles.

As noted previously, special materials are being developed specifically for the combustors. Supersonic transport studies show that the powerplant must have a 18,000 hour service life while operating near maximum temperatures for 90 percent of that time. The LPP combustor will not have the internal cooling which exists in present combustors so NASA's Enabling Propulsion Materials (EPM) program is researching ceramic matrix composites (CMCs). These materials can withstand high temperatures for long periods of time. EPM is also researching intermetallic matrix composites (IMC) for use in noise-reducing nozzles (NASA, A Material Issue).

Past studies and experiments have shown that composites may produce strength-to-weight improvements of up to 30-40 percent compared with today's superalloys. Composites will thus offer significant structural weight benefits. The weight of the engine is an important design consideration so it will be important to optimize the use of composites.

9.8 Final Engine Selection

An engine which meets all of the needs of our mission is still in the developmental stages. A variation of the non-afterburning, Rolls Royce Mid-Tandem Fan is used in this study. The engine is approximately 350 in. long and 100 in. diameter. The engine will produce a takeoff thrust of at least 80,000 lb with a thrust of at least 30,000 lb at Mach 2.4 and 66,000 ft. The total weight of the engine, including the inlet and nacelle, will not exceed 15,500 lb. The nacelle will hold two engines with a total length of 670 in.

The modified MTF will include an LPP combustor because of its low NO_x emissions. A simple, Concorde-type, two-bucket exhaust system will be used due to its light weight, simplicity and its low noise characteristics. The ideal engine will be composed of many composites which will decrease the overall engine weight while increasing the engine strength.

10. Stability and Control

An important consideration in the successful design of an aircraft system is that of stability and control. To be acceptable, the aircraft must meet or exceed certain flying handling qualities specifications and exhibit adequate control power in all of its flight conditions.

The overall mission requirements determine the control configuration of Aeolus as a canard based aircraft. These requirements range from accomodating structural design aspects of integrating the systems to load and unload the propane tanks, to ensuring that the incoming air flow to the control surfaces are least disturbed due to engine exhaust and/or interference from the wake of the wings; thus optimizing the surfaces' locations as to render them most effective in providing the needed forces and moments.

An important parameter to the design is the determination of the static margin limits, which characterizes the static longitudinal stability. The objective of the design is to be able to cruise with neutral stability, for such conditions alleviate the workload of the flight control systems and render the aircraft to be less prone to problems associated with sudden failures in the control effectiveness of the control surfaces . To accomplish this stability, fuel is shifted to change the center of gravity of the aircraft to correspond with the aerodynamic center.

There are three contraints on the determination of the static margin. The first constraint is imposed by considering the least possible drag coefficient induced by different center of gravity locations. The second contraint limits the range of the static margin by conforming to the range of center of gravity locations of the Aeolus during nose-up / nose down maneuvers. The third contraint is the limit imposed upon by fuel shift locations when such shifts are employed to maintain desired equilibrium states that may be perturbed due to the aerodynamic center shift that occurs during transition from subsonic to supersonic flight. Analysis of the Aeolus provides the following static margin limits at the three main flight regimes. These static margins, along with the distance that the fuel needs to be shifted to maintain neutral stability, are given in Table 10.1 .

FLIGHT CONDITIONS	STATIC STABILITY	Δ C.G. TO MAINTAIN NEUTRAL STABILITY
Take - Off / Landing	8.234 % unstable	6.95 ft
Cruise M = 0.9	5.093 % unstable	4.30 ft
Cruise M = 2.4	3.353 % unstable	2.83 ft

Table 10.1
Static Margins and Corresponding Fuel Shifts to Maintain Neutral Stability

10.1 Control Power Analysis

To enable the Aeolus to maneuver at all points in the flight envelope, it must possess enough control power. To ensure that the control surface areas provide adequate control power, the analysis for the determination of these areas were done at the critical conditions. For this mission the critical conditions are the take-off / landing conditions where there is relatively small dynamic pressures acting upon the control surfaces, thus possibly restricting the ability for the surfaces to induce the required moments. To assess control power, a set of standard specifications for assessment is used.

The two most commonly used regulatory standards used in assessing the characteristics of an aircraft are FAR Parts 23 and 25 and MIL-STD 1797. Because FAR Parts 23 and 25 provide only qualitative basis for assessment of the aircraft, MIL-STD 1797 is used.

The Aeolus's control configuration is that of a conventional type consisting of all-moving canards, ailerons at the outboard of the wing, elevons for take-off / landing at the inboard of the wing, and a vertical tail with a moving rudder. With this arrangement (see Configuration Section) , further analysis is done.

For best optimization of the determination of the control surface areas, a coupled analysis of control power availability and trim drag analysis is done. Thus the philosophy behind sizing the control surface areas is to induce the most moments and forces with as little area as possible. Not only will this approach reduce the inertias imposed upon the control surface hinges, but it will also reduce the drag associated with surface area. A consequence of this approach is that the control surface deflections have to be relatively large (maximum deflection is 40) .

Two methods for assessment were used. Initially, estimated values of control surface areas are inputted into the analysis methods provided by Eithoven. If the outputs are not in accordance with MIL-

STD 1797 , then the control surface areas in the geometry of the aircraft are modified and stability derivatives are calculated. And the analysis is performed again mainly to correct conditions that did not meet specifications, which is difficult since all the analysis input variables are coupled with one another. The second method involves setting the control deflections and certain states, such as bank and sideslip angles, at their maximum (thus meeting specifications), and solving for the aircraft's state equations coefficient matrix A ($\dot{x} = Ax + Bu$ where **x** and **u** are the state and control vectors, respectively) to determine the control surface areas from the induced stability derivatives that are exhibited in the A matrix components. The approach for the Aeolus configuration used a combination of these methods. The results from three iterations of analysis is given in Tables 10.2 and 10.3.

CONTROL POWER	MIL-STD-1797 SPECIFICATIONS	AEOLUS
Take-Off / Landing	1 < Mavail / Mreq	Mavail / Mreq = 1.2
Roll Axis in Crosswinds	$\delta a / \delta a_{max} \leq 0.75$ $\phi \leq 10$ deg	$\delta a / \delta a_{max} = 0.75$ $\phi = 10$ deg
Roll Axis with Asymmetric Thrust	$\delta a / \delta a_{max} \leq 0.75$ $\phi \leq 10$ deg	$\delta a / \delta a_{max} = 0.75$ $\phi = 10$ deg
Yaw Axis with Asymmetric Thrust	$\delta r / \delta r_{max} \leq 0.75$ $\phi \leq 10$ deg	$\delta r / \delta r_{max} = 0.75$ $\phi = 10$ deg
Yaw Axis in Crosswinds	$\delta a / \delta a_{max} \leq 0.75$	$\delta a / \delta a_{max} = 0.75$

Table 10.2
Control Power Assessed at Critical Conditions

CONTROL SURFACE	AREAS	PERCENTAGE OF WING
Canard	477.5 sq ft	4.8 %
Vertical Tail	640.2 sq ft	6.4 %
Ailerons	333.0 sq ft	3.3 %
Elevons (at T-O / Landing)	277.5 sq ft	2.8 %

Table 10.3
Control Surface Areas

10.2 Longitudinal Stability and Control

With respect to MIL-STD 1797 Aeolus is classified as a Class III aircraft being a large, heavy, low-to-medium-maneuverability airplane. The cruise segment of the flight envelope is classified as Category B while the take-off and landing segment is classified as Category C. Aeolus's stability derivatives are calculated using Aerodynamic Preliminary Analysis System II (APAS) by G. Sova and P. Diva of the North American Aircraft Operations, Rockwell International. These derivatives are shown in Table 10.4.

LONGITUDINAL STABILITY AND CONTROL DERIVATIVES			
Derivatives	Cat C: Take-Off / Landing	Cat B: Cruise (M = 0.9)	Cat B: Cruise (M = 2.4)
$C_{L\alpha}$	0.03299	0.03845	0.02545
C_{Lq}	2.00719	2.56021	0.80156
$C_{L\delta\ canard}$	0.00019	0.00009	0.00006
$C_{m\alpha}$	0.00260	0.00182	-0.00111
C_{mq}	-1.29553	-1.70477	-1.04649
$C_{m\delta\ canard}$	0.00267	0.00336	0.00180

Table 10.4
Longitudinal Stability and Control Derivatives

Incorporating these derivatives into Aeolus's longitudinal state equations of motion and analyzing the matrices of those equations resulted in the flying handling qualities as shown in Table 10.5.

LONGITUDINAL FLIGHT CHARACTERISTICS					
Flight Mode	Category	MIL-STD spec	Category C. Take-Off / Landing	Category B. Cruise (M = 0.9)	Category B. Cruise (M = 2.4)
Phugoid	Any	$\zeta p > 0.04$	$\zeta p = 0.1012$	$\zeta p = 0.1191$	$\zeta p = 0.0362$
Short Period	B	$0.30 < \zeta sp < 2.0$	-	$\zeta sp = 1.0000$	$\zeta sp = 0.1171$
	C	$0.35 < \zeta sp < 1.3$	$\zeta sp = 1.0000$	-	-

Table 10.5
Longitudinal Flying Handling Qualities Parameters

From these parameters, it is deduced that the Aeolus's phugoid and short period modes behavior at the aircraft's primary mission cruising speed of Mach 2.4 are unsatifsfactory. Thus a Stability Augmentation System (SAS) coupled with the Control Augmentation System (CAS) will have to be implemented as a provision for satisfying the standard specifications.

10.3 Lateral / Directional Stability and Control

The lateral / directional stability and control derivatives are calculated using APAS. The results are shown in Table 10.6.

LATERAL / DIRECTIONAL STABILITY DERIVATIVES			
Derivative	Takeoff		Cruise
C_{Lp}	0.00012	0.00012	0.00012
C_{Lr}	0.00112	0.00112	0.00112
$C_{Y\beta}$	-0.00317	-0.00363	-0.00241
CYp	0.00667	0.01241	0.00769
C_{Yr}	0.22806	0.26500	0.15677
$C_{Y\delta}$ aileron	-0.00073	-0.00109	-0.00002
$C_{Y\delta}$ rudder	0.00243	0.00295	0.00105
$C_{l\beta}$	-0.00027	-0.00033	-0.00020
Clp	-0.12156	-0.13097	-0.11471
C_{lr}	0.02391	0.02969	0.01900
$C_{l\delta}$ aileron	0.00211	0.00254	0.00092
$C_{l\delta}$ rudder	0.00024	0.00031	0.00011
C_{mp}	-0.00011	-0.00011	-0.00011
C_{mr}	0.00124	0.00124	0.00124
$C_{n\beta}$	0.00092	0.00117	0.00063
Cnp	-0.00783	-0.01188	-0.00772
C_{nr}	-0.17123	-0.19496	-0.13815
$C_{n\delta}$ aileron	0.00042	0.00062	0.00002
$C_{n\delta}$ rudder	-0.00149	-0.00184	-0.00072

Table 10.6
Lateral / Directional Stability and Control Derivatives

Incorporating these derivatives into Aeolus's lateral / directional state equations of motion and once again analyzing the resultant system matrices produces the flying handling qualities as shown in Table 10.7.

LATERAL / DIRECTIONAL FLIGHT CHARACTERISTICS					
Flight Mode	Category	MIL-STD-1797 Specifications	Category C Take-Off / Landing	Category B Cruise (M = 0.9)	Category B Cruise (M = 2.4)
Dutch Roll	B	$\zeta d > 0.08$ $\zeta d\omega d > 0.15$ $\omega d > 0.40$	- - -	$\zeta d = -0.1571$ $\zeta dwd = -0.0052$ $\omega d = 0.0330$	$\zeta d = -0.2375$ $\zeta d\omega d = -0.006$ $\omega d = 0.0253$
	C	$\zeta d > 0.08$ $\zeta d\omega d > 0.15$ $\omega d > 1.0$	$\zeta d = -0.1676$ $\zeta d\omega d = -0.005$ $\omega d = 0.0299$	- - -	- - -
Roll Subsidence	B C	$\tau r < 1.4$ $\tau r < 1.0$	- $\tau r = 13.0$ s	$\tau r = 12.1$ s -	$\tau r = 22.0$ s -
Spiral	B C	T2 > 20 s T2 > 12 s	- T2 = 990.2 s	T2 = 1155 s -	T2 = 231 s -

Table 10.7
Lateral / Directional Flight Characteristics

From these flying handling qualities parameters, it is concluded that the aircraft behaves unsatisfactorily in the dutch roll and roll subsidence modes. The negative damping ratios indicate that the system has become divergent, and can never naturally return to its equilibrium state. So a Stability Augmentation System (SAS) coupled with the Control Augmentation System (CAS) has to be implemented to create satisfactory flying handling qualities. The spiral mode, however, is allowed to be unstable. The only constraint for this mode is the minimum time to double amplitude, which in this case is satisfied.

11.1 Structural Design Process for HSCT

In order to design an aircraft structural concept for Aeolus one must conceive a design that has a high structural efficiency, that is heat resistant and is very reliable. The cost of the design must also be kept to a minimum. The structural design concepts for Aeolus was based upon:

1. Lockheed's previous structural concept studies
2. Boeing's previous structural concept studies
3. North American XB-70 structural configuration
4. Aerospaticale baseline design
5. Concorde Structural configuration.

The primary VPI HSCT configuration was developed from Aerospaticle's baseline design, otherwise referred to as the European design.

11.2 Structural Concept Formulation

The mission and environmental requirements for the structural design of Aeolus are as follows:

1. Cruise Speed, M = 2.4
2. Maximum Range = 5000 nmi.
3. Cruise altitude = 66000 ft.
4. TOGW =774916 lb.
5. Structural Life = 15 yrs * 4000 hrs/yr = 60000 flight hrs.

It would not be at all practical to test the design concept at every condition in the flight envelope. Alternatively, Aeolus' structure needs to be able to safely tolerate all the loading conditions sagely on the boundaries of a V-n diagram.

There are numerous considerations one needs to address in the structural design of Aeolus. The most dominant of these considerations are:

1. canard-fuselage, wing-fuselage, vertical tail-fuselage mating
2. heating and thermal expansion
3. fuselage pressurization
4. propane loading and support
5. weight loads (resting and inertial)

From the several structural assembly techniques, the most prominent is the use of ribs and spars and the assembly of premolded panels. The use of ribs and spars was chosen for the design of Aeolus because the small tolerances needed in the assembly of the HSCT are more difficult to obtain by assembling premolded panels like a puzzle.

It may no be surprising that structural weight has 3 times the impact on the viability of Aeolus than on a subsonic transport of comparable size. Aerospaticle realized this and thus used the following material and structural combinations:

1. main spar box of titanium
2. aluminum alloy fuselage (possibly advanced composites)
3. composite skin (Poisson-Quinton, 42).

A 40% weight savings was expected through this use of titanium and aluminum allows and the large scale introduction of composites. Wright lab has successfully demonstrated the use of composites in primary structure. The U.S. Military's B2-B construction also features composites used in primary load bearing structures (Noor, 21-22). On the other hand, titaniu, is the best choice of material for areas of highest temperature and the largest chance of impact of foreign objects. Titanium should also be used for pressure bulkheads. Otherwise, the structural designed of the HSCT will use composites wherever possible. Added bonuses from using composites is the ability to adhesively join the structure and the alleviation of stresses from uneven thermal expansion (Newaz,34).

Fuselage pressurization adds even more complexity and weight to the structure of Aeolus. Using round windows and eliminating windows over part of the cabin would reduce the structural weight considerably. Therefore, Aeolus' design will eliminate the window at every other seat in the "coach" section

of the cabin. Also, using a smaller diameter window will reduce the structural weight as well as elevate the maintainable minimum pressurization in the case of a window rupture (Poisson-Quinton, 42).

Aeolus will undergo severe temperature changes with sustained 'soaking' temperatures of near 350 deg F and peak temperatures close to 400 deg F. The temperatures Aeolus will be required to resist are displayed in Figure 11.1.

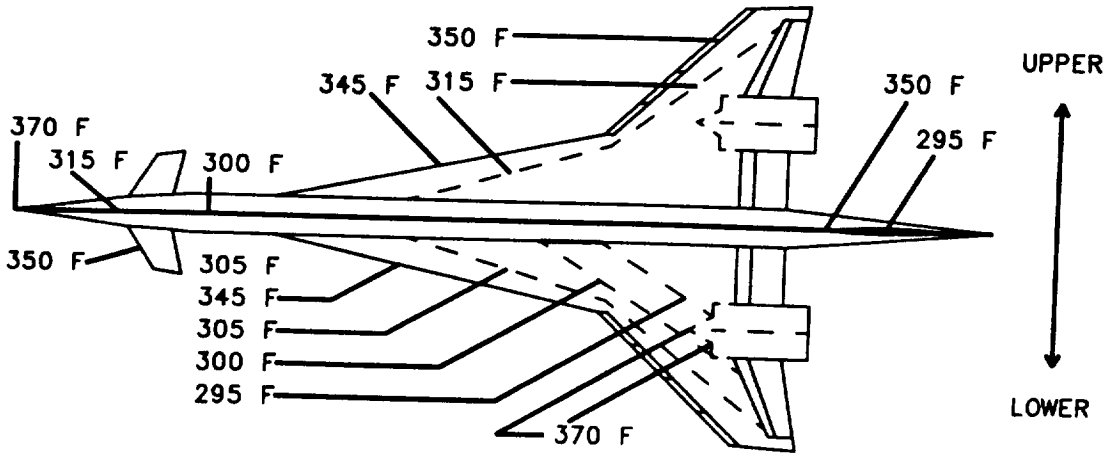

Figure 11.1
Projected temperature distribution (Mach 2.4)
(taken from Quist, Advanced Materials for a HSCT)

Structural materials tend to degrade at these elevated temperatures, especially composites. Their load carrying capabilities are dramatically reduced. Therefore, the thermal cycle fatigue of the selected materials should be tested and evaluated at these elevated temperatures. Another problem resulting from the heating is stresses induced from uneven thermal expansion. The wing of Aeolus is expected to grow at least 4 inches in the chordwise direction, while the fuselage will not. For this reason the HSCT needs to incorporate wing-fuselage mating technologies that will permit this uneven expansion (Piellisch,21). Possible solutions to the heating problem are as follows:

1. use aircraft capacity to act as a heat sink
2. use aircraft skin to act as a heat sink

3. apply a white finish to the aircraft skin

4. albation cooling

5. injection cooling

6. active cooling

7. magneto hydrodynamic cooling

The heat sink solution is much too heavy to use for an aircraft which will cruise at supersonic speeds. This method also does not work well with prolonged heating. Albation cooling involves the application of material which is taken off by impacting air particles. When a material particle leaves the aircraft skin it takes a small amount of heat with it. This method would not be very aerodynamicly or cost effective. Injection and active cooling involve the circulation of a coolant through the aircraft skin or structure, respectively. Active cooling can be more easily and cheaply utilized than injection cooling and, therefore, is the choice for the Aeolus' design. Magnetohydrodynamic cooling involves the use of a strong magnetic field to push the heat shock away from the aircraft surface. This method sounds very attractive if only the technology existed to implement it.

The major design considerations for Aelous' wing structure as follows:

1. landing gear weight loads (resting and inertial)

2. landing gear kick loads (braking)

3. Fuel wight loads

4. Aerodynamic loads (lift, control)

5. engine weight loads

6. thrust kick loads (forward and reversed)

7. fuselage bending loads (canard and landing rotation)

note: Aeolus' long wing will support the fuselage bending loads.

The banjo-wing configuration would be more aerodynamic, but it is much heavier. It would also would not allow eye level windows in the cabin. The differences between the two configurations can be seen in figure 11.2. The low-wing configuration is more structurally efficient, is lighter, and is much easier to assemble. Therefore, the low-wing configuration is used for Aeolus' design.

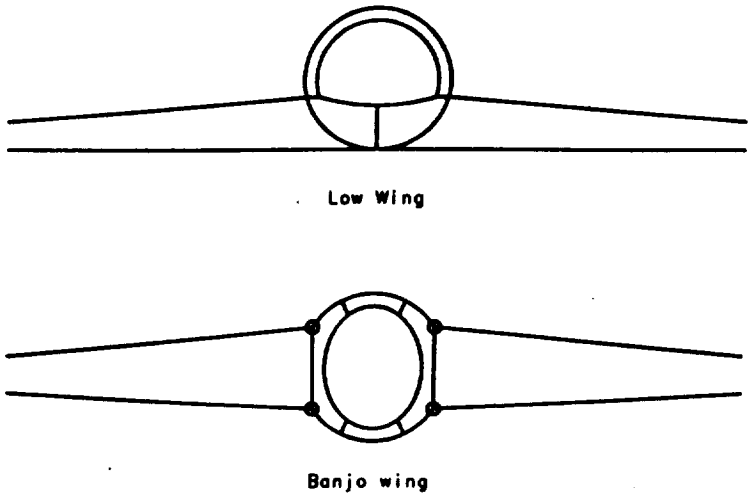

Figure 11.2
Banjo vs. low wing attachment

Aeolus' four engines are paired in single pods on each wing near the intersection of the wing and strake. For each pair of engines a five point connection is used in the engine installation: two points at the front center of each engine and 3 points at the intersection of the wing trailing edge and the engines. This configuration accounts for the engine thrust and weight loads. The engine connection points and overall structural and fuel tank layout can be seen in figure 11.3.

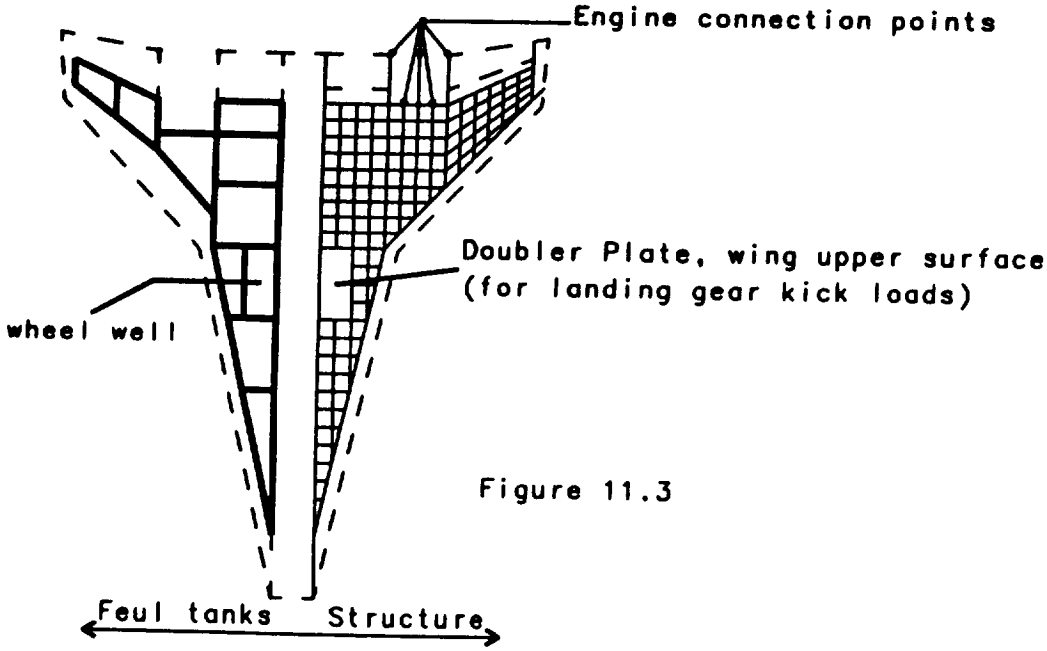

Figure 11.3

Figure 11.3
Aeolus main structural layout

11.3 Materials Requirements

The requirements for the structural materials for Aeolus are as follows:

1. high strength to weight ratio
2. heat resistant
3. durability
4. reliability

As mentioned earlier, most of the airframe materials must be able to tolerate temperatures of about 350 deg F for extended periods of time and peak temperatures of almost 400 deg F. The materials must also be durable enough to last the 60000 flight hours projected for the aircraft's 15 year life. The materials must withstand the heat and pressurization cycles involved in every mission the aircraft performs. These are strict requirements when we note that the Concorde had only 14000 flight hours of service.

11.4 Materials Investigation

Conventional materials such as steel and aluminum were first considered for Aelous' design for their large data base and their inexpensive and easy fabrication. But these materials have low strength to weight ratios, are easily corroded, and are very susceptible to fatigue as compared to materials like titanium and composites. Composites, on the other hand are very expensive, tend to absorb water, and may degrade at higher temperatures. Titanium is a material with almost no drawbacks. It is expected to be very inexpensive in the future because of its increased use in industry. It performs well in high temperatures, resists corrosion, and is very strong and impact resistant. It is ideal for active laminar flow and deicing or heating of the leading edge.

The primary materials for a HSCT structural design will be titanium, for its heat and impact resistance; and composites, for their high strength to weight ratios. The leading composite fibers on the market are as follows:

1. Hercules AS4 graphite
2. IM6 graphite

3. IM7 graphite

4. IM8 graphite

5. Kevlar

Composites using graphite fibers are stranger and lighter than Kevlar composites, but they are also more brittle. the distinguishing feature of Kevlar fibers is its high compressive strength. Resins commonly used today can be broken into three groups:

1. epoxies

2. thermosets

3. thermoplastics

Examples are:

epoxies

1. shell 1895

2. Lord

3. Dow

thermosets

1. LaRC - TPI

2. La RC - TEPI

3. Nomax

4. Cyanate Ester

thermoplastics

1. Derakane

2. ITX

Composite usage shall include, for the most part, thermoset and thermoplastic resins. Relative advantages of thermosets and thermoplastics are shown in table 11.1

THERMOSETS	THERMOPLASTICS
(Characteristics)	
-Undergo chemical change when cured	-Non-reacting, no cure required

-Processing is irreversible	-Post-formable, can be reprocessed
-Low viscosity/high flow	-High viscosity/low flow
-Long (2 hours) cure	-Short processing times possible
-Tacky prepreg	-Boardy prepreg
(Advantages)	
-Relatively low processing temperature	-Superior toughness to thermosets
-Good fiber wetting	-Reusable scrap
-Formable into complex shapes	-Rapid (low cost) processing
-Low viscosity	-Infinite shelf life without refrigeration
-Higher relative operation temperature	-High delimitation resistance
(Disadvantages)	
-Long processing time	-Less relative chemical solvent resistance
-Sensitive to moisture	-Requires high processing temperatures
-Restricted storage	-Outgassing contamination
-Requires refrigeration	-Limited processing experience available
	-Less of a database compared to thermoset

Table 11.1

Composites are usually manufactured in one of three ways:

1. Resin transfer molding (thermosets only)
2. Poltrusion
3. Layup

Silicon carbide/ceramic, metal matrices such as aluminum/lithium or aluminum/titanium may be used for engine parts. These composites are very strong and light and have a maximum operation

temperature of over 4700 deg F. Special care must be taken when deciding where to use these materials because they are very brittle.

Each is considerably expensive compared to conventional materials.

11.5 Materials Selection

All of the criteria discussed earlier was used to select materials for different structural components. For the main structural members such as longerons, spars, ribs, and frames, graphite thermosets are used. Minor components such as the trailing edges of the wing, vertical tail and canard; the aircraft skin, decks, landing gear doors, and rear fuselage cone will be fabricated from graphite thermoplastics. The leading edges of the wing, strake, canard, and vertical tail will be made of titanium or titanium honeycomb. The engine nacelles along with the main bulkheads/pressure bulkheads will be made of titanium honeycomb. The honeycomb structure should reduce the member weights by over 50%. The nose radome/nose cone will be composed of polymide quartz composite. The B-2 also features this material use. It is transparent to electromagnetic waves and is very heat resistant. The inside of the fuel tanks will be overlaid with titanium sheets to prevent fuel-induced microcrack formation of the composite materials. Also, selected composites will have nickel fibers added to the composition of their outer 3 or 4 layers for protection against lightning strikes on the airframe. A figure of the material placements can be seen below in figure 11.4. Finally figure 11.5 shows a isometric view of the fuel tank and structural layout.

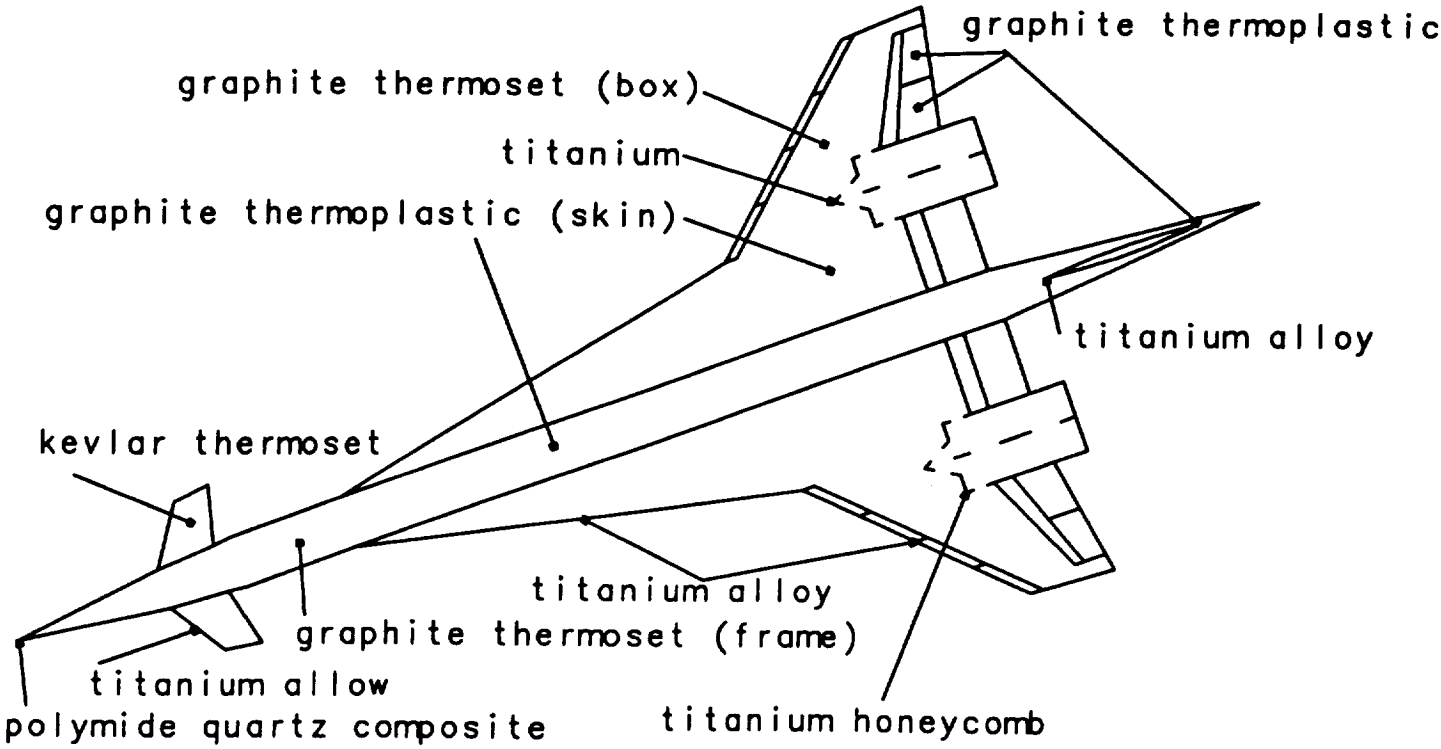

Figure 11.4
Materials placement

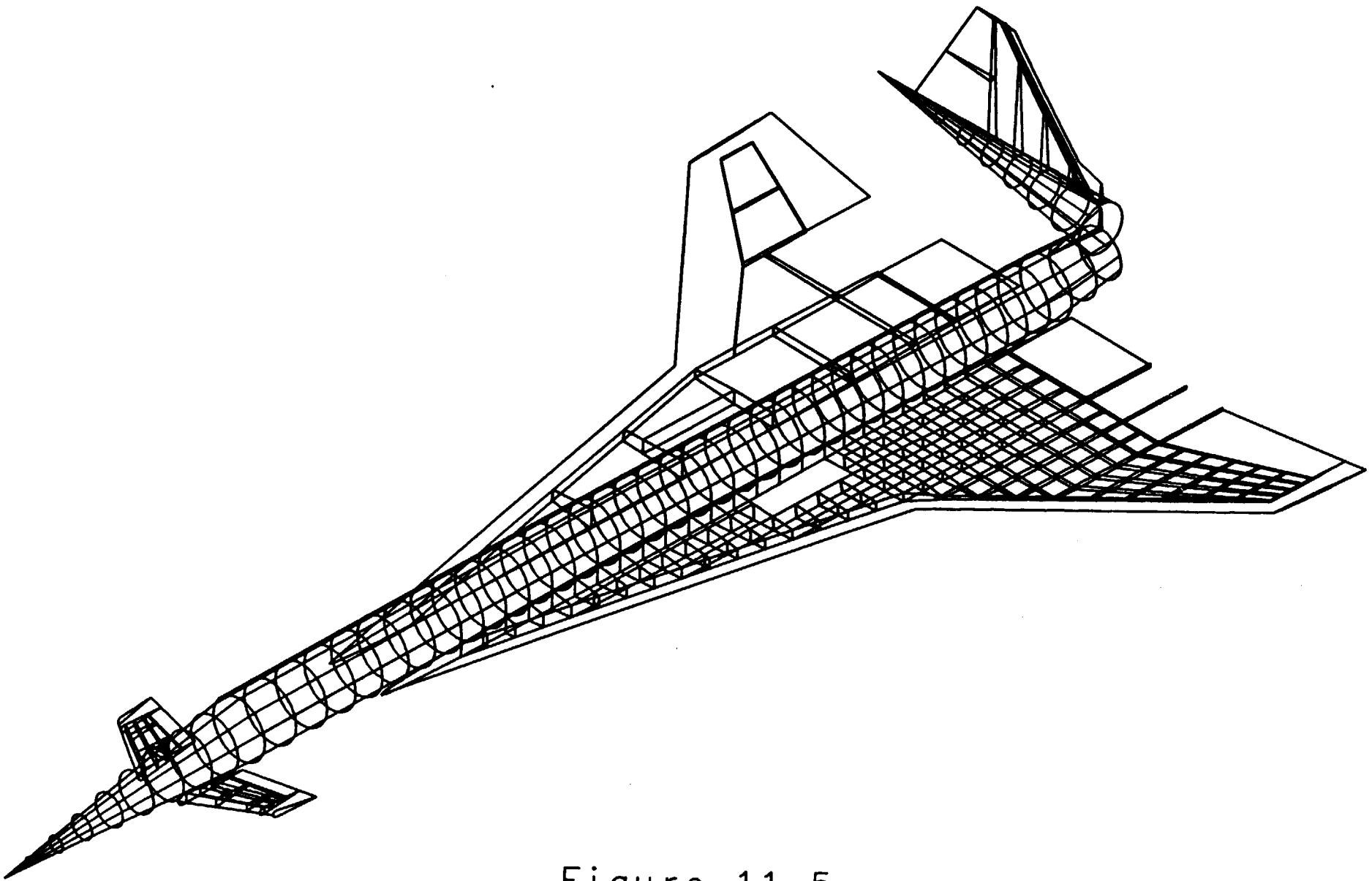

Figure 11.5

12. Aircraft Systems

An important key to ensuring a safe, efficient, and economical flight is the systems package used for the Aeolus. There are 9 major components:

- Flight Control and Avionics
- Electronics
- Fuel Systems
- Environmental Control Systems
- De-Icing and De-Fogging Systems
- Hydraulics and Landing Gear
- Emergency Systems
- Accommodations for Passengers
- Propane Loading and Releasing

Sections 1 through 9 will discuss each topic in detail. Section 10 will discuss the bases for operation.

12.1 Flight Control and Avionics

The Flight Control Systems package is a fully Fly-By-Light system. Compared to the Fly-By-Wire systems commonly used, Fly-By-Light, (FBL) is lighter in weight. Its optical signals require smaller, lighter wiring and allow for less electromagnetic interference (which allows for better shielding form lightning strikes). This system can transmit data at a higher rate (the speed of light) and has fewer components and less maintenance required. There is also no resistance heating in the cabling which eliminates fire hazard and increases the overall efficiency.

The FBL system is quadruple-redundant. The pilot's inputs are sent to four independent channels, located in the primary flight control computer (PFCC), located directly below the cockpit. There they are converted to optical signals which are then sent to Optical Amplifier Systems (OAS) via fiber-optic wires. These inputs are sent at the speed of light. Each input is amplified by the OAS and sent to an electrohydrostatic actuator located on each control surface.

Redundancy is necessary to prevent flight control failure. Although failure cannot be prevented 100%, a quadruple system, consisting of four independent processing computers as well as four independent channels in each computer, can lower the error percentage. The pilot's command is received by the four channels where each branch compares its input to the others to choose the correct command for the control surface. Each pair of channels is manufactured by a different company to prevent failure of all four channels if there was a manufacturing problem. Once a decision is made on the input the signal is then sent to the OAS's, two for each control surface group (the second is used as a back-up). This comes to total of 12 OAS's -- two for the rudder, two for the canards, two for each group of elevons on each wing, and two for the leading edge flaps on each wing. If the PFCC fails the inputs are rerouted to the secondary FCC, located directly aft the nose landing gear in an avionics bay, where the input again is sent to four independent channels. The third and fourth FCC's are located in avionics bays forward and aft of the cargo bays, respectively (Figure 12.1).

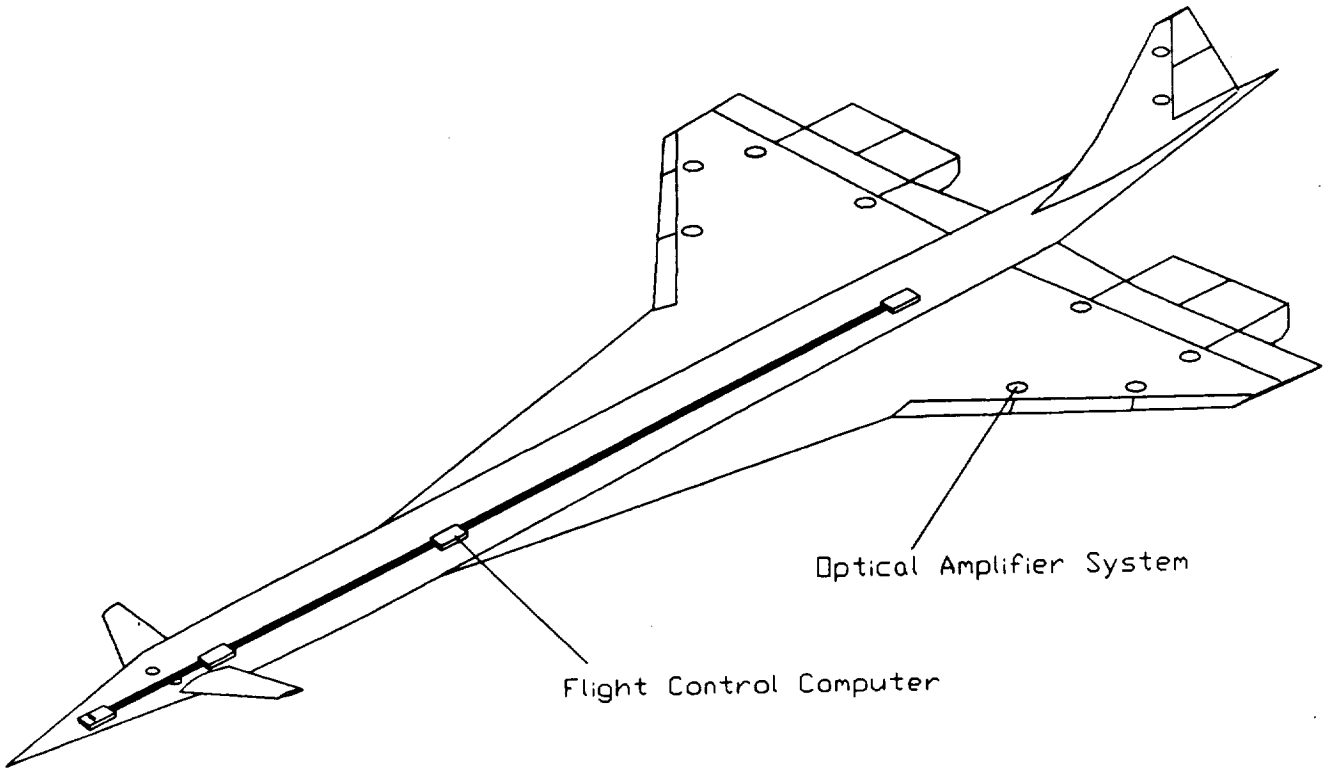

Figure 12.1
Flight Control System Layout

Electrohydrostatic actuators have their own mini-hydraulic system, pump, and motor eliminating the need for large accumulators. Each control surface is split into several parts and has two electrohydrostatic actuators for each part (one as backup). This also allows for redundancy in case both actuators fail for a control surface in a group. The surface deflection is fed back to the PFCC through a feedback loop to ensure that the deflection is equivalent to the pilot's command.

A Gust Alleviation and Stability Augmentation System is included in the flight control package for in-flight attitude disturbances. A sensor placed in the radome independently moves control surfaces to counter the effects of small disturbances and to dampen out any induced oscillatory motion. This system also compensates for weight reduction and cg travel due to fuel consumption by trimming the aircraft as the fuel burns.

A Global Positioning System (GPS) is employed to navigate the aircraft with an Inertial Navigational System (INS) as a backup, an autopilot, an autothrottle, and an autolanding system, each with a backup system. A GPS essentially allows the "autopilot" to navigate the aircraft using satellites to give its position at any point along the flight. An INS works by feeding in required route segments for the entire mission and navigating the airplane for each juncture point. Once a point is reached the autopilot then engages the flight control system to prepare the aircraft to reach the next juncture. At any point during the flight, the pilot may interrupt this process to take control of the aircraft in case of emergency. Also located in avionics is the Fully Automated Digital Engine Control (FADEG) which automatically controls the thrust and power levels during landing.

The cockpit for the Aeolus was designed based on predicted models for futuristic aircraft. The cockpit accommodates a pilot, co-pilot, and two flight crew members. The flight crew will be split into flight engineer and propane engineer for the primary mission, whereas only the flight engineer is necessary for the transport mission. Each pilot has a Multi-Function Display (MFD) with all instrumentation easy to reach and readable under all lighting conditions. Displays are necessary since cameras are needed for landing to allow the pilots to see the runway. The pilots can call a variety of information to the screens including landing gear positions, door ajarment, engine performance, control surface position, fuel levels, weather, radar images, etc. During refueling the pilots can call up a view of the fuel boom with reference to the

plane to make guiding into refueling easier. The propane engineer will be able to observe the release of the propane as well as the temperature and pressure of the tanks. Loading procedures and safety checks may also be monitored at this station. All seats are electronically adjustable and movable for easy access.

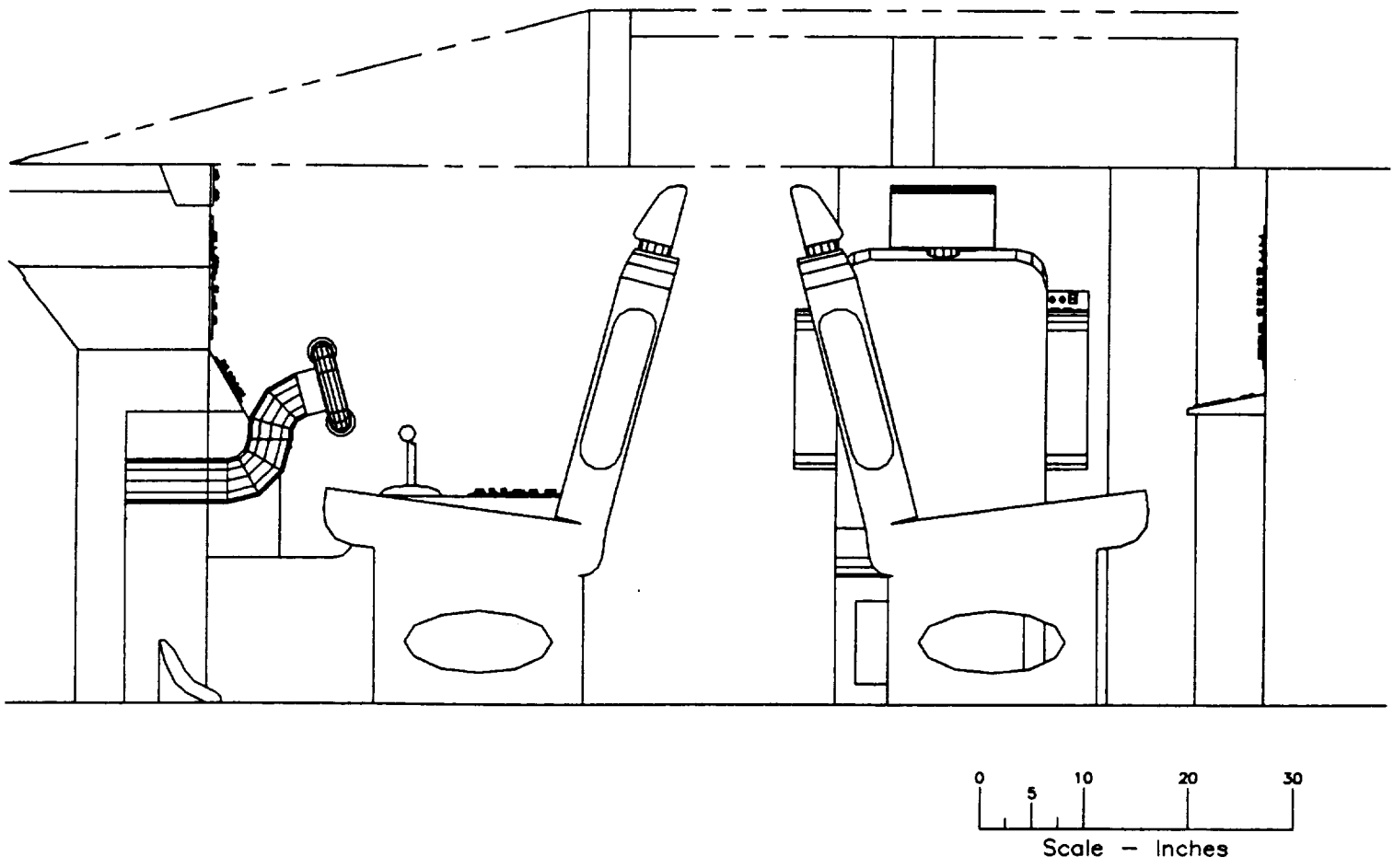

Figure 12.2a
Side View of the Cockpit showing Head Clearance

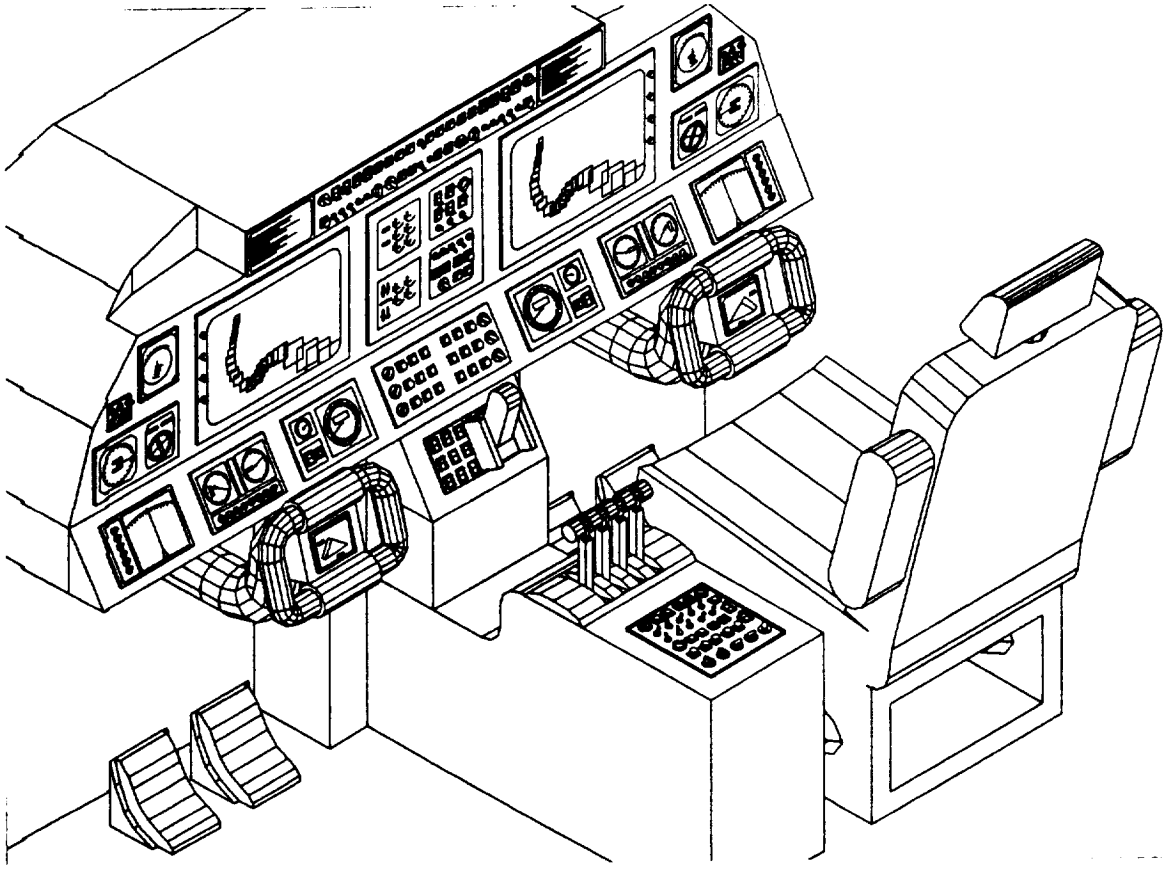

Figure 12.2c Main and Center Console

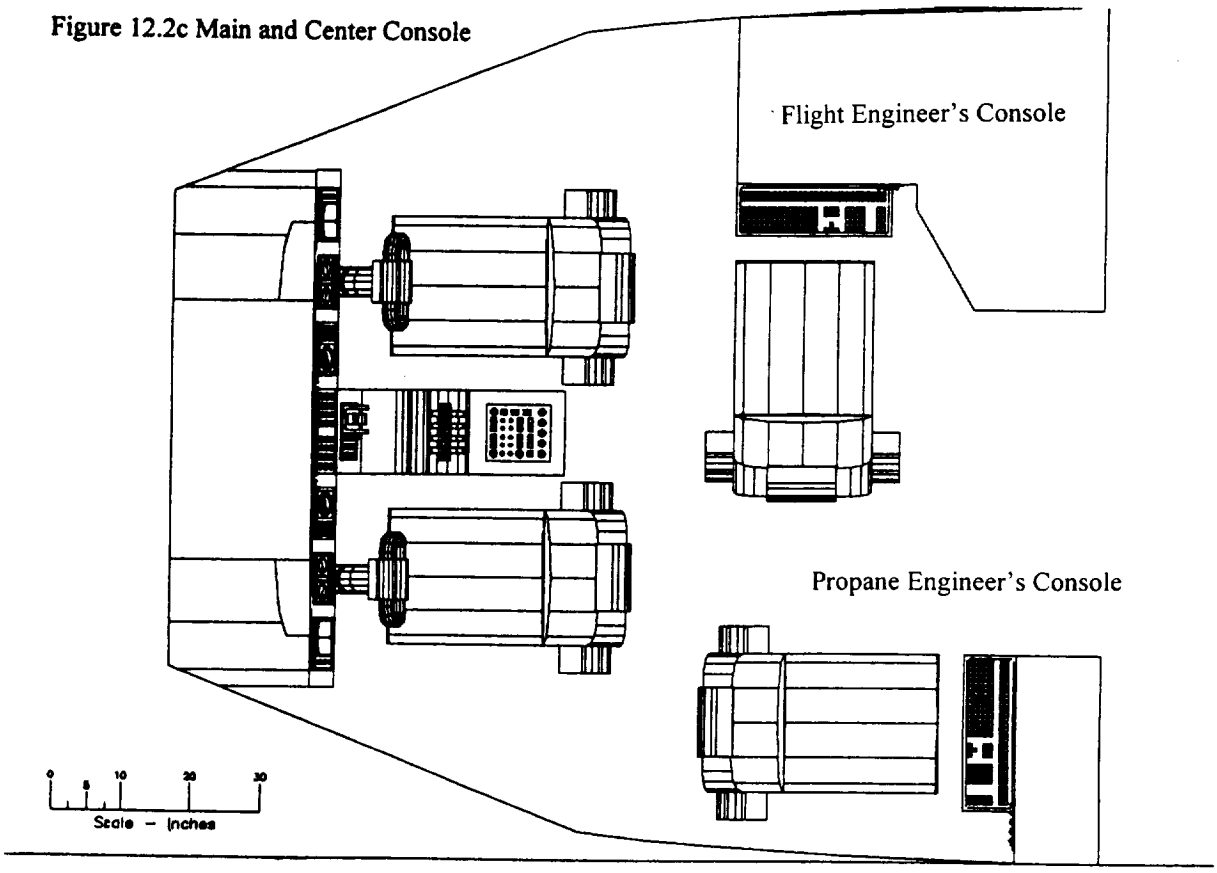

Figure 12.2b Overhead of Cockpit

The following is a list of the elements included in the cockpit:

Multi-Function Displays
- Velocity Vector
- Glidescope
- Flight Director Curve
- Rate of Climb
- Landing Gear Deployment

Status Display
- Terrain and Collision Avoidance
- Navigation
- VHF Omni Range
- Distance Measuring Equipment
- Warning and Caution System
- Central Aural Warning System
- Autopilot Indicators

Top Control Panel
- Engine Controls
- Environmental Control System
- Defense System
- Auxiliary/Lighting/Cockpit Ventilation
- De-Icing/De-fogging Systems
- Fully Automated Digital Engine Control (FADEG) System
- Fuel Management System
- Electrical Systems

Base Panel
- Flight Mode Selector
- Compass
- Diagnostics
- Fuel Management

Side Panels
- Visor Systems
- Fire Suppression System
- Lighting

Center Console
- Communications
- UHF/HF/VHF
- Friend or Foe Indicator/Selective ID Feature
- Line of Sight/SATCOM

Propane Console
- Intercom
- Tank Pressure and Temperature Sensors
- Loading and Attachment Secure Systems
- Exit Nozzle and Propane Release Management System
- Emergency Jettison Exhaust System
- Split Tail Operation

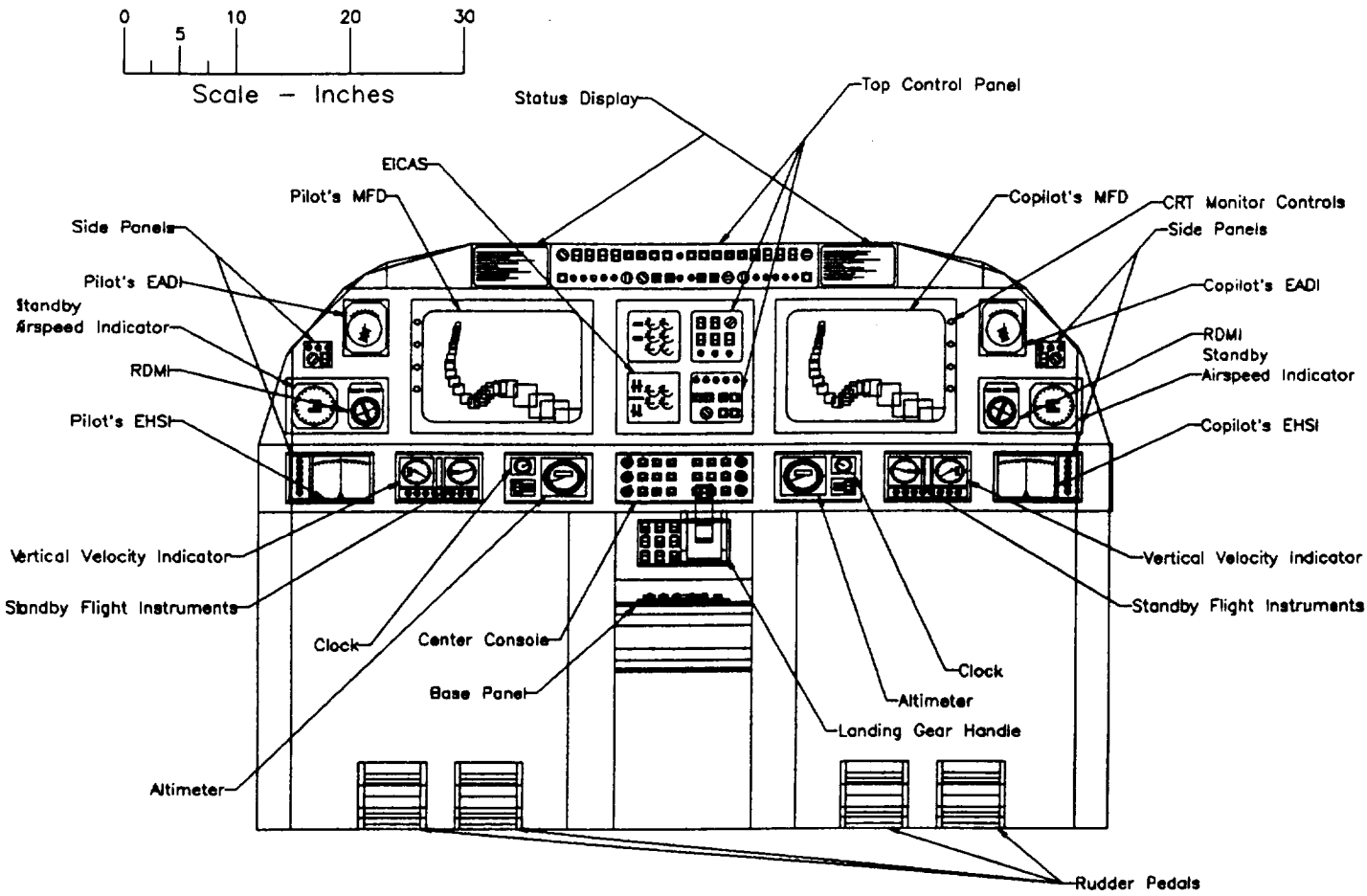

Figure 12.3
Detail of Main Cockpit Console

12.2 Electronics

The electronics system is triple-redundant and provides power for the flight controls, avionics, engine starting systems, heating and cooling systems, transport systems, fuel transfer, and lighting. Primary in-flight power is provided by engine generators with backup power provided by batteries and a Ram Air Turbine (RAT). Ground electronic power is provided by the Auxiliary Power Unit (APU) which can cold start the engines as well as run the air conditioning system on ground to keep the fuel tanks warm or cool (depending on the outside climate).

Batteries are used as a source of secondary power and will immediately come on-line if any electronic system fails. The RAT will be located aft of the last avionics bay and will be deployed due to in-flight failure of the electronics and batteries. The RAT will run a generator that will allow enough power to let the plane return to the nearest airport. The APU itself may be started in-flight by an electrical starter motor which would draw power from the engines.

Exterior lighting is provided by electrical power with landing gear lights at each wing root and two for the nose gear. Anti-collision strobe lights are placed on the fuselage, and left and right navigational lights are located on the wing tips and tail. Landing gear camera lights are located near each gear strut facing forward and aft. Interior lighting is located along the passenger overhead compartments as well as individual lights over each seat. Fuel transfer to and from the tail tank to the wing tanks is necessary for controlling the cg shift (which should move as the ac moves) during supersonic flight. This is electronically driven as well as are the hydraulics that drive landing gear, brakes, nose wheel steering, and flaps.

12.3 Fuel Systems

The fuel tanks have been designed to carry a total of 312,050 lbs of fuel, with 262,050 lbs in the main tanks located in the wings and a 50,000 lb tank in the tail cone, located aft of the double bulkhead. Sump and vent tanks have been placed in the outer areas of the wings. The fuel used is the conventional JP-8, which has a density of 44.3 lb/ft^3. An automatic fuel management system is used as a tank selection system which allows the flight crew to regulate the flow from various tanks to different engines. This system also manages the transfer of fuel from the tail tank to the wing tanks and vice versa. Fuel quantity sensors allow the pilots to know the correct level of fuel in extreme aircraft attitudes. Upon takeoff the tanks will be filled to 287,050 lbs. Taking off without the maximum amount of fuel decreases loads on the landing gear and it is in-flight where the Aeolus will refuel to its maximum capacity. Approximately 70,000 lbs of fuel is utilized from takeoff to the refueling point. A KC -10A is the tanker used for in-flight refueling; this tanker can deliver 200,000 lbs of fuel to delivery vehicles before returning to its base. Since each delivery vehicle will only need to refuel 95,000 lbs, each tanker can refuel two planes safely, with extra fuel to spare in case of emergency. In-flight refueling will occur directly outside the polar vortex for the primary mission while there will be no refueling in-flight for the transport mission.

In-flight refueling will be performed on top of the nose cone using a Universal Aerial Refueling Receptacle-Slipway System (1993/1994 Design Report, p.43) located aft of the radome and ahead of the pressurized cockpit. Fuel lines will then run beneath the cockpit and around the nose wheel well to the main tanks in the wings. The 1993/1994 design team had originally placed the refueling system along the

backbone of the fuselage, but the nose was picked due to safety concerns for the pressurized cabin. Also the pilots will have a better view of the refueling process than if it was to occur behind the cockpit. An alarm will sound once the probe has entered the refueling receptacle to allow the flight engineer to begin the fuel flow. Ground refueling is made possible by a single pressure point located at each wing root for the main tanks which automatically transfers fuel to the tail tank to prepare for takeoff.

12.4 Environmental Control Systems

Engine bleed air is the primary source for the air conditioning and pressurizing systems as well as the cooling systems for the fuel tanks, avionic bays, and wheel wells. Cabin pressure and temperature are set at 8,000 ft and 75^{o} Fahrenheit, respectively. Pressurization changes with altitude are automatic. Backup compressors powered by electronic motors which draw off free stream air can also drive the air conditioning and pressurization systems. Cabin service air is piped into overhead compartments via eight main riser ducts (four forwards and aft of the wing leading edges and trailing edges, respectively), and then onto each individual service nozzle above the seat. Cabin air is recirculated 100% every three minutes. This cooling is also used for the primary mission to keep the propane tanks at a temperature level of about 70^{o} Fahrenheit. Separate ducts direct cooling air to the electronic and avionic bays, flight deck and galleys as well as the wheel wells and fuel tanks. Ground environmental control is provided by the APU.
An auxiliary oxygen system will come on-line due to failure in the pressure system. Oxygen tanks with masks are provided for the flight crew along with individual masks located above each seat for the passengers.

12.5 De-Icing and De-fogging Systems

When ice forms on an aircraft several consequences are expected: an increase in drag, a decrease in lift, and changes in pitching moment. Fortunately flying at supersonic altitudes relieves this problem somewhat since the outer skin will be heated up to temperatures as high as 325^{o} Fahrenheit. Icing is unlikely to occur. However during the subsonic leg of the mission, ice is a potential problem. Therefore de-icing systems have been incorporated into the aircraft's system package.

De-icing systems are located in the nose, wing and tail leading edges, canard leading edges, Pitot sensors, and engine inlets and cowls for the subsonic leg of the primary mission (along with any possibility of ice buildup during takeoff and landing for the transport missions). The system located in the engine cowls and inlets is an electric-thermal de-icing system. This system consists of hot wires in the leading edges of these locations to heat up the areas in order to remove any ice buildup. The other areas mentioned use an electro-impulse de-icing system which sends electrical bursts to the iced area to shatter the ice. Anti-icing systems are used as backup. De-fogging for the windscreen and camera lenses will be provided by hot wires embedded in the glass.

12.6 Hydraulics and Landing Gear

Hydraulics are used for the nose wheel steering, landing gear deployment and retraction, wheel brakes, swinging tail cone, and wing flaps are deployed completely by hydraulics. Landing gear and flap hydraulics are coupled using two accumulators as are the braking and steering hydraulics (one accumulator for backup in each system). The flap hydraulics are doubly redundant, with two actuators for each flap. The swinging tail cone, pivoted at the right side, is opened and closed by a large hydraulic jack located in the dorsal fin of the vertical tail. The tail cone has its own accumulator. The hydraulic systems will be run by the APU on ground and by the electric system in-flight. On ground the APU will be backed up by batteries. As part of the automatic landing system, lowering of the landing gear will turn the APU on and charge the hydraulics for braking and steering. All pumps are 4,000 psi powered.

The landing gears were designed to absorb landing shocks and loads, to allow for ground maneuvering, to provide braking capability, and to protect the ground surface. The 26 wheels are arranged in a tricycle pattern for ground stability and steering, and provide a level floor. All gears retract forward; the main gear retracts into the wings and the nose gear retracts into the center of the fuselage. The nose wheels are arranged in the twin pattern. The main gears are arranged in a quad tandem model to reduce the vertical stowage space occupied by the wheels in the wing.

The tires were chosen from Goodyear tire data sheets and were selected using the following parameters: maximum allowable static load (dynamic load for nose gear), maximum runway speed of at least 200 mph, and the smallest possible diameter (especially for main gears). For the main 24 tires, a static load capacity of no less than 23,500 lbs was determined. The nose gear tires' specifications were determined to be a dynamic load of 33,000 lbs, a runway speed of at least 200 mph, and a minimum diameter. One tire met the requirements for both the nose and main gear tire specifications. The tire selected (29.75 in x 11.5 in, 26 ply, Type McD SCD 32 411504-1) has a maximum static load rating of 25,000 lbs, a dynamic load of 37,500 lbs, a maximum runway speed of 230 mph, a tire pressure of 243 psi, and weighs 66.6 lbs.

Carbon-carbon anti-skid brakes have been chosen for these landing gears as a result of their 40% weight reduction and improved braking capabilities compared to conventional braking, especially on wet or icy runways (Roskam, vol.4, p.61). Designed to have a shock stroke of 34 in. on the main gear and 7 in. on the nose gear (determined by a sink rate of 12 fps, a loading factor of 2.0, and the methods used in Roskam), oleo-pneumatic shocks were employed in the design for their efficiency in energy absorption.

Constructed almost completely from titanium with steel axles the total weight of the landing gears is about 36,000 lbs. The nose gear, steered through its torque links and steering system, is capable of rotating 78^{o} to the left or right. The main bogies can rotate while retracting so that they will remain horizontal when stowed into the wheel well. This allows the bogies and wheels to fit into the wing envelope. Additionally a pivot in the bogie has been placed behind the shock strut, between the second and third row of tires, in order to create a smaller turning radius (157 ft. 10 in.) by translating the plane's ground rotation point off the main landing gear. All landing gears will be contracted after takeoff to fit inside the wheel wells. The nose gear and main gear configurations are shown in the following figures.

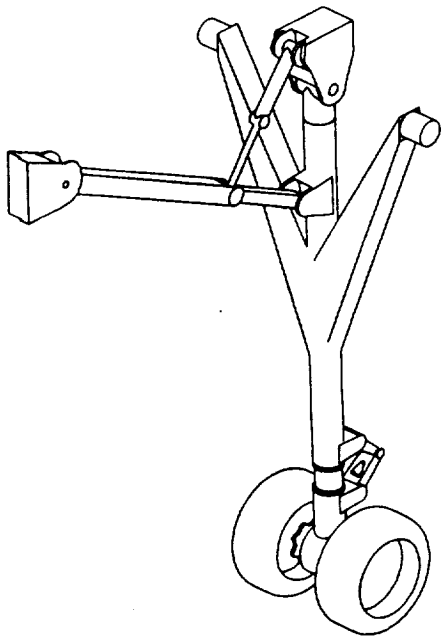

Figure 12.4a
View of Nose Gear

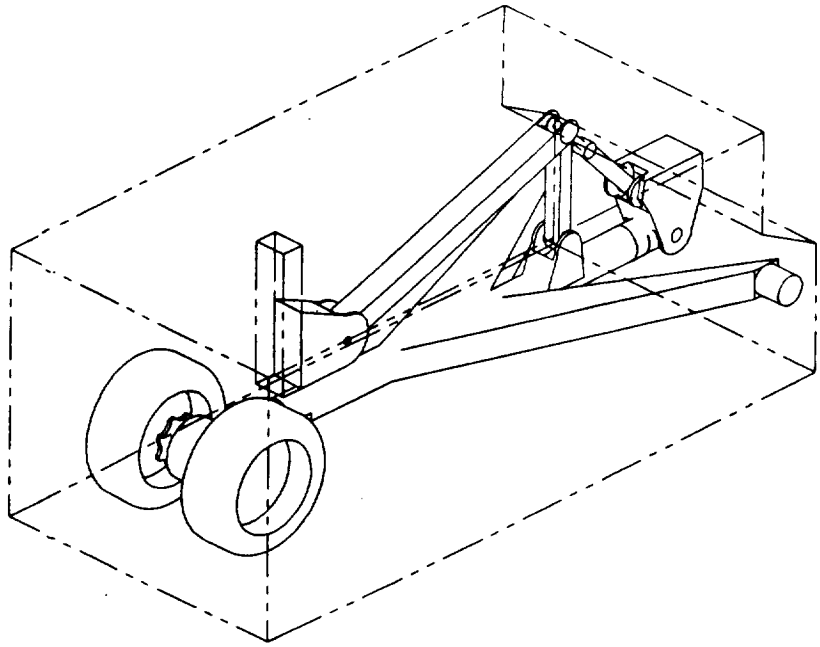

Figure 12.4b
Nose Gear Retracted into the Wing

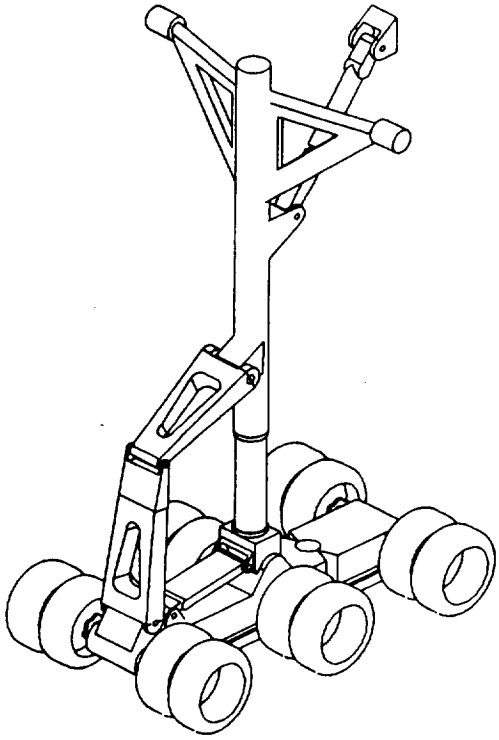

Figure 12.5a
View of Main Gear Stowed in Wing

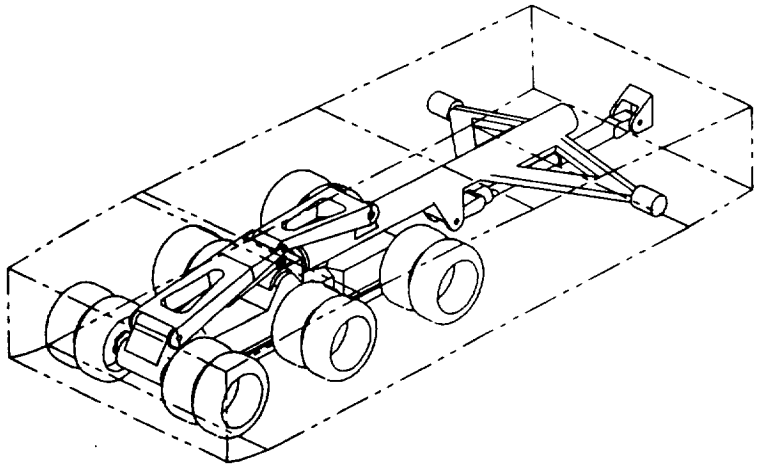

Figure 12.5b
Main Gear Deployed

12.7 Emergency Systems

Emergency exits will be located on both sides of the fuselage for a total of eight exits (Figure 12.6). The doors behind the cockpit will be equipped with inflatable rafts that may also be used as water rafts. Slides are also located in the leading and trailing edges of the strakes and wings, respectively, along side the fuselage. Anti-skid material will be applied near all wing exits to allow passengers to walk safely to the slides. A fire suppression system releases Halon or its future equivalent. Extinguishers are located in all avionic bays, at each engine, in all battery and APU compartments, and in all three galleys.

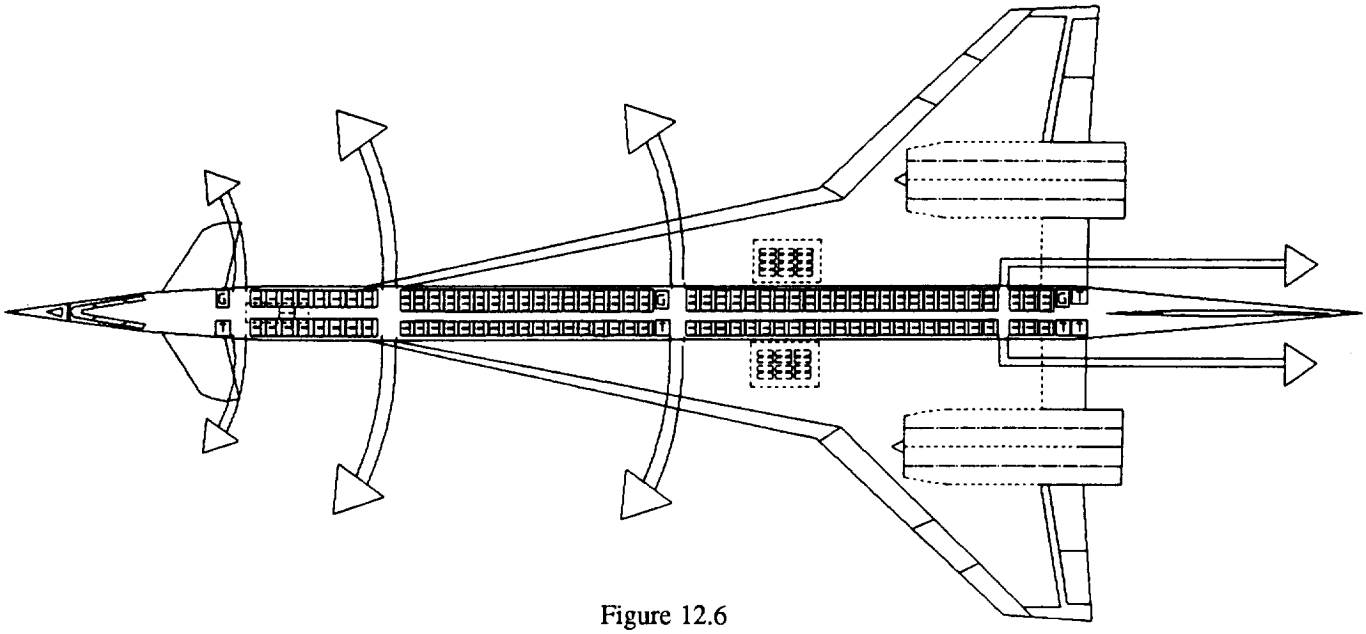

Figure 12.6
Emergency Layout

12.8 Accommodations for Passengers

The Aeolus can comfortably fly 237 passengers and their luggage with 32 in first class and the rest economy, or 244 passengers as an all economy flight. First class will have a window in each aisle. Economy seating will have a window every other aisle. There are three galleys located directly behind the cockpit, midway along the aircraft, and near the tail cone double bulkhead. Five lavatories are located conveniently for passengers and flight crew: one in first class, one midway by the galley and three in the rear of the aircraft. All seats, lavatories, and galleys are removable excluding the first class lavatory and galley. This allows for modification between propane and transport missions by allowing one lavatory and galley for the primary mission flight crew.

12.9 Propane Loading and Releasing

A total of 2.2×10^8 lbs of propane will be released over a three week time period, in the polar vortex. Each plane will perform two operations a day and carry a total payload of 76,162 lbs. The payload consists of 62,620 lbs of propane, evenly distributed into nine cylinder tanks with spherical end caps weighing a total of 4,542 lbs, and the plumbing systems weighing 9,000 lbs. The tank and plumbing weights were taken from the 1993/1994 study. This determines a fleet size of 83 which agrees with the 1993/1994 design team's proposed fleet size. A multiple tank system is utilized to minimize cg shift, to reduce the in-flight stresses on the tanks, and to provide safety in a redundant system. The tail cone opens and closes electronically with the help of a hydraulic jack located in the dorsal fin of the vertical tail. A propane loading attachment (support frame track) will be placed inside the plane after all seats, lavatories, and galleys have been removed, (except for the first class galley and bathroom). Propane ducting and nozzles are then attached to the aircraft. Release nozzles for the propane are located at each wing tip and at the end of the tail cone. Once these modifications are made the next step is to load the tanks.

The tanks will be stacked in a pyramid configuration (three tanks at a time) and placed in a support frame whose outer shell is rigidly fixed to the airframe at one end and is relatively free at the other end in order that the torsional and bending moments of the aircraft are reduced when transferred to the tanks. The tanks and support frame are shown in Figure 12.7. The tanks are loaded, empty, through the tail cone of the aircraft. The tanks are covered with polystyrene to prevent any damage from loading. They are then loaded into the plane using a scissors lift platform to lift the tanks to the heignt of the cabin, inside the plane. The tanks' support frame will be equipped with tracks which move along airframe mounted ball bearings for ease of use (1992/1993 USRA/NASA Design Report, p.39-43). The support frame and tanks are then secured to the airframe. The next pyramid stack is loaded and secured followed by the last pyramid stack. All nine tanks are then filled with propane using check valves to prevent back flow in the lines when the pressure changes.

The total cg of the tanks will be placed at the aircraft's cg. An atmospheric temperature system stores the propane at the atmospheric temperature and a gage pressure of 10 atmospheres in order to keep the propane at approximately 85% liquid state. The release valves are connected to the ducting for the nozzles. The propane engineer will be in the cockpit during this process and will be able to monitor the entire process, from the modification attachments to closing the tail cone. An intercom system allows him to communicate any problems to the loading crew and vice versa. He will also monitor the pressure and temperature of the propane as well as the state of the propane in the tanks throughout the flight. The propane control station is also equipped with an emergency jettison exhaust system and each tank is furnished with a relief valve. If an emergency state were to arise or if the pressure was to increase to more than 1% of 10 atmospheres at any time during flight, an alarm will sound in the cockpit and the emergency system will come on-line. The propane engineer may then activate the system (or deactivate it depending on the situation) and the propane may be prematurely released.

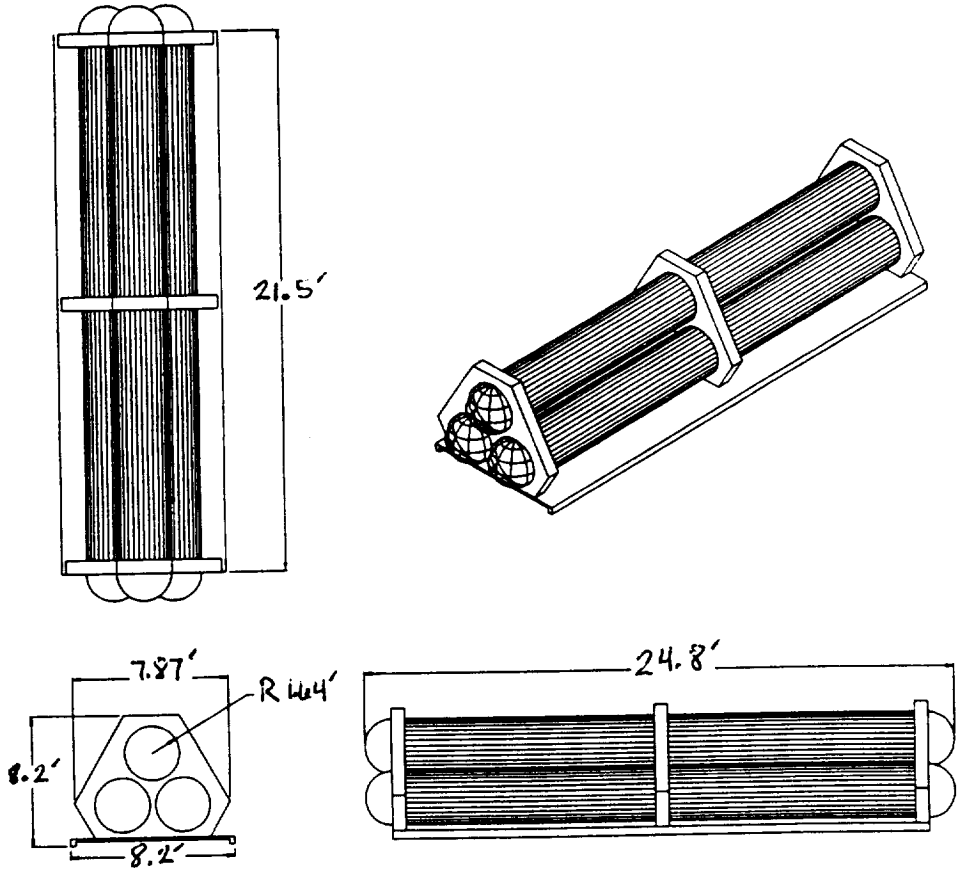

Figure 12.7
Propane Storage Tanks and Support System
From: 1993/1994 NASA/USRA Design Report - adapted from 1992/1993 Design Report

The tanks are made from a graphite/epoxy composite and are 24.8 ft long with a radius of 1.64 ft and a wall thickness of 1.81×10^{-2} in. The density of the tank material is 96.5 lb/ft^3. The propane tanks and support system were designed by the 1992/1993 design team. The 1993/1994 design team decided to release the propane through one exit nozzle with a diameter of 15.75 in. However placing such a large nozzle on the aircraft produced a problem; the only location that would allow such a large extruding component would be the tail cone. This location would demand a split tail cone which created unnecessary complication by adding extra actuators, more weight, and the possibility of jamming or failure of the actuators. Therefore the nozzle has been split into three smaller nozzles. A nozzle will be located at each wing tip and a larger nozzle will be located at the tail cone. The wing tip nozzles have a diameter of 4.75 in. A length of 3.0 ft of the tail cone will be removed and the exit nozzle (with a diameter of 6.25 in) will be attached to the propane delivery pipe inside (aft of the tail cone fuel tank). The delivery pipe is permanently fixed inside the tai cone as are the pipes inside the wings leading to the tip exit nozzles (Figure 12.8).

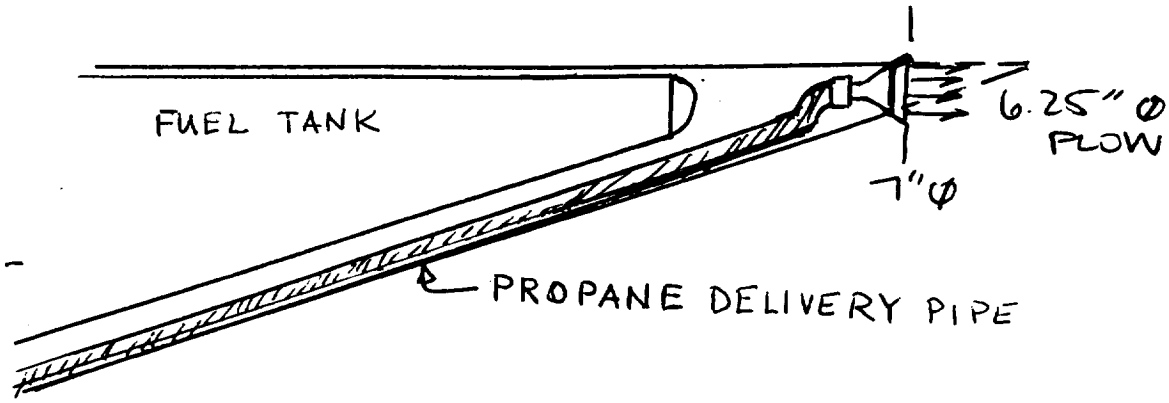

Figure 12.8
Tail Cone with Tip Removed and Nozzle Attached

The base area of the nozzle (30.68 in^2) should be small enough to lay inside the boundary layer wake of the 300 ft fuselage allowing almost little or no drag to ensue. The turbulence in the wake will aid in the integration of the propane with the polar air. Vortex flow at the tips of the wings will also help integrate the propane into the atmosphere. The forward three tanks will be connected to the tip nozzles while the other six tanks will be connected to the tail cone nozzle. A 3.6 ppbv concentration must be achieved for the propane delivery to be feasible. The nozzles will be variable geometry to ensure that the release rate of the propane is exact. All nozzles will be covered with swirl vanes to assist in the mixing of the propane with the atmosphere and flame arrestors to protect any possibility of ignition of the propane due to jet exhaust (Figure 12.9).

In-flight propane flow control is regulated with a series of pipes and valves. The pipes through which the propane is loaded and unloaded are aluminum. Each of the nine tanks are individually connected to a settling chamber with a butterfly valve to maintain a constant pressure. This valve throttles the propane release as needed and is used in the emergency jettison system. The tanks loaded inside the aircraft are shown in Figure 12.10.

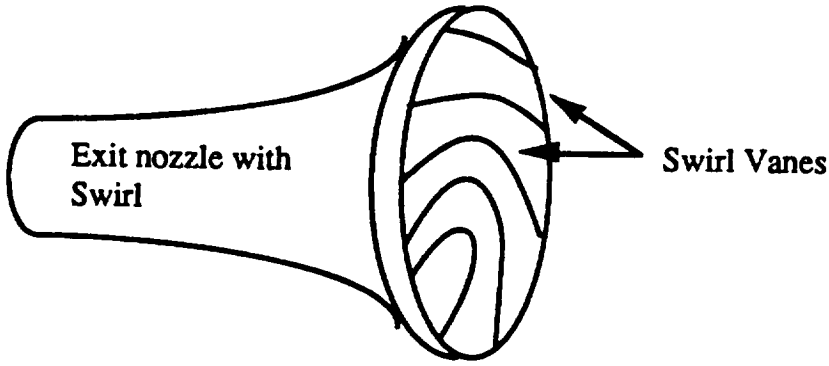

Figure 12.9
Swirl Vanes on Nozzle
(From: 1993/1994 NASA/USRA Design Report - adapted from 1992/1993 Design Report)

Figure 12.10
Propane Configuration

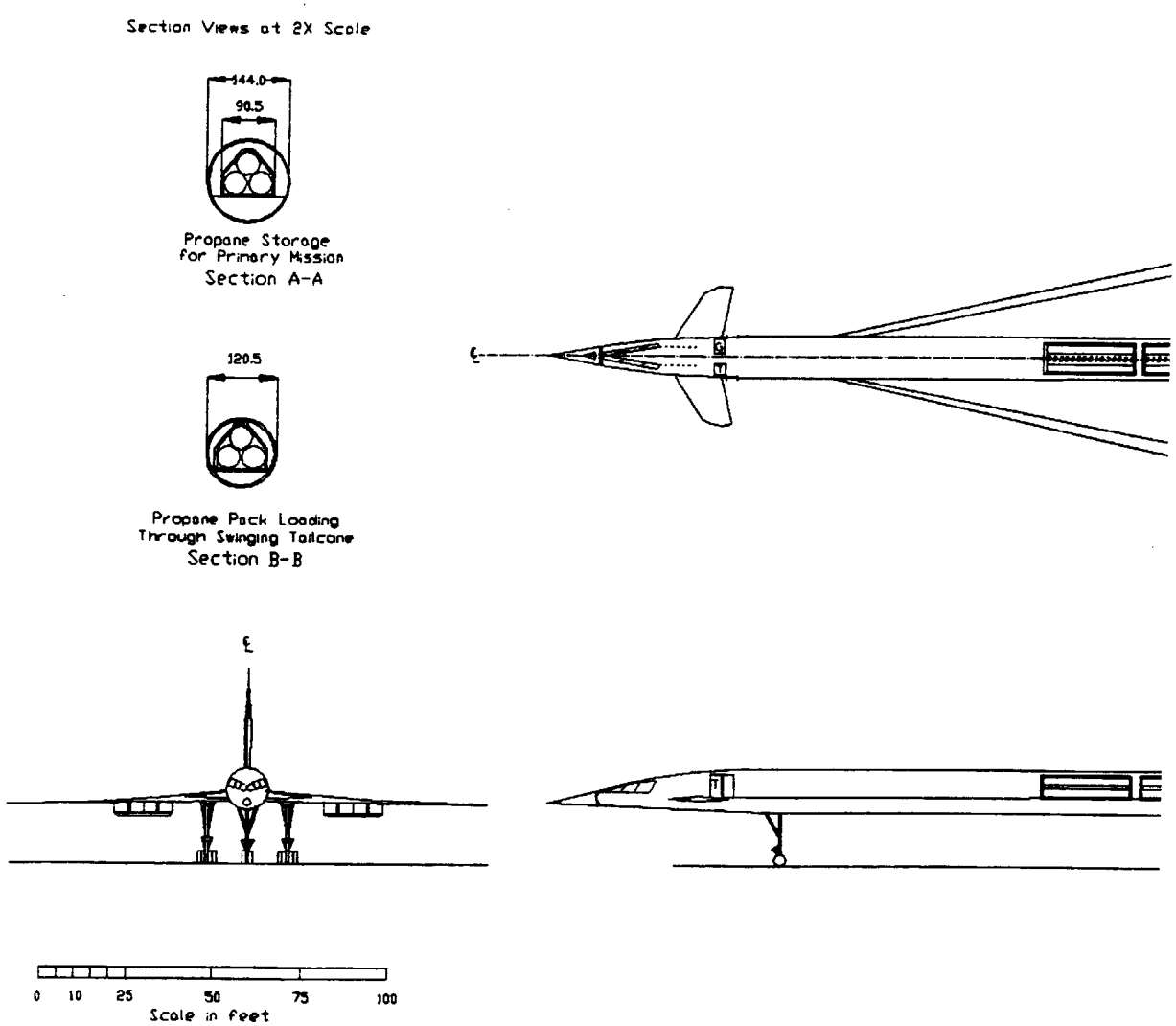

12.10 Bases of Operation

The bases of operation for the Aeolus and the refueling tankers were studied and decided upon by the 1993/1994 design team. A total of 9 airports were investigated in locations of southern South America, Africa, and Australia. Due to their close proximity the airports were narrowed down to those located in South America with the possibility of an emergency landing in Australia or New Zealand. Since the Aeolus required a landing field length of at least 10,000 ft, the Rio Gallegos airport was chosen as its base. It has a field length of 11,650 ft. A separate airport in Buenos Aires was chosen as the base for the tanker operations since having all operations out of one airport would disrupt the normal airport schedule. In the evnt of an in-flight emergency on the far side of the polar vortex, the Aeolus could abort the return leg of the delivery run and divert to one of the alternate airports located in Christchurch, New Zealand and Avalon, Australia. A large amount of storage space is necessary for the storage of the propane and this space may be limited by safety reasons to areas far from airport facilities. Therefore it is necessary to truck the propane in from a remote storage facility outside of the airport base. A facility may be built for this storage if one is not available.

13.0 Weights

One of the primary objectives in the design of the Aeolus was to minimize the takeoff gross weight (TOGW). Although weight reductions do induce some initial cost penalty, the savings in the total operating cost outweigh these penalties in the long run. To minimize the TOGW certain areas were considered for weight reduction:

- Wing
- Fuselage
- Empennage
- Engines
- Fixed Equipment
- Landing Gear

Examples of weight reduction include the use of composites on the wings, fuselage, and empennage (approximately 60%), ceramics for engine materials, a Fly-By-Light flight control system, and carbon brakes. Table 13.1 lists the main weight values used for cost feasibility.

	Weight (lbs)
Empty Weight	184705
Operating Weight	192124
Fuel Weight	300000
Maximum TOGW	604711

Table 13.1
Cost Related Weights

The horizontal and vertical centers of gravity (cg) are determined from the following formulas:

$$X_{cg} = \frac{\sum x_i W_i}{\sum W_i} \quad Z_{cg} = \frac{\sum z_i W_i}{\sum W_i}$$

The horizontal and vertical locations of the aircraft components are taken from the nose and ground, respectively. Table 13.2 lists the components' weights and cg locations. The weights are taken from ACSYNT and the cg locations were computed using a PASCAL program written specifically to compute cg.

Component	Weight (lbs)	Xcg(ft)	Zcg(ft)
Airframe Structure			
Wing	31530	196.7	16.5
Fuselage	15665	150.0	18.0
Vertical Tail	1131	277.9	36.1
Canard	1205	44.3	16.5
Nacelles	14502	206.6	16.0
Landing Gear (retracted)	3600	174.6	16.5
Propulsion			
Engines	62080	226.2	16.0
Fuel System	6800	206.2	16.3
Fixed Equipment			
Hydraulics	2540	172.1	17.6
Electrical	2884	24.6	15.0
Avionics	1358	49.2	15.0
Instrumentation	771	19.7	20.1
De-Icing & Air Cond.	2599	177.0	16.5
APU	1250	230.0	16.0
Furnishings & Equipment			
Seats	8423	157.4	17.3
Cockpit	205	24.6	20.1
Cabin Finishing	4930	147.5	18.3
Cabin Emergency Eqpt	896	147.5	21.95
Flight Controls	4439	32.1	15.8
Operating Items			
Flight Crew	680	24.6	20.1
Crew Baggage	375	150.8	16.2
Flight Attendants	1040	152.5	20.4
Passenger Service	5394	151.3	19.5
Fuel	287050	200.3	16.5
Payload	76162	185.3	17.6
Passengers	40290	163.3	19.08
Baggage	9580	164.2	13.3

Table 13.2
Weights and CG Locations for Aircraft Components

As fuel is consumed the plane's center of gravity moves. The cg is also shifted aft during supersonic flight to correspond with the supersonic ac location. The pressure profile over the wing during supersonic flight is different from the profile during subsonic flight and ultimately the ac is shifted back. Therefore the cg must also be shifted back in order for the plane to be neutrally stable. This is done by utilizing the automatic fuel management system previously discussed. The following figure is the path the cg travels throughout the primary mission. These locations were computed using ACSYNT analysis.

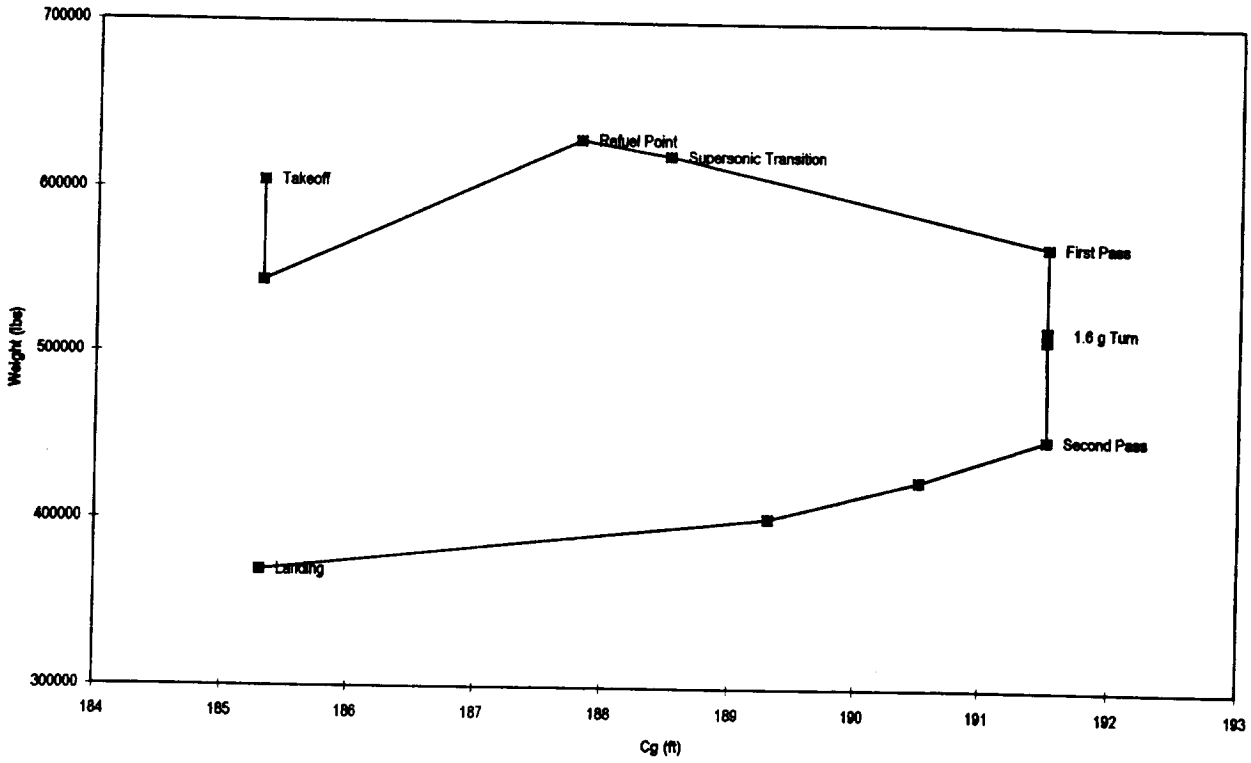

Figure 13.1
Plot of the CG Locations Throughout the Propane Mission

14. Cost

The future of the Aeolus concept depends on its economic viability. The primary mission, in order to be successful must be combined with a profitable secondary mission. The most profitable secondary mission for this concept is as a high-speed commercial transport. Many factors are involved in determining the cost of the Aeolus concept, including; passenger load, aircraft range, manufacture of materials, and engine choice. The quantitative cost analysis was conducted using ACSYNT. The total number of aircraft to be built was equivalent to the number needed for the primary mission, 86. The analysis was done using equilvalent 2005 dollars.

14.1 Determination of Cost

The Aeolus concept was sized to be a profitable commercial transport. It can carry a two class passenger load totaling 237 people. The forward located first class section has 28 seats, while the economy class section contains up to 205 seats. The cost of tickets on the Aeolus aircraft must be competative with travel on subsonic transports.

The Aeolus has an unfrefueled range of 5500 nmi with a full passenger payload. This range is adequate for either a trans-Atlantic or a trans-Pacific crossing. Thus the Aeolus could cover the routes of its subsonic competators.

The Aeolus concept contains a large percentage of composite materials, about 60% of the aircraft. This large amount of composites was necessary to reduce the aircraft weight while maintaining structural integrity. These materials presently cost a great deal more than traditional aircraft materials to manufacture, but by the time the Aeolus reaches the production stage, the use of large amounts of composites in aircraft will be commonplace.

The engine choice for the Aeolus was based both on performance and emissions. The mid-tandem turbofan (MTF) engine was chosen for its capabilities in both of these areas. The initial cost of the MTF will be high. Since it is still in the developmental stages, further research and testing will also be costly. But after the final development and testing stages have been completed, the MTF will be less expensive.

The composites that make up much of the engine will also be initially more expensive. This engine will, however, prove cost effective in the long run due to its long life and environmental soundness.

14.2 ACSYNT Cost Analysis

ACSYNT determined the cost of the Aeolus program. Factors were weighted in an input file to calculate the costs of various stages of the Aeolus development. These factors include material technology, research and testing programs, delivery and commercial profits. The material technology factors reflected the increase in manufacturing cost with an increase in the use of composites. The research and testing factors included number of research hours, engineering hours, tooling and manufacturing hours, and the cost of the labor involved in these processes. One vehicle was set to be built for ground testing, while two aircraft will be used for flight testing. Table 14.1 shows the breakdown of the research and development costs.

A production and delivery scheme was also devised by ACSYNT and is shown in Figure 14.2. It calls for a research and development phase of five years, followed by the production of aircraft at a rate of approximately 0.9 per month. This production schedule, along with a per unit aircraft price of $975.652 million gives a net cashflow at the end of 15 years of 22995.9 million dollars. This cost per aircraft also gives a breakeven unit number of 76 aircraft. With an aircraft price of 780.521 million dollars per unit, breakeven was never achieved and the manufacturers suffered a loss of 10566.492 million dollars. At a cost of 1170.782 million dollars per aircraft brought a breakeven point of 53 units and a profit of 22995.9 million dollars. The chosen aircraft price was in the middle of these two extremes and brought a profit of 6214.859 million dollars. The final cost statistics for this analysis were:

TOTAL COST	(86. aircraft)	83906.633
AVERAGE UNIT AIRPLANE COST	(including spares)	975.659
AVERAGE UNIT AIRPLANE COST	(excluding spares)	912.107

DEVELOPMENT PHASE	Cost (in millions)
RESEARCH,DEVELOPMENT,TEST,AND EVALUATION	39992.262
AIRFRAME DEVELOPMENT (Eng. labor $70./hr)	2254.166
CONCEPT FORMULATION (150. man-yrs)	16.380
CONTRACT DEFINITION (500. man-yrs)	72.800
AIRFRAME ENGINEERING (14869. man-yrs)	2164.986
SUBSYSTEMS DEVELOPMENT	4139.273
AVIONICS DEVELOPMENT (1.00x Factor)	3185.572
PROPULSION DEVELOPMENT (55.% Spares)	23061.625
DEVELOPMENT SUPPORT	4389.237
GROUND TEST VEHICLES (1. aircraft)	643.993
GROUND TEST SPARES (10.0% of GTV)	64.399
FLIGHT TEST SPARES (20.0% of FTV)	386.854
TOOLING EQUIPMENT (Tooling labor $65./hr)	1511.831
FLIGHT TEST OPERATIONS (2. aircraft)	1340.625
GROUND SUPPORT EQUIPMENT	402.849
TECHNICAL DATA	38.685
FEE (8.0% profit)	2962.390

Table 14.1
Research and Development Cost Breakdown

Year	Production Rate	Cumulative Deliveries	R&D Cost	Manufacturing Cost	Sustaining Cost	Income	Net Cashflow
2005	0.	0.	4612.3	0.	0.	242.3	-4370.1
2006	0.	0.	7007.1	0.	0.	388.3	-6618.8
2007	0.	0.	8104.4	0.	0.	782.7	-7321.7
2008	0.	0.	8104.4	0.	0.	1192.3	-6912.1
2009	0.	0.	8104.4	2106.2	1344.1	1644.9	-9909.8
2010	4.3	4.3	1097.3	2419.4	2174.0	5715.3	24.6
2011	4.3	8.6	0.	2577.8	1696.5	5222.1	947.8
2012	8.6	17.2	0.	3320.7	1827.5	9111.1	3962.9
2013	10.8	27.9	0.	3219.5	1582.5	9833.1	5031.1
2014	10.8	38.7	0.	2933.6	1355.6	10367.5	6078.3
2015	10.8	49.4	0.	2738.8	1222.5	9891.0	5929.7
2016	10.8	60.2	0.	2557.2	1118.9	9461.0	5784.9
2017	10.8	70.9	0.	2194.1	949.6	8286.4	5142.8
2018	8.6	79.5	0.	1643.3	707.1	7154.8	4804.4
2019	6.5	86.	0.	680.4	292.1	4613.4	3640.8
Totals		86.0	37029.9	26391.1	14270.3	83906.1	6214.9

Production Size = 86.

Aircraft Unit Cost = $975.652 million

Table 14.2
Production and Delivery Schedule and Costs

1.6-G Turn Analysis

Inputs:

W=604,711 lb

h=66,000 ft

V=2325 ft/sec.

$$V = Ma = 2.4(968.644) = 2324.7456 \text{ft / sec.}$$

q=457.7 $^{slug}/_{ft\ sec.^2}$

$$q = \tfrac{1}{2}\rho V^2 = 0.5(.00016938)(2325)^2 = 457.7 \text{slug/ftsec.}^2$$

S=9950 ft^2

g=32.2 $^{ft}/_{sec.^2}$

k=0.353

C_{Do}=0.005812

sfc=1.3 $^{1}/_{hr}$

Equations:

Evaluated at n=1.6

$$R = \frac{V^2}{g\left[\tan(\arccos(1/n))\right]} = \frac{2325^2}{32.2\left[\tan(\arccos(1/1.6))\right]} = 134379\text{ft}$$

$$D = \pi R = (3.14)(134379) = 422165\text{ft}$$

$$\text{Time} = \frac{D}{V} = \frac{422165}{2325} = 181.6\text{sec.}$$

$$\text{lift} = nW = (1.6)(604711) = 967538\text{lb}$$

$$C_l = \frac{\text{lift}}{qS} = \frac{967538}{(457.7)(9950)} = 0.212452$$

$$C_d = C_{D_o} + kC_l^2 = 0.005812 + (0.353)(0.212452)^2 = 0.21745$$

$$T_{req'd} = C_d qS = (.021745)(457.7)(9950) = 99030\text{lb}$$

$$\text{mfr} = \frac{T_{req'd}\,\text{sfc}}{3600} = \frac{(99030)(1.3)}{3600} = 35.761\text{lb/sec.}$$

$$\text{fuel} = (\text{mfr})\text{Time} = (35.761)(181.6)6494.0\text{lb}$$

References

Bunker, D., et al, *Design of a Vehicle Based System to Prevent Ozone Loss*, 1992/1993 NASA/USRA

Carlson, H.W. and Mann, M.J.,*Survey and Analysis of Research on Supersonic Drag-Due-to-Lift Minimization With Recommendations for Wing Design*, NASA Technical Paper 3202, Sept. 1992

Chipperfield, M., "Satellite Maps Ozone Destroyer, " *Nature*, Vol. 362, Apr. 15, 1993, p.592.

Cicerone, R.J., S. Elliott, and R.P. Turco, "Reduced Antarctic Ozone Depletions in a Model with Hydrocarbon Injections," *Science*, Vol. 254, Nov. 22, 1991, pp. 1991-1194.

Dornheim, Michael, "Atmospheric Tests, Models Show Little SST Ozone Loss," *Aviation Week & Space Technology*, Nov. 21, 1994, pp.88-89.
Design Team

Eby, S., et al, *Design of a Vehicle Based System to Prevent Ozone Loss*, 1993/1994 NASA/USRA Design Team.

Einthoven, P., *Aircraft Handling Qualities Evaluation Software - Background and User's Guide*, Depaertment of Aerospace and Ocean Engineering, Virginia Polytechnic Institute and State University, 1994

Etkin, B., *Dynamics of Flight - Stability and Control, 2nd Edition*, John Wiley & Sons, 1982.

Guynn, M., *Aerodynamic Preliminary Analysis System - Beginner's Guide*, NASA Langley Research Center.

Hamill, P. and O. Toon, "Polar Stratospheric Clouds and Ozone Hole," *Physics Today*, Vol. 44, Dec. 1991, pp. 34-39.

Hamlyon, Christopher O., *The Concorde Story*, p. 121.

Kandebo, Stanley W., "High-Speed Propulsion Effort to Narrow Focus," *Aviation Week and Space Technology*, Nov. 21, 1994, pp. 71-72, 74.

Kandebo, Stanley W., "HSCT Engine Research Makes Steady Gains," *Aviation Week and Space Technology*, Sept. 13, 1993, pp. 46-47, 50.

Kandebo, Stanley W., "U.S., Europe Select HSCT Engine Concepts," *Aviation Week and Space Technology*, Nov. 8, 1993, pp. 22-23.

Kawa, S. R., D. W. Fahey, L. E. Heidt, W. H. Pollock, S. Solomon, D. E. Anderson, M. Lowenstein, M. H. Proffitt, J. J. Margitan, and K. R. Chan, "Photochemical Partitioning of the Reactive Nitrogen and Chlorine Reservoirs in the High-Latitude Stratosphere", *Journal of Geophysical Research*, Vol. 97, No. D8, May 30,1992.

Kay, Jacob, "A Review of the Stratospheric Ozone Depletion Problem and Considerations for the Development of Vehicle-Based Intervention Schemes," USRA Summer Inter, Virginia Polytechnic Institute and State University, Aug. 24, 1992.

Kay, J. et. al., *Control Authority Issues in Aircraft Conceptual Design : Critical Conditions, Estimation Methodology, Spreadsheet Assessment, Trim and Blibliography*, VPI-Aero-200 Report, Department of Aerospace and Ocean Engineering, Virginia Polytechnic Intstitute and State University, 1993

Kuchemann, D., *The Aerodynamic Design of Aircraft,* Pergamon Press, 1978. pp 404 - 405.

Lipske, Michael, "Living Under an Angry Sun," *National Wildlife*, Aug./Sept. 1992, Vol. 30, pp.30-34.

Mattingly, Jack D., *On-Design and Off-Design Cycle Analysis Computer Program,* ONX and OFFX User Guide.

Myklebust, Arvid. "Putting the ACSYNT on Aircraft Design." Aerospace America. Sept. 1994: p26-30.

NASA Contractor Report 4233, *High-Speed Civil Transport Study*, Prepared for Langely Research Center by Boeing Commercial Airplanes, Seattle, Washington, Sept. 1989.

NASA Headquarters Office of Aeronautics and Space Technology, "High-Speed Transports: No Noisy Neighbors," Washington, DC 20546, pp. 24-25.

NASA Headquarters Office of Aeronautics and Space Technology, "Technology Advances to Protect the Environment," Washington, DC 20546, p. 29.

NASA Headquarters Office of Aeronautics and Space Technology, "Tomorrow's Engines-A Material Issue," Washington, DC 20546, p. 28.

NASA Headquarters Office of Aeronautics and Space Technology, "Ultra-Low NO_X Emissions," Washington, DC 20546, p. 27.

NASA/USRA, Undergraduate Design Team, "Design of a Vehicle Based System to Prevent Ozone Loss," Virginia Polytechnic Institute and State University, Blacksburg, VA, 1994.

Newaz, Golam M., "Advanced Thermoplastic Composites." ASTM Standardization News, Vol. 15, Number 10, Oct. 1987.

Noor, Ahmed K., "Structures." Aerospace America, Dec. 1993.

ONERA, Wind Tunnel Data on Concorde., Poisson-Quinton.

Phillips, Edward H., "NASA Research Program Directed at Reducing Supersonic Transport Noise," *Aviation Week and Space Technology*, Nov. 25, 1991, pp. 69-72.

Poisson-Quinton, Philippe. "Future SST's. A European Approach." Aerospace America. Sept. 1994.

Prather, M. and R. Watson, "Stratospheric Ozone Depletion and Future Levels of Atmospheric Chlorine and Bromide," *Nature*, Vol. 344, Apr. 19, 1990, pp.729-731.

Prellisch, Richard, "Mach 2 and More." Aerospace America, Jan. 1994.

Raymer, D.P., *Aircraft Design: A Conceptual Approach,* AIAA Education Series, 1989 pp. 257-300.

Razgonyaev, V. and Mason, W.H., "An Evaluation of Aerodynamic Prediction Methods Applied to the XB-70 for Use in High Speed Aircraft Stability and Control System Design," AIAA Paper 95-0759, American Institute of Aeronautics and Astronautics, 1995.

Roskam, J., Dr., *Airplane Design Part I: Airrplane Flight Dynamics and Automatic Flight Controls.* Roskam Aviation and Engineering Cp, Ottawa, 1994.

Roskam, J., Dr., *Airplane Design Part IV: Layout Design of Landing Gear and Systems*, 1986.

Sforza, P.M., "Aircraft Vortices: Benign or Baleful?", *Space/Aeronautics,* April 1970.

Sova, G. and Divan, P., *Aerodynamic Preliminary Analysis System II, Part II User's Manual,* North American Aircraft Operations, Rockwell International.

Stratoshperic Ozone, 1st Report, United Kingdom Stratopheric Ozone Review Group, 1987.

Stevens, B.L. and Lewis, F.L., *Aircraft Control and Simulation,* John Wiley & Sons, 1982.

Svitil, Kathy, "Holey War," *Discover,* Jan. 1993, Vol. 14, pp.75-76.

Talbot, J. E., "Aerodynamics of Power Plant Installations," *Supersonic Engineering,* 1962, pp. 143-150.

Torenbeek, Egbert. Synthesis of Subsonic Airplane Design. Kluwer Academic Publishers, Dordrecht, the Netherlands. 1982, p 75.

Wayne, Richard P., *Chemistry of Atmosphere 2nd Ed.,* Clarendon Press: Oxford, 1991.

Zurer, Pamela, "Ozone Depletion's Recurring Surprises Challenge Atmospheric Scientists," *Chemical & Engineering News,* Vol. 71, May 24, 1993, pp.8-11.

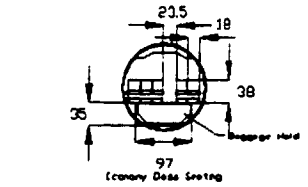

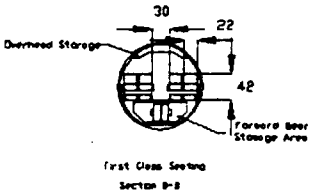

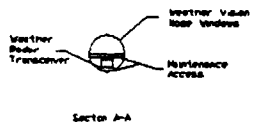

Section Views at Double Scale
Dimensions in Inches

① Unpressurized nose section & Radome
② Front pressure bulkhead
③ Movable canard
④ Forward landing gear and stowage area
⑤ Stroke
⑥ Main landing gear and stowage area
⑦ Subsonic Aerodynamic Center
⑧ CG
⑨ Leading edge flaps
⑩ Ailerons
⑪ Flaperons
⑫ Elevator / Flap
⑬ Engines - two per pod
⑭ Back-to-Back Bulkheads
⑮ Vertical Tail
⑯ Rudder
⑰ Tail wheel at max stroke
⑱ Cargo bay doors (2 each side)
⑲ Passenger doors (8)
⑳ Refueling Receptacle
㉑ Four crew cock
㉒ Galley (3)
㉓ Toilet facilities
㉔ Cargo Bays and stowage
㉕ Overhead stora
㉖ Lift Dumpers
㉗ Swinging Tailcone

32 First Class Sea
40 inch pitch
205 Economy Class
@ 32 inch pitch

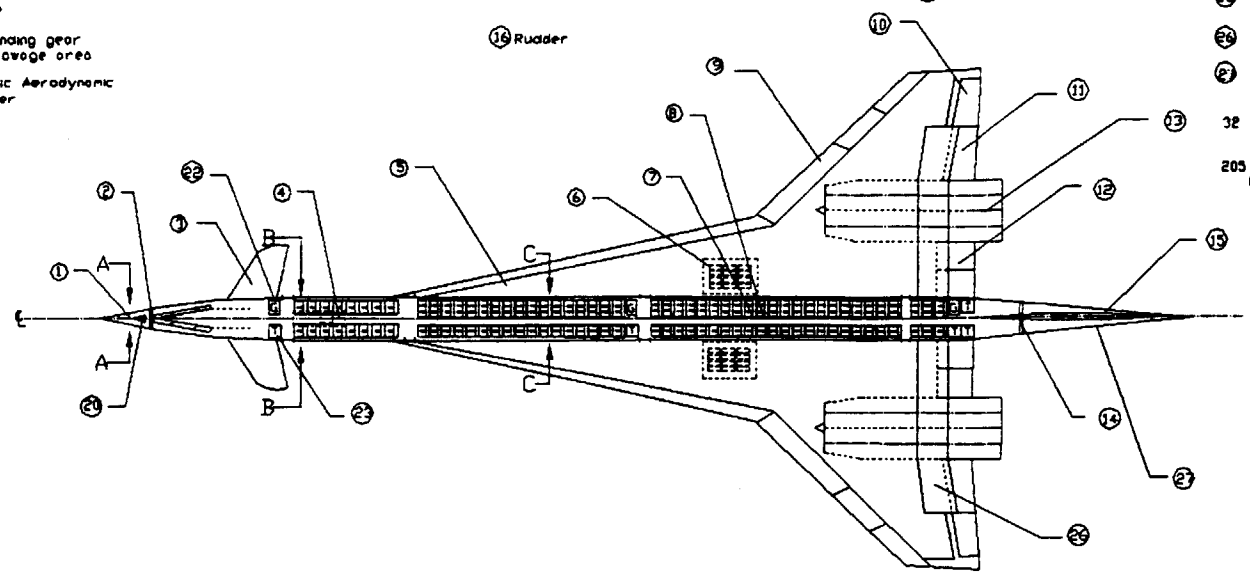

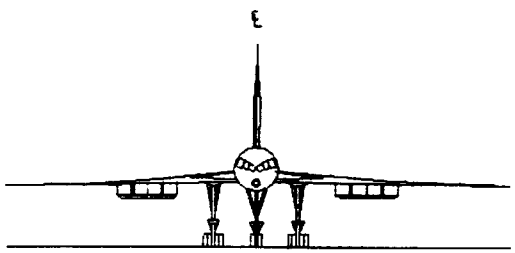

Note:
Flat Top Over Crew Cabin and Inflight Refueling Receptacle

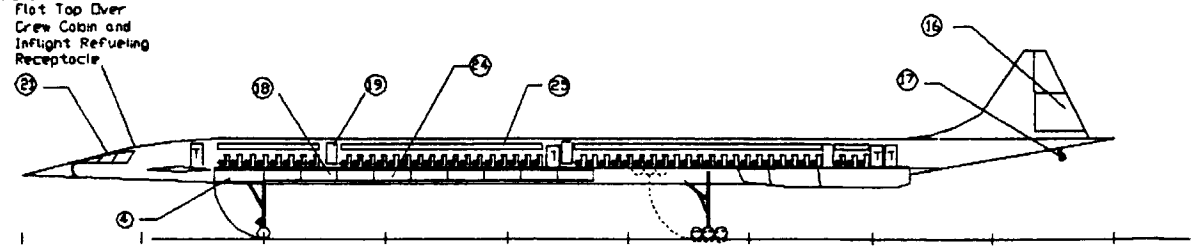

100 500 900 1300 1700 2100 2500 2900 3300 3700

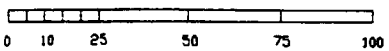

AEOLUS Concept	INBOARD PROFILE	Drawn By: Kristin Olson 4/29/9

DATA SUMMARY

LENGTH OVERALL	300 ft.
PRESSURIZED LENGTH	237 ft.
MAX FUSELAGE WIDTH	12 ft.
AIRCRAFT SUBSONIC CG/AC	185/183 ft aft
WEIGHTS	
TOGW	604711 lbs
FUEL	485840. lbs
PAYLOAD	
PASSENGER/CARGO (237)	50000 lbs.
PROPANE	77000 lbs.
ENGINES - ROLLS ROYCE MID-TANDEM FAN	
MAX SLS THRUST	80000
BYPASS RATIO	
SUBSONIC	2.5
SUPERSONIC	0.7

	WING	CANARD	VERT. TAIL
AREA-FT^2	9950.0	477.5	640.2
AR	1.82	2.714	.843
TR	0.2	0.4	0.2
t/c root/tip	.025/.02	.12/.07	.05 / .02
SWEEP$_{LE}$	47° / 78.8°	40.6°	27°
AILERON AREA	163.5 ft^2	--	--
RUDDER AREA	--	--	320.11 ft^2
ELEVON AREA	138.75 ft^2	--	--

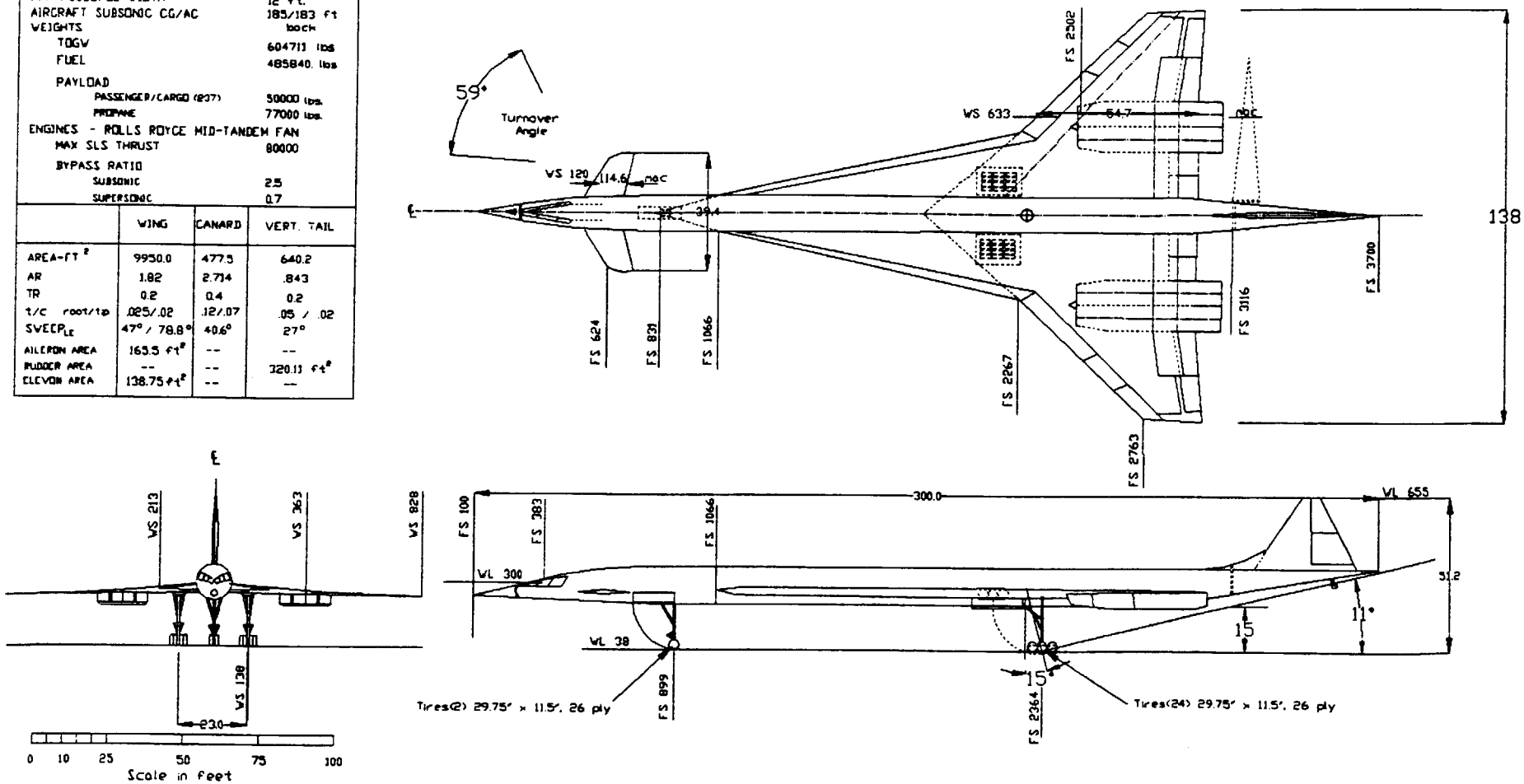

AEOLUS Concept	THREE VIEW WORKING DRAWING	Drawn By: Kristin Olson 4/29/95